Graduate School ETD Form 9
(Revised 12/07)

PURDUE UNIVERSITY
GRADUATE SCHOOL
Thesis/Dissertation Acceptance

This is to certify that the thesis/dissertation prepared

By Amiraj Banga

Entitled Functional Effects of Carbon Nanoparticles on Barrier Epithelial Cell Function

For the degree of Doctor of Philosophy

Is approved by the final examining committee:

Dr Cynthia Stauffacher
Chair

Dr Teri Belecky-Adams

Dr Bonnie Blazer-Yost

Dr Frank Witzmann

Dr Ellen Chernoff

To the best of my knowledge and as understood by the student in the *Research Integrity and Copyright Disclaimer (Graduate School Form 20)*, this thesis/dissertation adheres to the provisions of Purdue University's "Policy on Integrity in Research" and the use of copyrighted material.

Approved by Major Professor(s): Dr Bonnie Blazer-Yost

Approved by: Dr Simon Atkinson 09/21/2011
Head of the Graduate Program Date

Graduate School Form 20
(Revised 9/10)

PURDUE UNIVERSITY
GRADUATE SCHOOL

Research Integrity and Copyright Disclaimer

Title of Thesis/Dissertation:

Functional Effects of Carbon Nanoparticles on Barrier Epithelial Cell Function

For the degree of Doctor of Philosophy

I certify that in the preparation of this thesis, I have observed the provisions of *Purdue University Executive Memorandum No. C-22,* September 6, 1991, *Policy on Integrity in Research.**

Further, I certify that this work is free of plagiarism and all materials appearing in this thesis/dissertation have been properly quoted and attributed.

I certify that all copyrighted material incorporated into this thesis/dissertation is in compliance with the United States' copyright law and that I have received written permission from the copyright owners for my use of their work, which is beyond the scope of the law. I agree to indemnify and save harmless Purdue University from any and all claims that may be asserted or that may arise from any copyright violation.

Amiraj Banga

Printed Name and Signature of Candidate

09/21/2011

Date (month/day/year)

*Located at http://www.purdue.edu/policies/pages/teach_res_outreach/c_22.html

FUNCTIONAL EFFECTS OF CARBON NANOPARTICLES ON BARRIER EPITHELIAL CELL FUNCTION

A Dissertation

Submitted to the Faculty

of

Purdue University

by

Amiraj Banga

In Partial Fulfillment of the

Requirements for the Degree

of

Doctor of Philosophy

December 2011

Purdue University

Indianapolis, Indiana

Dedicated to my mom, dad and husband for their unconditional support

ACKNOWLEDGMENTS

I would like to express my sincere gratitude to my advisor Dr Bonnie Blazer-Yost for her motivation, enthusiasm, support and guidance throughout this program. I am also grateful to all the members of my thesis committee: Dr Cynthia Stauffacher, Dr Frank Witzmann, Dr Teri Belecky-Adams and Dr Ellen Chernoff for their valuable suggestions and guidance. I would also like to thank Dr Frank Witzmann for doing proteomics analysis, Dr Somenath Mitra for doing physicochemical studies and Dr Mangilal Agarwal and Dr Horia Petrache for helping me in particle size and zeta potential studies.

TABLE OF CONTENTS

Page

Page

Page

LIST OF TABLES

Table Page

LIST OF FIGURES

Figure Page

LIST OF ABBREVIATIONS

AC ..... alternate current

ADH ..... anti-diuretic hormone

AFM ..... atomic force microscopy

AIC ..... air-interface culture

ANOVA ..... analysis of variance

ATCC ..... American type culture collection

BAL ..... bronchoalveolar lavage

BAPTA-AM .....

..... [1,2-bis(2-aminophenoxy)ethane-N,N,N,N'-tetraacetic acid tetrakis(acetoxymethyl ester

BSA ..... bovine serum albumin

C_{60} ..... fullerenes

CaCC ..... calcium activated chloride channel

cAMP ..... cyclic adenosine monophosphate

CFTR ..... cystic fibrosis transmembrane regulator

CNP ..... carbon nanoparticle

CNT ..... carbon nanotube

DAPI ..... 4',6-diamidino-2-phenylindole

DIDS ..... 4,4'-diisothiocyanatostilbene-2,2'-disulfonate

DLS ..... dynamic light scattering

DMEM/F-12 ..... Dulbecco's modified Eagle's medium/Hams F-12

DNA ..... deoxyribonucleic acid

DS ..... dielectric spectroscopy

DTT ..... dithiothreitol

EDS ..... energy dispersive X-ray spectroscopy

EDTA ..... ethylenediaminetetraacetic acid

ENaC ..... epithelial sodium channel

ESI ..... electrospray ionization interface

FAK ..... focal adhesion kinase

FBS ..... fetal bovine serum

FDR ..... false discovery rate

FFA ..... flufenamic acid

G-CSF ..... granulocyte-colony stimulating factor

GST ..... glutathione-S-transferase

GM-CSF ..... granulocyte macrophage-colony stimulating factor

HBSS ..... Hanks balanced salt solution

HEPES ..... 4-(2-hydroxyethyl)-1-piperazineethanesulfonic acid

HPLC ..... high performance liquid chromatography

IFNr ..... interferon regulator

IL-1 ..... interleukin-1

IL-6 ..... interleukin-6

IL-8 ..... interleukin-8

IL-12 ..... interleukin-12

IP-10 ..... Interferon inducible protein-10

IPA ..... ingenuity pathway analysis

IPI ..... international protein index

HEK ..... human embryonic kidney

LCC ..... liquid covered culture

LDH ..... lactate dehydrogenase

LFQMS ..... label free quantitative mass spectrometry

LTQ ..... linear trap quadrupole

MCP-1 ..... monocyte chemotactic protein-1

MIP-1a ..... macrophage inflammatory protein-1-alpha

MMP ..... matrix metalloproteinase

$mpkCCD_{cl4}$ ..... mouse principal kidney cortical collecting duct clone 4

MS ..... mass spectrometry

MWNT ..... multi wall nanotubes

NCBI ..... national center for biotechnology information

NGSBB ..... normal goat serum in blocking buffer

NPPB ..... 5-nitro-2-(3-phenypropylamino)-benzoic acid

PCNA ..... proliferating cell nuclear antigen

PKA ..... protein kinase A

RANTES ..... regulated on activation, normal T expressed and secreted

ROS ..... reactive oxygen species

SCC ..... short circuit current

SCF ..... stem cell factor

SEM ..... scanning electron microscopy

SOD ..... superoxide dismutase

SWNT ..... singe wall nanotube

TBARS ..... thiobarbituric acid reactive substances

TBST ..... tris buffered saline with tween-20

TEER ..... transepithelail electrical resistance

Th1 ..... T-helper cells, type-1

TMEM16A ..... transmembrane 16A

TNF-α..... tumor necrosis factor-alpha

TPP ..... transproteomic pipeline

XIC ..... extracted ion chromatogram

ABSTRACT

Banga, Amiraj. Ph.D., Purdue University, December 2011. Functional Effects of Carbon Nanoparticles on Barrier Epithelial Cell Function. Major Professor: Bonnie L Blazer-Yost.

As mass production of carbon nanoparticles (CNPs) continues to rise, the likelihood of occupational and environmental exposure raises the potential for exposure-related health hazards. Although many groups have studied the effects of CNPs on biological systems, very few studies have examined the effects of exposure of cells, tissues or organisms to low, physiologically relevant concentrations of CNPs. Three of the most common types of CNPs are single wall nanotubes (SWNT), multi wall nanotubes (MWNT) and fullerenes (C_{60}). We used electrophysiological techniques to test the effects of CNP exposure (40 $\mu g/cm^2$ – 4 ng/cm^2) on barrier function and hormonal responses of well characterized cell lines representing barrier epithelia from the kidney ($mpkCCD_{cl4}$) and airways (Calu-3). $mpkCCD_{cl4}$ is a cell line representing principal cell type that lines the distal nephron in an electrically tight epithelia that aids in salt and water homeostasis and Calu-3 is one of the few cell lines that produces features of a differentiated, functional human airway epithelium *in vivo.* These cell lines respond to hormones that regulate salt/water reabsorption ($mpkCCD_{cl4}$) and chloride secretion (Calu-3).

In $mpkCCD_{cl4}$ cells, after 48 hour exposure, the transepithelial electrical resistance (TEER) was unaffected by high concentrations (40 – 0.4 $\mu g/cm^2$) of C_{60} or SWNT while lower, more relevant levels (< 0.04 $\mu g/cm^2$) caused a decrease in TEER. MWNT decreased TEER at both high and low concentrations. CNT exposure for 48 hour did not change the transepithelial ion transport in response to anti-diuretic hormone (ADH). In Calu-3 cells, after 48 h of exposure to CNPs, fullerenes did not show any effect on TEER whereas the nanotubes significantly decreased TEER over a range of concentrations (4 $\mu g/cm^2$-0.004 ng/cm^2). The ion transport response to epinephrine was also significantly decreased by the nanotubes but not by fullerenes. To look at the effect of exposure times, airway cells were exposed to same concentrations of CNPs for 24 and 1h. While the 48 h and 24 h exposures exhibited similar effects, there was no effect seen after 1h in terms of TEER or hormonal responses.

In both the cell lines the magnitude of the transepithelial resistance change does not indicate a decrease in cellular viability but would be most consistent with more subtle changes (e.g., modifications of the cytoskeleton or changes in the composition of the cellular membrane). These changes in both the cell lines manifested as an inverse relationship with CNP concentration, were further corroborated by an inverse correlation between dose and changes

in protein expression as indicated by proteomic analysis. These results indicate a functional impact of CNPs on epithelial cells at concentrations lower than have been previously studied and suggest caution with regard to increasing CNP levels due to increasing environmental pollution.

PUBLICATION

Nanotoxicology, September 2011; 5(3): 354–371

informa
healthcare

Effect of carbon nanoparticles on renal epithelial cell structure, barrier function, and protein expression

BONNIE L. BLAZER-YOST[1,2], AMIRAJ BANGA[1], ADAM AMOS[1], ELLEN CHERNOFF[1], XIANYIN LAI[2], CHENG LI[3], SOMENATH MITRA[3], & FRANK A. WITZMANN[2]

[1]*Department of Biology, Indiana University Purdue University at Indianapolis, Indianapolis, Indiana,* [2]*Department of Cellular and Integrative Physiology, Indiana University School of Medicine, Indianapolis, Indiana, and* [3]*Department of Chemistry and Environmental Science, New Jersey Institute of Technology, Newark, New Jersey, USA*

(Received 2 March 2010; accepted 4 August 2010)

Abstract

To assess effects of carbon nanoparticle (CNP) exposure on renal epithelial cells, fullerenes (C_{60}), single-walled carbon nanotubes (SWNT), and multi-walled carbon nanotubes (MWNT) were incubated with a confluent renal epithelial line for 48 h. At low concentrations, CNP-treated cells exhibited significant decreases in transepithelial electrical resistance (TEER) but no changes in hormone-stimulated ion transport or CNP-induced toxicity or stress responses as measured by lactate dehydrogenase or cytokine release. The changes in TEER, manifested as an inverse relationship with CNP concentration, were mirrored by an inverse correlation between dose and changes in protein expression. Lower, more physiologically relevant, concentrations of CNP have the most profound effects on barrier cell function and protein expression. These results indicate an impact of CNPs on renal epithelial cells at concentrations lower than have been previously studied and suggest caution with regard to increasing CNP levels entering the food chain due to increasing environmental pollution.

Keywords: *Carbon nanotubes, fullerene, cortical collecting duct, dielectric spectroscopy, proteomics, transepithelial resistance*

Introduction

Carbon nanoparticles (CNPs) are important components of the rapidly expanding nanotechnology field. Due to their size and unique electrical, mechanical, and thermal properties, they have found widespread application in electronic, aerospace, medical, agricultural, pharmaceutical, and other industries. Consequently, mass production and widespread application of nanoparticles continues to rise and, along with it, the likelihood of occupational and environmental exposure (Maynard et al. 2004; Borm et al. 2006; Lam et al. 2006) and potential for exposure-related inflammation, human illness, and dysfunction. Depending on the manufacturing process, CNPs are released to the air and water and ultimately contaminate soil and food products (Reijnders 2006).

Despite recent efforts to characterize potential health hazards, the overall understanding of the biological effects of CNP exposure is far from complete. Three of the most common types are single-walled carbon nanotubes (SWNT), multi-walled carbon nanotubes (MWNT), and fullerenes (C_{60}). SWNT consist of covalently bound carbon atoms arranged in a long, thin tube-like structure with a diameter of approximately 1.4 nm (Jia et al. 2005). MWCNT have a similar structure, but multiple layers of graphene sheets are concentrically rolled up for their formation with a diameter in the range of 10–50 nm (Jia et al. 2005). C_{60}, also known as fullerenes or 'buckyballs', typically consist of 60 carbon atoms covalently linked together to form a spherical molecule.

Recent research has revealed diverse effects of CNPs on biological systems. One study indicated that SWNT and MWNT inhibit growth by apoptosis and loss of cell adhesion (Cui et al. 2005), while other studies suggest that carbon nanotubes seem to

Correspondence: Dr Frank A. Witzmann, PhD, Department of Cellular & Integrative Physiology, Indiana University School of Medicine, Biotechnology Research & Training Center, 1345 West 16th Street, Room 308, Indianapolis, IN 46202, USA. Tel: +1 317 278 5741. Fax: +1 317 278 9739. E-mail: fwitzman@iupui.edu

ISSN 1743-5390 print/ISSN 1743-5404 online
DOI: 10.3109/17435390.2010.514076

increase the growth of mesenchymal cells, cause fibrogenesis, and granuloma formation (Donaldson et al. 2006). We have previously shown that MWNT alter expression of genes for cellular transport, metabolism, cell cycle regulation, and stress response (Witzmann and Monteiro-Riviere 2006). MWNT are of special interest because of their structural similarity to asbestos (Poland et al. 2008). Early experiments with SWNT have shown them to be cytotoxic, and they have been shown to bind to ion channels (Park et al. 2003). Various types of nanoparticles are endocytosed and can alter the cytoskeletal organization (Gupta and Gupta 2005).

Assuming the possibility of systemic availability of nanoparticles via lung, skin, or gastric/intestinal absorption, secondary renal exposure is a distinct likelihood (Chen et al. 2006), particularly if the CNP exposure is chronic. Lacerda et al. (2008) have shown that mice injected with purified non-functionalized MWNTs contain both aggregated and individual carbon nanotubes in the glomerular capillaries. In elegant electron microscopy images, the authors show that aggregated nanoparticles appear to remain in the capillaries while individual nanotubes pass into Bowman's space by crossing the endothelial fenestrations in a longitudinal conformation. From Bowman's capsule they traverse the nephron and enter the urinary bladder.

Our current study examines the effect of carbon nanoparticles on the function of the epithelial cells lining the renal nephron. The model used in this study is the mouse principal cell type of the kidney cortical collecting duct, clone 4 ($mpkCCD_{cl4}$) cell line. $mpkCCD_{cl4}$ cells grow to form a confluent monolayer that simulates the barrier epithelial function and hormone responsiveness found *in vivo* in renal distal tubule and collecting ducts (Bens et al. 1999). Principal cells are of particular interest because they are responsible for much of the hormonally-regulated ion transport in the kidney. If the CNP exposure alters the hormonal responsiveness of these cells, salt homeostasis could be modulated, resulting in changes in blood pressure. If the barrier function of the intact epithelium is compromised, the resulting equilibration between the filtrate and the renal interstitium can have serious consequences ranging from an inability to concentrate urine to complete renal failure.

Experiments were conducted to determine functional, structural, and proteomic changes induced by application of CNPs to the renal barrier epithelial cells. Electrophysiological studies were used to determine the effect of CNPs on transepithelial electrical resistance (TEER), a measure of barrier integrity, and hormone responsiveness. Quantitative proteomic studies were conducted to correlate the observed structural and functional studies with CNP-induced changes in the expressed cellular proteome.

Methods

Materials

CNPs were purchased from SES Research (Houston, TX, USA) and used with no further purification. As reported by the manufacturer, C_{60} (#600-9980) was 99.95+%, ultra-pure and vacuum oven-dried; SWNT (#900-1301) (long) were purified single-walled nanotubes with an outer diameter <2 nm, length ranging from 5–15 μtivm, purity >90%CNT (>50% SWNT), ash <2% wt and amorphous carbon <5% wt; and purified MWNT (# 900-1203) with an outer diameter of 40–60 nm, length ranging from 5–15 μm, >95% nanotubes vs. amorphous carbon (<2%), and ash content <0.2%.

ADH ($[Arg^8]$-Vasopressin), amiloride, transferrin, sodium selenide, and triiodothyronine were purchased from Sigma Chemical Co. (St Louis, MO, USA). DMEM/F12 tissue culture media, Glutamax, penicillin, streptomycin were purchased from Invitrogen (Carlsbad, CA, USA); fetal bovine serum came from ICN Biochemicals, Inc (Irvine CA); and ciprofloxacin from Mediatech Inc. (Herndon, VA, USA). Permeable tissue culture supports in six-well format were obtained from Costar-Corning (Acton, MA, USA). Mouse monoclonal antibody to proliferating cell nuclear antigen (PCNA) was obtained from Sigma Chemical Co. and goat anti-mouse Alexafluor red 594 was obtained from Invitrogen-Molecular Probes (Eugene, OR, USA).

CNP preparation

SWNT, MWNT, and C_{60} were diluted in fetal bovine serum to 5 mg/ml. A control was prepared by treating with fetal bovine serum in the absence of added nanoparticles. Using a Branson Sonifier 450, samples were sonicated at a duty cycle of 30% and an output control of 3 for 20 sec. Before sonication of each sample, the probe of the Branson Sonifier 450 was cleaned with ethanol and coated for 10 sec with normal serum. After sonication, the samples were sterilized via autoclave and diluted to a final concentration of 2% FBS-CNP in media. The final experimental concentrations of CNP varied over 6 orders of magnitude. In the manuscript we have expressed the concentrations as concentration per cm^2 of epithelial cell layer. For conversion, X $\mu g/cm^2$ = 2.5X μg/ml.

Background experiments performed using untreated and autoclaved serum in matched cultures showed that adding autoclaved serum to the confluent cultures for 48 h did not alter the TEER or the hormonal responses of the cell line as compared to untreated serum.

Cell culture

mpkCCD$_{cl4}$ cells were grown in a humidified chamber at 37°C and 5% CO_2. The cell line was maintained in plastic culture flasks and, for CNP exposures, cells were seeded onto Transwell filters or six-well tissue culture plates. The media was replaced thrice weekly and consisted of Dulbecco's modified Eagle's medium (DMEM): Ham's F12 basal media supplemented with 2% fetal bovine serum, 1 mM Glutamax, 25 U/ml penicillin, 25 mg/ml streptomycin, 12 mg/l ciprofloxacin, 5 mg/l transferrin, 20 μg/l sodium selenite, and 10^{-7} M triiodothyronine. Cultures were used for exposures only after achieving a confluent monolayer of cells.

Electrophysiology

Electrophysiological techniques were used to monitor TEER as well as to observe changes in ion flux across the cellular monolayers in response to hormonal stimulation. Cells were grown to confluency over a period of 13 days on Transwell filters with CNP treatment in the last 48 h at concentrations indicated in the Figures. The filters were excised, mounted in a Ussing chamber, and connected to a DVC-1000 Voltage/Current Clamp (World Precision Instruments) with voltage and current electrodes on either side of the membrane as described in detail previously (Shane et al. 2006). The spontaneous transepithelial potential difference was clamped to zero, and the resultant short-circuit current (SCC) was monitored continuously. The cells were bathed in serum-free medium maintained at 37°C via water-jacketed buffer chambers on either side of the filter. Medium was circulated and kept at constant pH using a 5% CO_2/95% O_2 gas lift. TEER was recorded every 200 sec throughout each experiment by applying a 2 mV pulse and the resulting deflection in the SCC was measured and used to calculate the TEER by Ohm's law. After the basal current stabilized, anti-diuretic hormone (ADH, vasopressin; 100 mU/ml) was added to the serosal bathing medium, and 30 min after the addition of ADH, amiloride (10^{-5} M), a specific blocker of the epithelial Na^+ channel, was added to the apical bathing medium. Groupwise comparisons of TEER were conducted using one-way ANOVA and all pairwise multiple comparison procedures used the Holm-Sidak method, at $P < 0.05$.

Histochemistry

Confluent cellular monolayers were washed with Hanks Balanced Salt Solution (HBSS), fixed in 4% paraformaldehyde, and permeabilized with 0.1% Triton X-100 in DI water. After rinsing with 4-(2-hydroxyethyl)-1-piperazineethanesulfonic acid (HEPES) buffer, cells were treated for 8 min with hot citric acid buffer, washed with HEPES and blocked with Normal Goat Serum diluted [1:10] in Blocking Buffer (NGSBB; 0.75 g Blocking Reagent/150 ml 1× Tris Buffered Saline with Tween-20 (TBST)) for 2 h at room temperature. Mouse monoclonal PCNA antibody in NGSBB (1:3000) was added to the cells overnight at 4°C. Cells were washed with HEPES buffer, and goat anti-mouse Alexafluor Red 594 secondary antibody in Blocking Buffer (1:1000) was added to the cells for 2 h at room temperature. Cells were washed with HEPES buffer and treated with DAPI. Cells were visualized using a Nikon Eclipse TE2000-U Microscope fitted with a Nikon Digital Camera (DXM1200F).

Cytokine assay

The expression pattern of eight cytokines; IL-1a (interleukin-1a), IL-1b (interleukin-1b), G-CSF (granulocyte-colony stimulating factor), GM-CSF (granulocyte macrophage-colony stimulating factor), MCP-1 (monocyte chemotactic protein-1), MIP-1a (macrophage inflammatory protein-1 alpha), SCF (stem cell factor), and RANTES (Regulated on Activation, Normal T Expressed and Secreted), was profiled using a kit, Mouse Inflammation ELISA Strip for Profiling 8 Cytokines (Signosis, Sunnyvale CA, USA). Apical and basolateral media from mpkCCD$_{cl4}$ cell cultures were assayed in triplicate according to the manufacturer's protocol. Briefly, 100 μl of media were added to wells coated with a primary antibody against a specific cytokine and incubated for 1 h at RT. Medium was aspirated from wells followed by three washes with 200 μl of assay wash buffer. 100 μl of biotin-labeled antibody mixture was added to each well and incubated for 1 h at RT. Wells were aspirated then washed three times with 200 μl of assay wash buffer. Streptavidin-HRP conjugate (100 μl) was added to each well and incubated for 45 min at RT followed by the aspiration and wash procedure. 100 μl of substrate was added and incubated for 10 min; subsequently 50 μl of stop solution was applied to each well. A microplate reader determined

the optical density of each well at 450 nm. The concentrations of the inflammatory cytokines were directly proportional to the color intensity of the samples.

LDH assay

Media was collected from both apical and basolateral sides of exposed cells for electrophysiological studies and assayed for lactate dehydrogenase (LDH). The LDH assay was performed using Promega CytoTox 96 non-radioactive cytotoxicity assay kit (Promega, Madison, WI, USA). This is a colorimetric assay that quantitatively measures lactate dehydrogenase, a stable cytosolic enzyme released upon cell lysis. The released LDH oxidizes lactate to pyruvate which promotes conversion of tetrazolium salt INT to formazan, a water soluble molecule with absorbance at 490 nm. The amount of LDH released is proportional to the number of cells damaged or lysed. As a positive control for toxicity, we used cadmium dioxide (CdO_2) (Sigma-Aldrich, St Louis, MO, USA), known for its cytotoxic properties. The CdO_2 was prepared exactly like the other nanoparticles. The cells were exposed to CdO_2 for 48 h and media collected from both apical and basolateral sides.

Scanning electron microscopy (SEM) and energy dispersive X-ray spectroscopy (EDS)

SEM and EDS data were collected on a LEO 1530 VP Scanning Electron Microscope equipped with an energy-dispersive X-ray analyzer. A few drops of SWNT and MWNT dispersions in cell culture media were placed on silicon wafers and allowed to air-dry. The silicon wafers were then mounted on aluminum stubs for SEM and EDS analysis.

Particle size analysis and dielectric spectroscopy of carbon nanotubes in media

The samples (the culture medium blank and CNPs dispersed in the medium at two different concentrations) for particle size analysis and dielectric spectroscopy were prepared at IUPUI. Particle size distribution of the samples was measured at 26°C using dynamic light scattering (Beckman Coulter N4-Plus submicron particle size analyzer) operating at 90° detector angle). Dielectric spectroscopy was carried out at NJIT with a Novacontrol BDS-80 broadband dielectric spectrometer, using a liquid sample cell with the size of 11.04 × 6.6 mm (diameter × thickness). The bias voltage was set at 1 volt, and the dielectric spectra were collected at room temperature in the frequency range 1–10^5 Hz.

Atomic force microscopy

To study CNP agglomeration on cell surfaces, morphology of these surfaces was evaluated with tapping-mode atomic force microscopy (AFM) using a Digital Instrument Nanoscope II.

Proteomics

Proteins from duplicate samples were analyzed by label-free quantitative mass spectrometry (LFQMS) (Higgs et al. 2008; Wang et al. 2008). Cultured cell proteins were extracted *in situ* using a lysis buffer containing 8 M urea and 10 mM dithiothreitol (DTT) and protein concentrations were determined by Bradford assay (Bradford 1976). The same lysis buffer was used as the background reference for the protein assay and for BSA protein standards. The resulting protein extracts were reduced and alkylated with triethylphosphine and iodoethanol (Hale et al. 2004). Protein mixtures were digested with trypsin and filtered through 0.45 μm spin filters before being applied to the high-performance liquid chromatography (HPLC) system. Prior to tryptic digestion, each sample was spiked with chicken lysozyme as an internal reference to assess technical variation.

Tryptic peptides (20 μg) were injected randomly onto a Surveyor HPLC system (Thermo-Finnigan) with a C18 microbore column (Zorbax 300SB-C18, 1 mm × 65 cm). Peptides were eluted with a linear gradient from 5–45% acetonitrile developed over 120 min at a flow rate of 50 μl/min and the effluent was electro-sprayed into the LTQ mass spectrometer (Thermo Fisher Scientific, Waltham, MA, USA). Data were collected in the 'Triple Play' (MS scan, Zoom scan, and MS/MS scan) mode. The acquired data were filtered and analyzed by a proprietary algorithm (Higgs et al. 2005) licensed to Monarch Lifesciences LLC, Indianapolis IN. Database searches against the International Protein Index (IPI) mouse database and the non-redundant *Mus musculus* database (NCBI) were carried out using the X!Tandem (Craig and Beavis 2004) and SEQUEST (Eng et al. 1994) algorithms.

Only those proteins identified with >90% confidence were evaluated quantitatively as described previously (Higgs et al. 2005, 2008). Briefly, when raw files were acquired from the LTQ mass spectrometer, all extracted ion chromatograms (XICs) were aligned by retention time. After alignment, area under the curve (AUC) for each individually aligned peak from each sample was measured,

normalized, and compared for relative abundance. Significant differences in protein expression across dose groups were determined by ANOVA. To eliminate technical bias, randomization of order of measurement and 'quantile normalization' was used (Bolstad et al. 2003) and data normalized using a log2 scale.

Pathway analysis

To assist with interpretation of the numerous protein expression effects, we analyzed the differentially expressed protein data using Ingenuity Pathways Analysis (IPA) tools (Ingenuity Systems, Mountain View, CA; http://www.ingenuity.com/index.html), a web-delivered application that enables the discovery, visualization, and exploration of molecular interaction networks and canonical pathways in protein expression data (see Tables VII and VIII). Lists of differentially expressed proteins were uploaded into the IPA system and proteins that were associated with a specific functional network or canonical pathway in the Ingenuity Pathways Knowledge Base were considered for evaluation. The IPA computes a score for each network according to the fit of the user's set of proteins of interest. The score is derived from a p value and indicates the likelihood that the selected proteins are categorized in a network due to random effects.

Results

Characterization of nanoparticles in aqueous media

The nanomaterials used in these studies were 'as-manufactured' particles of the types that are likely to occur as environmental or workplace contaminants. An analysis of the three types of particles indicate that the fullerenes are virtually free of contaminating metals while the carbon nanotubes have measureable levels of iron, nickel and/or cobalt which are likely contaminates from the manufacturing process (Figure 1). SEM of SWNT and MWNT indicated that these materials are relatively free of amorphous carbon.

As-manufactured, unrefined nanotubes are sparingly dispersible in aqueous media. The highest concentrations of nanotubes used in these experiments, 40 and 4 μg/cm^2 (100 and 10 μg/ml), show substantial agglomeration and precipitation onto the apical surface of the cellular monolayers. Figure 2 shows the particles that remain on the surface of the cells after removal of the media. Lower concentrations show no visible aggregates.

Atomic force microscopy

In agreement with the visual observations (Figure 2), AFM demonstrated that at high dose (40 μg/cm^2) exposures, roughness factor (Ra) is high, suggesting

Element	C_{60}%wt	SWNT %wt	MWNT %wt
C	73.7	95.3	92.2
O	26.3	3.1	3.7
Fe	-	0.4	-
Ni	-	1.0	0.3
Co	-	0.2	4.3

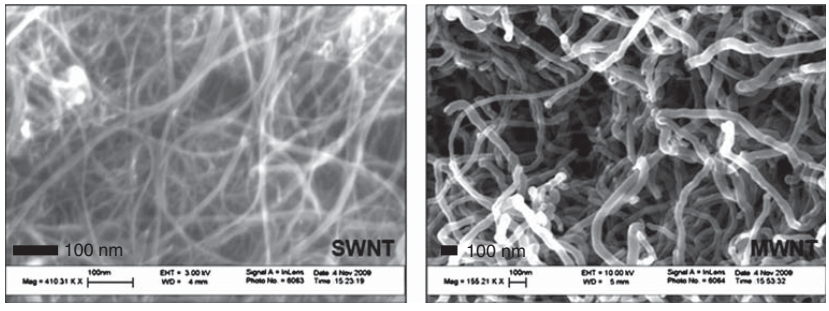

Figure 1. Elemental analysis of the carbon nanoparticles determined by energy dispersive X-ray spectroscopy and SEM of SWNT and MWNT.

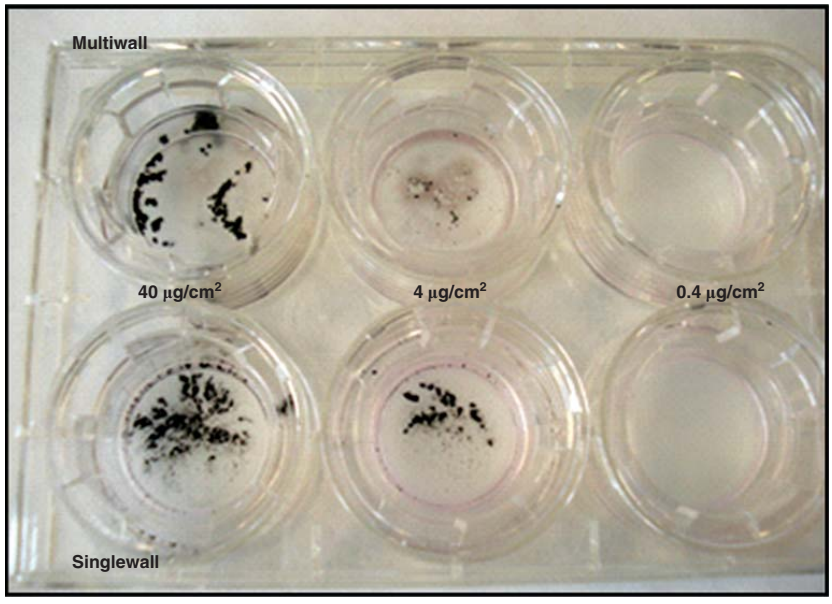

Figure 2. Nanotube agglomeration in the tissue culture media. Multi-wall and single-wall nanotubes were prepared in serum and diluted into tissue culture media as described in *Methods*. The solutions, at the concentrations indicated, were added to six-well Transwell chambers and incubated for 48 h at 37°C. The media was removed. The Figure shows the agglomerated particles that were deposited on the apical side of the cellular monolayers under these incubation conditions.

that large agglomerates are associated with the cell surface (Table I). These measurements represent the general filter surface and not the large black CNT particles seen in Figure 2. At a lower dose (0.4 μg/cm^2), Ra is very low (near blank levels), suggesting that the particles are more dispersed and may, therefore, have greater potential for cellular interaction and biological activity. Agglomeration at cell surface would serve as a barrier which would prevent the dispersed CNPS from interacting with the cells.

Particle size analysis and dielectric spectroscopy of CNTs in media

Results of particle size analysis of CNPs (C_{60}, SWNT, and MWNT) dispersed in the culture media are listed in Table II. The particle size is expressed as 'mean diameter'. The increase in particle size of fullerene dispersion was negligible when the concentration was increased by an order of magnitude, indicating little aggregation of fullerene in the culture medium. On the other hand, the increase in particle size with increasing CNT concentration is an indication of nanotube aggregation at higher concentration. Note that, at higher concentration of 0.04 μg/cm^2, although the mean diameter of the MWNT dispersion was very close to that of the SWNT dispersion, the much higher standard deviation (STD) was observed for the former (7.1 vs. 1.0). This indicates that some

Table I. Results of AFM-Roughness (Ra) values on cell surface.

CNP	Ra value
Blank	147.5
SWNT 0.4 μg/cm^2	113.5
MWNT 0.4 μg/cm^2	160.1
C_{60} 40 μg/cm^2	622.2
SWNT 40 μg/cm^2	432.2
MWNT 40 μg/cm^2	214.0

Table II. Results of particle size analysis of CNTs in cell culture media.

CNPs	Mean diameter (nm)	STD
C_{60} 0.004 μg/cm^2	230	0.7
C_{60} 0.04 μg/cm^2	233	0.6
SWNT 0.004 μg/cm^2	218	0.1
SWNT 0.04 μg/cm^2	260	0.6
MWNT 0.004 μg/cm^2	224	1.0
MWNT 0.04 μg/cm^2	263	7.1

larger agglomerates were formed in the case of the MWNT.

We applied dielectric spectroscopy (DS) for the investigation on the dispersion of CNPs in the cell culture medium. DS has been used extensively to characterize colloidal suspensions. The measurements were carried out using a liquid sample cell at a bias voltage of 1 volt. Dielectric spectra were collected in the frequency range of $1–10^5$ Hz. Frequency dependence of AC conductivity of C_{60}, SWNTs or MWNTs dispersed in the medium at two different concentrations (0.004 μg/cm^2 and 0.04 μg/cm^2) is shown in Figure 3. Frequency dependence of AC conductivity of the medium blank is included for comparison. The conductivity of the medium blank and the C_{60} dispersions are relatively low and underwent little change over the entire frequency range. An increase in the conductivity with increasing frequency is evident for all media with dispersed CNTs. This could be attributed to the effect of interfacial polarization due to surface charge on CNT particles. The difference in the conductivity of the medium matrix and the conductivity of the CNTs caused interfacial polarization resulting in the motion of the surface charge which is trapped at the interface of components.

In the case of SWNT, conductivity increased with an increase in the concentration of SWNT. For example, at 9.8 kHz, AC conductivity was increased from 3.62×10^{-4} S/cm for the medium blank to 3.66×10^{-3} S/cm at 0.004 μg/cm^2 SWNT concentration and further to 1.02×10^{-2} S/cm at 0.04 μg/cm^2 SWNT concentration. The conductivity reached a plateau at higher frequency because the polarization process can no longer follow the change in the applied electrical field. Increased conductivity with concentration indicates finely dispersed SWNTs even at higher concentrations.

As for MWNT, at 0.004 μg/cm^2 MWNT concentration, conductivity was comparable to that of the medium with SWNT at the same concentration level at higher frequency range but reached a plateau at lower frequency. The difference between the MWNT and SWNT dispersed in the medium is that the conductivity decreased with the increase in MWNT concentration, contrary to the trend shown in the case of SWNT dispersion. One possible reason is that, compared to SWNT, the MWNTs tend to form large agglomerates at higher concentration. Higher agglomeration in MWNTs resulted in the reduction of effective conduction pathways. In general, the dielectric spectroscopy data provide an insight into agglomeration pattern in the biological suspensions, which is expected to affect CNP-cell interactions at both physical and biological levels. It is interesting to observe that the SWNT and MWNT behaved so differently. This is consistent with the DLS data, where the formation of larger agglomerates led to a

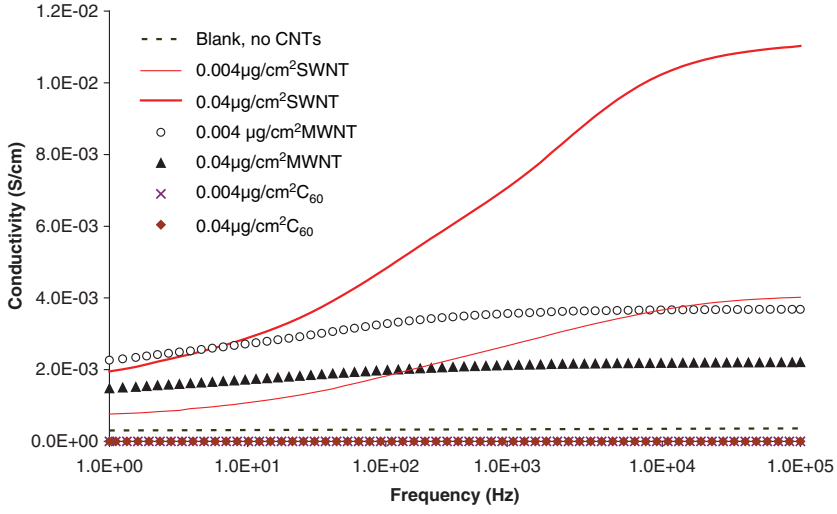

Figure 3. Frequency dependency of AC conductivity for a culture medium (dashed line), and the media with 0.004 μg/cm^2 (thin solid line) or 0.04 μg/cm^2 (thick solid line) of SWNT, the media with 0.004 μg/cm^2 (open circle) or 0.04 μg/cm^2 (filled triangle) of MWNT, and the media with 0.004 μg/cm^2 (cross) or 0.04 μg/cm^2 (filled diamond) of C_{60}.

significantly higher variability in the particle size distribution.

Cellular effects of nanoparticle exposure

PCNA staining was used to visualize cellular proliferative responses (Figure 4). At high concentrations, where agglomeration of particles is pronounced, in the immediate vicinity of the agglomerated nanotubes, there is an increase in cellular proliferation. This effect was never seen in C_{60} exposures, nor was it observed at SWNT or MWNT concentrations ≤ 0.4 μg/cm^2.

While the agglomerated particles induce specific effects on the cellular proliferation, we hypothesized that more subtle functional effects may be exerted at lower concentrations where the particles were not agglomerated and could, potentially, enter the cells or permeate the cellular junctions as individual particles. To mimic the *in vivo s*ituation of a healthy epithelium, the cells were exposed to nanoparticles only after they had achieved at high-resistance monolayer (13 days). The effects of 48 h incubation with various nanoparticles on the transepithelial resistance (TEER) of the mpkCCD$_{cl4}$ renal cell line were measured using standard Ussing-type electrophysiological techniques. 48 h incubation with

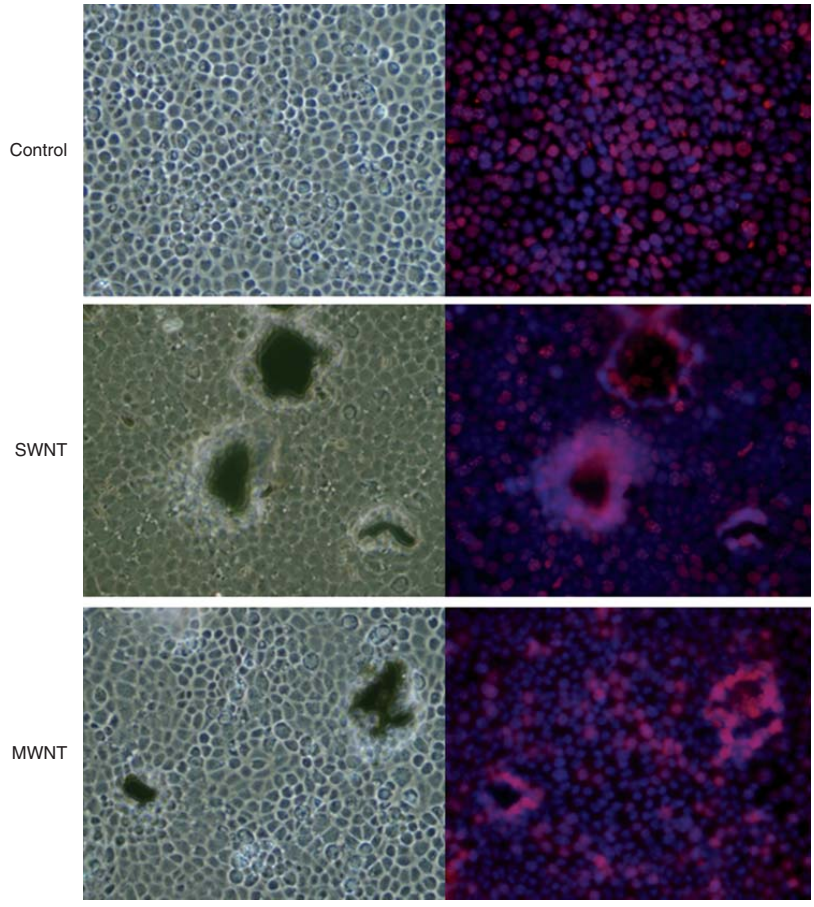

Figure 4. Effects of CNP exposure in the mpkCCD$_{cl4}$ cell line. Cells were seeded in 24-well plates and exposed to 40 μg/cm^2 of SWNT or MWNT for 48 h. The cells were fixed and stained with proliferating cell nuclear antigen (PCNA) to indicate the nuclei or proliferating cells and DAPI to stain all cell nuclei (red and blue respectively in the merged images on the right). The brightfield images (left-hand panels) clearly show the agglomerated nanoparticles as irregular black spots. The panels on the right indicate the increased cellular proliferation (PCNA; red) in the areas surrounding the nanoparticles.

multi-walled nanotubes decreases the TEER of the renal cells with equal efficacy over a 6 order of magnitude dose response range. The single-walled nanotubes and fullerenes, on the other hand, show an inverse dose response relationship with the lower concentrations showing a significant decrease in TEER while the higher concentrations are without effect (Figure 5).

After measurement of the TEER, the cells were exposed to antidiuretic hormone (ADH; vasopressin). Figure 6 illustrates the response to ADH in control and nanoparticle-exposed cellular monolayers. The mpkCCD$_{cl4}$ cells respond to three hormones that stimulate ion transport in renal principal cells – aldosterone, insulin and ADH (Shane et al. 2006). We have chosen to study the effects of ADH because this peptide hormone elicits a multi-phasic response consisting of both Cl^- secretion via the cystic fibrosis transmembrane regulator (CFTR) and Na^+ absorption via the epithelial Na^+ channel (ENaC). Aldosterone and insulin both cause an increase in ENaC-mediated Na^+ absorption with no detectable change in Cl^- secretion. Thus, studying the response to ADH maximizes the ability to detect potential nanoparticle effects on ion transporters. Figure 6 contains the data from control, 40 μg/cm^2 (highest dose) and 0.4 ng/cm^2 (lowest dose). Nanoparticle exposure did not alter either the Cl^- secretory or the Na^+ absorption response to ADH. The experiments were repeated at every concentration shown in Figure 5 and all doses were without effect (data not shown).

Cytokine profiles and LDH measurements (data not shown) revealed that none of the CNP exposures, at any dose, altered their levels, indicating the absence of any irritation or cell damage. Regarding cell viability, none of the changes in TEER reached levels that represent a decrease in cell viability. The observed decreases in TEER are indicative of a healthy and high resistance, intact epithelium. Therefore, no other measures of viability were deemed necessary.

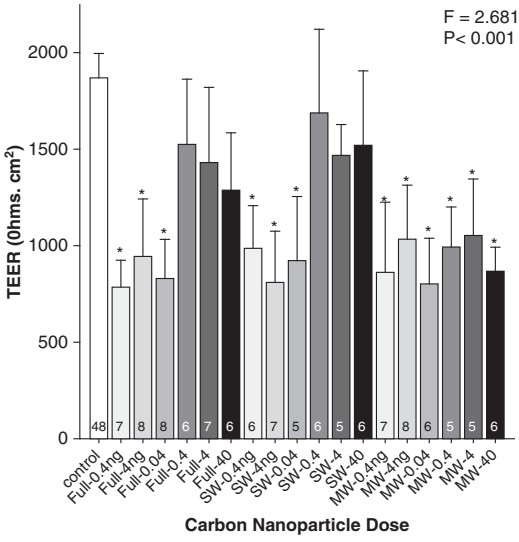

Figure 5. Effect of nanoparticle incubation on the TEER in the mpkCCD$_{cl4}$ cell line. Cells were grown to confluence on Transwell permeable supports and incubated for 48 h with media containing the indicated concentrations of nanoparticles provided as concentration per cm^2 diagonally under each bar. After the incubation, the Transwells were removed and placed in Ussing chambers and allowed to stabilize for 0.5–1 h before measuring the TEER. The bars represent the means ± SEM. * indicates experiments where the mean values were significantly different than the mean control value. The number of replicate experiments performed at each concentration is indicated as the values in the bars.

Proteomic effects of nanoparticle exposure

Carbon nanoparticle treatment induced significant alterations in protein expression as measured by label-free quantitative mass spectrometry. Across all samples analyzed, an average of 1,878 proteins were identified, quantified, and compared. As Table III indicates, all CNPs caused differences in protein expression compared to controls and the number of proteins whose expression was significantly altered declined with increasing dose, with C_{60} having the least effect overall.

A complete list of the detected proteins and their pertinent information can be found in the supplementary material, available online. When all doses and CNP-types were compared, no differentially expressed proteins common to all exposure conditions were found. This was also true across all three doses within individual CNPs. However, at the two lowest doses, 0.04 and 0.004 μg/cm^2, expression of a number of proteins was affected by the respective CNP, and these are listed in Table IV.

At the lowest dose, the expression of seven proteins was altered by all three CNPs (Table V), while only histone cluster 2, H2ac was altered by all three CNPs at the 0.04 μg/cm^2 dose, and none at 40 μg/cm^2.

When comparing the effect of the two nanotubes, 26 proteins were similarly affected by exposure to SWNT and MWNT at the 0.004 μg/cm^2 dose. These are listed in Table VI. At the 0.04 μg/cm^2, only members J and X of the H2A histone family and histone cluster 2 were altered by both SWNT and

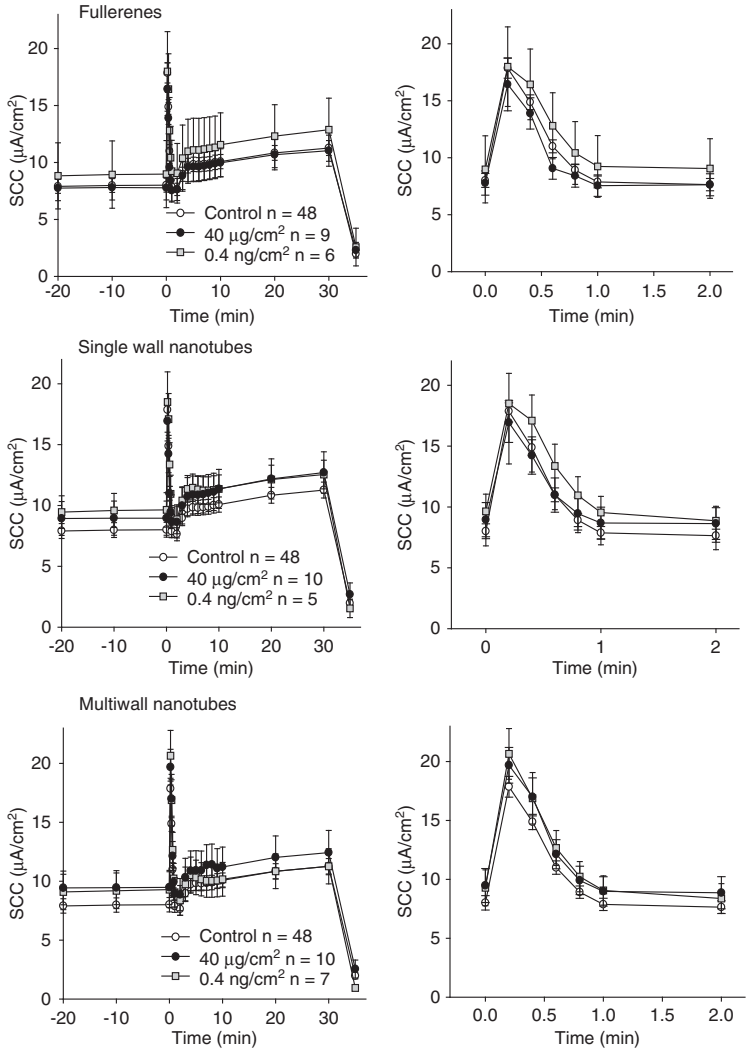

Figure 6. Response of mpkCCD$_{cl4}$ renal cells to ADH in control and nanotube-exposed cultures. Cells were grown in Transwell supports until they formed a confluent monolayer. The media was then replaced with either control or nanoparticle containing media and the incubation was continued for 48 h. The cells were mounted in Ussing chambers and the basal SCC was allowed to stabilize. ADH was added to the serosal bathing media at time zero. The panels on the left denote the entire time course of the response of the mpkCCD$_{cl4}$ cells to ADH. The hormone causes an immediate response that consists of a CFTR-mediated Cl^- secretory phase (~ 0–1 min) followed by an ENaC-mediated increase in Na^+ flux (~ 5–30 min). Amiloride, a specific inhibitor of ENaC, was used to terminate the experiment at time t = 30 min. Panels on the right show the first 2 min which is the Cl^- secretory phase. This Figure contains the data from control, 40 μg/cm^2 (highest dose) and 0.4 ng/cm^2 (lowest dose).

MWNTs, while at 40 μg/cm^2, catenin, beta like 1 (CTNNBL1) was upregulated.

To interpret the biological significance of the affected proteins, Ingenuity Pathways Analysis was used to categorize proteins differentially expressed by mpkCCD$_{cl4}$ cells in response to each dose and CNP exposure, and those 254 proteins altered across all exposures. Pathway analysis technology enables the mapping of protein expression data into relevant molecular interaction networks and canonical pathways based on functional annotations and known molecular interactions. Tables VII and VIII list the

Table III. Number of proteins altered ($P \leq 0.01$) by CNP exposure.

	CNP dose (μg/cm^2)		
CNP	0.004	0.04	40
C_{60}	61	16	5
SWNT	116	29	12
MWNT	105	17	10

most significant ($P \leq 0.001$) functional networks and canonical pathways involving proteins altered by the CNP exposures. Table VII lists the various CNP exposures and corresponding number of up- and down-regulated proteins (corresponding to totals listed in Table III) in one column and, in a second column, the functional networks corresponding to the number of proteins (included parenthetically) from the first column that were statistically assigned to IPA networks. Table VIII lists the various CNP exposures along with canonical pathways identified by IPA that are impacted by each exposure. Only those pathways in which three or more differentially expressed proteins were determined statistically ($P < 0.001$) to be members are included. Interpretation of these results is presented in the *Discussion* section.

To compare the proteomic results with multiple previous studies, it is also informative to highlight proteins that did not change in response to CNP exposure. The general absence of toxicity is exemplified by the observation that numerous proteins typically upregulated by ROS or cellular toxicity were unaffected at all doses. The following glutathione-S-transferases were identified and quantified: A3, mu-1, mu-2, mu-4, mu-5, mu-7, mu-7, omega-1, P1, P2, and theta-3. With the exception of GST mu-4, which was up-regulated (10.1%) by SWNT at 0.004 μg/cm^2, and GST omega-1 which was up-regulated slightly by fullerenes (10.7%) at 0.04 μg/cm^2 and down-regulated by SWNT (10.6%) at 0.004 μg/cm^2, all others were normally expressed, as were glutathione reductase and formylglutathione lyase (glyoxalase I). Similar observations were made for both superoxide dismutases Mn and Cu-Zn and stress proteins. Seventeen proteins associated with the peroxiredoxin family of antioxidant enzymes and with peroxisomes were unaffected at all exposures, as were four members of the cytochrome P450 family. Seventy-eight kinases were profiled and none with toxicity-related signaling function were affected by the exposures.

Table IV. mpkCCD$_{cl4}$ cell proteins altered in both lower dose exposures (0.004 and 0.04 μg/cm^2) in response to specific CNP.

CNP	Gene ID	Protein name
C_{60}	CPPED1	calcineurin-like phosphoesterase domain containing 1 ▲,▼
SWNT	ACBD3	acyl-Coenzyme A binding domain containing 3 ▲,▲
	GAPDHS	glyceraldehyde-3-phosphate dehydrogenase ▲,▲
	H2AFX	histone family, member X ▲,▲
	MIF	macrophage migration inhibitory factor (glycosylation-inhibiting factor) ▲,▲
	RPL17	ribosomal protein L17 ▼,▼
	RPL27	ribosomal protein L27 ▼,▼
	EG237361	ribosomal protein L27a ▼,▼
	RPS8	ribosomal protein S8 ▼,▼
	GM5121	ribosomal protein S8 isoform 1 ▼,▼
	RPS17	ribosomal protein S17 ▼,▼
	SECTM1B	secreted and transmembrane 1B ▼,▼
MWNT	H2AFJ	H2A histone family, member J ▲,▼
	H2AFX	H2A histone family, member X ▲,▼
	H2AFY	H2A histone family, member Y ▲,▼
	HIST2H2AC	histone cluster 2, H2ac ▲,▼
	HADH	hydroxyacyl-Coenzyme A dehydrogenase ▼,▲
	SHMT2	serine hydroxymethyltransferase 2 (mitochondrial) ▼,▲

In each row, the first arrow refers to change associated with the 0.004 μg/cm^2 exposure; the second arrow refers to change associated with the 0.04 μg/cm^2 exposure.

Table V. mpkCCD$_{cl4}$ cell proteins altered by all CNPs (C_{60}, SWNT, MWNT) at the lowest dose (0.004 μg/cm^2).

Gene ID	Protein name
HIST1H2BF	histone cluster 1, H2bf ▲,▲,▼
HNRNPU	heterogeneous nuclear ribonucleoprotein U ▼,▼,▼
LHX9	LIM homeobox 9 ▼,▼,▼
MYBBP1A	MYB binding protein (P160) 1a ▼,▼,▼
PDE2A	phosphodiesterase 2A, cGMP-stimulated ▲,▲,▲
PIWIL1	piwi-like 1 (Drosophila) ▼,▲,▼
TMPO	thymopoietin ▼,▼,▼

In each row, the first arrow refers to the effect of C_{60}; the second arrow refers to the effect of SWNT; and the third arrow refers to the effect of MWNT.

Discussion

Raw, non-functionalized nanoparticles such as the materials used in this study form the basis for the synthesis of other functionalized particles and composite materials that are useful in both industry and medicine. As such, it is the non-functionalized forms that will be manufactured in large quantities and are, therefore, the most likely forms that will contribute to environmental contamination as well as work-place exposures. As shown in the Results these particles are very sparingly dispersible, even after sonication in a protein-rich solution such as serum. The results predict that there may be two very different types of effects of the nanoparticles on cellular response – those manifested in response to the presence of large

Table VI. mpkCCD$_{cl4}$ cell proteins altered by both SWNT and MWNT exposures at the lowest dose (0.004 μg/cm^2).

Gene ID	Protein name
ACBD3	acyl-Coenzyme A binding domain containing 3 ▲,▼
AHNAK	AHNAK nucleoprotein ▼,▼
DNAHC9	dynein, axonemal, heavy chain 9 ▲,▼
GAPDH	glyceraldehyde-3-phosphate dehydrogenase ▲,▼
H2AFX	H2A histone family, member X ▲,▼
H2AFY	H2A histone family, member Y ▲,▼
HIST1H2BF	histone cluster 1, H2bf ▲,▼
HNRNPU	heterogeneous nuclear ribonucleoprotein U (scaffold attachment factor A) ▼,▼
KCNN3	K^+ intermediate/small conductance Ca^{++}-activated channel, subfamily N, member 3 ▲,▼
LHX9	LIM homeobox 9 ▼,▼
ABCG3	similar to ATP-binding cassette transporter ▲,▼
MAT2B	methionine adenosyltransferase II, beta ▼,▲
MIF	macrophage migration inhibitory factor (glycosylation-inhibiting factor) ▲,▼
MYBBP1A	MYB binding protein (P160) 1a ▼,▼
OIP5	Opa interacting protein 5 ▲,▼
PDE2A	phosphodiesterase 2A, cGMP-stimulated ▲,▲
PFN1	profilin 1 ▼,▲
PIWIL1	piwi-like 1 (Drosophila) ▲,▼
PPIL1	peptidylprolyl isomerase (cyclophilin)-like 1 ▼,▼
RDH5	retinol dehydrogenase 5 (11-cis/9-cis) ▲,▼
RPS5	ribosomal protein S5 ▼,▼
SHMT1	serine hydroxymethyltransferase 1 (soluble) ▼,▲
SHMT2	serine hydroxymethyltransferase 2 (mitochondrial) ▼,▲
SLC39A10	solute carrier family 39 (zinc transporter), member 10 ▲,▼
TLN1	talin 1 ▼,▲
TMPO	thymopoietin ▼,▼

In each row, the first arrow refers to the effect of SWNT; the second arrow refers to the effect of MWNT.

Table VII. Functional networks in mpkCCD$_{cl4}$ cells impacted by CNP exposure ($P \leq 0.001$).

CNP	Functional network
C_{60} 0.004 ug/cm^2 (34▲; 27▼)	1) **Gene Expression, Cell Death,** Energy Production (13▲; 4▼) 2) **Cancer, Cellular Growth & Proliferation, Cell Cycle** (6▲; 6▼)
C_{60} 0.04 ug/cm^2 (11▲; 5▼)	No significant relationship to networks
C_{60} 40 ug/cm^2 (4▲; 1▼)	No significant relationship to networks
SWNT 0.004 ug/cm^2 (57▲; 59▼)	1) Protein Synthesis, **Gene Expression, Cellular Growth & Proliferation** (4▲; 14▼) 2) Carbohydrate Metabolism, **Cancer, Genetic Disorder** (13▲; 4▼) 3) **Cancer, Cellular Movement, Connective Tissue** Development & Function (8▲; 5▼)
SWNT 0.04 ug/cm^2 (14▲; 15▼)	1) **Cancer, Cell Death, Cellular Growth & Proliferation** (7▲; 6▼)
SWNT 40 ug/cm^2 (7▲; 5▼)	No significant relationship to networks
MWNT 0.004 ug/cm^2 (45▲; 60▼)	1) **Cancer, Cell Cycle, Cell Death** (7▲; 8▼) 2) Inflammatory Disease, Skeletal & Muscular Disorders (9▲; 7▼) 3) Neurological Disease, **Connective Tissue** Disorders (10▲; 4▼) 4) Endocrine Disorders, **Cellular Movement,** Metabolic Disease (9▲; 7▼)
MWNT 0.04 ug/cm^2 (10▲; 7▼)	1) DNA Replication, Recombination & Repair, **Cancer, Genetic Disorder** (3▲; 2▼)
MWNT 40 ug/cm^2 (3▲; 7▼)	No significant relationship to networks

Numbers in parentheses indicate the number of proteins whose abundance increased ▲ or decreased ▼. Protein alterations in the left column refer to those altered at each exposure (corresponding to Table III). Protein alterations appearing in the right column are only those corresponding to the specific functional networks determined by IPA, represented by the altered proteins (i.e., other proteins had no significant relationship to other networks). Those networks appearing in bold are those that are common to one or more CNPs.

agglomerants of particles that adhere to the surface of the epithelial cells (micro effects) and those manifested by exposure to individual particles (nanoeffects). At concentrations above 1 μg/ml (0.4 μg/cm^2), both single- and multi-walled nanotubes form visible aggregates. These observations are corroborated by the dielectric spectroscopy results and AFM analysis.

In a previous study examining the effect of MWNT on human epidermal keratinocytes (Witzmann and Monteiro-Riviere 2006), the authors observed significant alterations in protein expression, particularly in membrane-related proteins, such as those involved with organization of membrane domains and/or - membrane-cytoskeleton linkages, certain exocytotic and endocytotic transport steps, cytoskeletal integrity, and related signaling functions. A subsequent experiment in which mpkCCD$_{cl4}$ cells were exposed to very high concentrations of CNPs (200 μg/cm^2) (Amos et al. 2008) demonstrated significant declines in TEER but minor proteomic alterations. However, those proteins that were affected were related to junctional and cell adhesion functions. This leads us to hypothesize that MWNT and other related CNPs might alter barrier function in these and other epithelial cells that play such a protective role.

Studies have suggested that carbon nanoparticles may have carcinogenic properties (Murr et al. 2005). MWNT have been specifically implicated due to their structural similarity to chrysotile asbestos that is widely accepted to cause carcinogenic responses in humans (Kane and Hurt 2008; Poland et al. 2008). After exposure to high concentrations of nanotubes, we observed changes in cells surrounding agglomerations of SWNT and MWNT. Cells seemed to exhibit proliferating nuclei as indicated by PCNA staining. Under control conditions, once confluence is reached, cells no longer actively divide. The results with the nanotubes indicate that SWNT and MWNT agglomerations cause cells to replicate abnormally, suggesting that hyperplasia is occurring. Despite elevated PCNA staining at agglomerant foci, PCNA expression was detected but remained unchanged at all doses analyzed using quantitative mass spectrometry.

The mpkCCD$_{cl4}$ studies were conducted to show the effects of relatively short-term exposure to nanoparticles. High resistance cell lines most closely mimic the *in vivo* situation if potential effectors are added to the cultures after the cells have achieved a confluent monolayer, thus limiting the timing of the experiments to several days. However, the effects seen in this model could portend additional, more serious, outcomes with longer-term exposures.

In some organs, nanoparticles may remain embedded in the tissues for long periods of time. MWNT administered intratracheally persisted in the lung tissue for more than 60 days (Muller et al. 2005). In the rodent models and in cultured lung cells, high levels of MWNT caused inflammatory and fibrotic reactions as well as evidence of mutagenesis (Muller et al.

Table VIII. Canonical pathways in mpkCCDcl4 cells impacted by CNP exposure (only ≥ 3 proteins) ($P < 0.001$).

CNP	Canonical pathway
C_{60} 0.004 μg/cm^2	Fatty Acid Elongation in Mitochondria ▲ Glycolysis/Gluconeogenesis ▲▼ Mitochondrial Dysfunction ▲ Methane Metabolism ▲ Phenylalanine, Tyrosine and Tryptophan Biosynthesis ▲
C_{60} 0.04 μg/cm^2	No multiprotein pathways
C_{60} 40 μg/cm^2	No multiprotein pathways
SWNT 0.004 μg/cm^2	Glycolysis/Gluconeogenesis ▲ Pentose Phosphate Pathway ▲ Galactose Metabolism ▲ Fructose and Mannose Metabolism ▲ Methane Metabolism ▼
SWNT 0.04 μg/cm^2	Tight Junction Signaling ▲ NRF2-mediated Oxidative Stress Response ▲
SWNT 40 μg/cm^2	Xenobiotic Metabolism Signaling ▼ NRF2-mediated Oxidative Stress Response ▼
MWNT 0.004 μg/cm^2	Glycolysis/Gluconeogenesis ▲ Methane Metabolism ▲ One Carbon Pool by Folate ▲ Glycine, Serine and Threonine Metabolism ▲ Cellular Effects of Sildenafil ▲▼
MWNT 0.04 μg/cm^2	Lysine Degradation ▼
MWNT 40 μg/cm^2	No multiprotein pathways

Arrows indicate whether proteins in those pathways increased ▲ or decreased ▼, or both ▲▼; Shaded areas emphasize pathways common to all three CNPs.

2005, 2008). In contrast, a single oropharyngeal aspiration of SWNT caused no inflammatory response 1 or 21 days post-exposure. However, at 21 days, the investigators did observe small interstitial fibrotic lesions in the alveolar regions, particularly near groups of macrophages containing micron-sized aggregates of the nanotubes (Mangum et al. 2006).

While studies employing high concentrations of CNPs are useful for predicting effects, concentrations above 1 μg/ml are unlikely to occur *in vivo* except during topical exposure of keratinocytes and perhaps in lung epithelia in an industrial setting. Thus, the current studies also explored the effects of very low concentrations of nanoparticles on cellular function and protein expression in renal cells. To our knowledge these are the first studies to comprehensively examine concentrations in the low ng/ml (ng/cm^2) range.

TEER is a measure of monolayer integrity and is also a very sensitive measure of cellular viability. As cellular viability decreases, TEER falls precipitously. In the experiments shown in Figure 5, TEER was significantly decreased after treatment with all concentrations of MWNT from 40 μg/cm^2 down to 0.4 ng/cm^2. Interestingly, after incubation with fullerenes or SWNT, resistances were lowered only by exposure to concentrations below 0.4 μg/cm^2.

It is important to note that none of the changes in TEER reached levels that represent a decrease in cell viability. Control monolayers had an average TEER of 1867 $\Omega \cdot cm^2$. A decrease to values between 750 and 1000 $\Omega \cdot cm^2$ is still considered a high resistance, intact epithelium. The changes in resistance indicate more subtle changes within the cells, and perhaps between them. Examples of cellular alterations which could be manifested in the magnitude of the changes observed would be minor modifications of the cytoskeleton which is a major component in determining the impermeability of the junctional complexes or changes in the composition of the cellular membrane which would be sufficient to alter permeability. We have not tested concentrations below those listed in Figure 5 so cannot yet comment on the lowest concentration that causes this change in transepithelial resistance.

To further investigate nanotube-induced changes in cellular function, the responses to external stimuli were assessed using the method of short circuit current (SCC), a measure of net ion transport. Interestingly, there were no alterations in the cellular response to ADH, a hormone known to regulate both Na^+ and Cl^- in the principal cells. Thus, this cellular function is maintained in the presence of nanoparticle exposure.

The proteomic analyses have highlighted several important aspects of the responses to nanoparticle exposure. The first observation is that, in general, the effects on protein expression correspond to the results of the transepithelial resistance in that they are, interestingly, inversely related to dose. Both the number of altered proteins and the fold-changes increase as dose declines. No one has previously studied carbon nanoparticle doses this low so there are no parallels in the published literature. Size measurements suggest that at high doses where there is significant agglomeration, particles act at a microscale, while at the lower doses, CNPs may act at a nanoscale level where little if any agglomeration is observed.

Second, none of the protein groups reflect a 'traditional' set of toxicity-related proteins. Thus, at least in the mpkCCD$_{cl4}$ cells we are not observing a 'toxic effect' in the classic sense. This finding is in agreement with the lack of cell death in the TEER and LDH measurements and lack of substantial stress responses as measured by cytokine secretion. In fact, stress responses proteins such as those

upregulated by ROS were notably unchanged by CNP exposure.

Third, there is little overlap among the three nanoparticle types in terms of the types of proteins, molecular interaction networks and pathways, suggesting the physico-chemically distinct particles act differently at the biochemical and molecular level, with respect to effects on the proteome. While the nanomaterials decreased TEER in the mpkCCD$_{cl4}$ cells, the protein alterations observed do not provide evidence of mechanism in this regard. There is only one exception where SWNT at 0.04 μg/cm^2 upregulated tight junction signaling proteins (Table VII). However, we have only conducted the cytoskeletal and proliferating nuclei labeling experiments at high concentrations, where the carbon forms can be located for analysis of surrounding cells, while the proteomic changes are observed predominately at the lower concentrations. Therefore additional experimentation will be necessary to fully explain the correlation, if any, between the observed changes in cellular proliferation and actin cytoskeleton structure and the proteomic changes that have been observed.

In general, the proteomic results demonstrate a complex and diverse biological response to CNP exposure, at the lowest concentrations ever studied. Furthermore, as already noted, this response is inversely related to dose, is CNP-specific, and occurs in the absence of overt irritation, inflammation, or toxicity. The inverse relationship between CNP exposure concentration and protein expression is not surprising when considered in the context of particle size. At 40 and 4 μg/cm^2, significant agglomeration is evident while visible particles are absent below that level. Physico-chemical characterization evidence supports this.

When one examines mpkCCD$_{cl4}$ cell proteins whose expression was altered by CNP exposure, the 40 μg/cm^2 had little effect. At $P < 0.01$ one would expect ~ 19 proteins to be altered by chance alone, thus one can conclude this exposure was insignificant relative to protein expression, despite the decline in TEER observed in MWNT. However, at exposures several orders of magnitude lower, CNP-mediated protein expression was significantly greater and these alterations parallel significant declines in TEER. This is likely the result of CNP agglomerants (at 40 μg/cm^2) exerting focal effects that may be significant in those foci, but are rendered largely undetectable when all cells on the transwell are examined. As mentioned earlier, this accounts for focal elevations of PCNA staining, but no significant change overall in PCNA as measured by label-free quantitative mass spectrometry.

As Table IV indicates, the lowest two SWNT exposures studied by proteomics resulted in a decreased expression of six ribosomal proteins. Neither C_{60} nor MWNT exerted such an effect. Ribosomal proteins are integral components of basic cellular machinery involved in protein synthesis and individual ribosomal proteins are known play a role in regulating cell growth, transformation and death (Warner and McIntosh 2009). It has been suggested that both the differentiation state and the proliferative status of the cells affect the expression of ribosomal protein mRNAs (Bevort and Leffers 2000) and both L and S-type ribosomal protein gene expression have been shown to decline in nephrotoxicity (Leussink et al. 2003).

Of the proteins altered by MWNT low-dose exposure, conflicting responses were observed. The four histone family proteins were up-regulated by the 0.004 μg/cm^2 exposure, while the same proteins were significantly down-regulated by the higher 0.04 μg/cm^2 exposure. One of these, H2AFX, is a major component of the nucleosome core structure that comprises 10–15% of total cellular H2A family proteins in mammalian cells, is critical to genomic stability and DNA repair (Fernandez-Capetillo et al. 2004), and play an important role in the regulation of gene expression and cellular proliferation (Svotelis et al. 2009).The conflicting effects of MWNT on these members of the histone H2A family at these exposures are difficult to interpret but they suggest significant MWNT effects on nuclear function of these barrier epithelia.

To aid in interpretation of the complex proteomic results, we used Ingenuity Pathways Analysis. As mentioned above, protein expression was relatively unaffected by the 40 μg/cm^2 exposure and no statistically significant relationships to functional networks were detected.

One of the effects observed in all three CNP exposures only at the 0.004 μg/cm^2 dose was a general up-regulation of glycolysis/gluconeogenesis pathways. As Table VIII indicates, expressions of proteins in this pathway were generally increased. These included enolase 2, enolase 3, and lactate dehydrogenase A (C_{60} exposure); aldolase A, enolase 1, glyceraldehyde-3-phosphate dehydrogenase, glucose phosphate isomerase, lactate dehydrogenase A, phosphofructokinase, phosphoglycerate kinase, phosphoglucomutase, pyruvate kinase and triosephosphate isomerase (SWNT exposure); and aldolase B, enolase 2, enolase 3, phosphoglycerate kinase, phosphoglycerate mutase, and pyruvate kinase (MWNT exposure). The only proteins associated with this pathway that were down-regulated were hexokinase 1 (C_{60} exposure); alcohol dehydrogenase 4 (SWNT exposure);

and glyceraldehyde-3-phosphate dehydrogenase (MWNT exposure).

Gou et al. (2008) reported a dose-dependent adsorption and depletion of nutrients from RPMI cell culture medium by purified SWNTs that contained 10% Fe. HepG2 cells cultured in these depleted media showed significantly reduced viability that was restored by replenishment of folate. However, those effects occurred at doses of 10 μg/ml (corresponding to 25 $\mu g/cm^2$) and above, higher than the doses used in the present study. Alternatively, one can view the increased glycolysis/gluconeogenesis pathway as a generalized response to stress. Systemically, such phenomena are usually manifested in a fight or flight response. However, the stimuli for a more subtle, analogous change at a tissue or molecular level are not well documented.

These altered components of the glycolysis/gluconeogenesis pathway are also reflected in the Functional Networks presented in Table VII. For instance, in low-dose C_{60} exposure, the predominant interaction network affected is a network of gene expression, cell death, and energy production. This network received a significance score of 32 (with 35 being the maximum), the highest in this exposure analysis (thus the proteins have a 1 in 10^{32} probability of having been assigned to this network by chance). The network contains the following differentially expressed (13 up-regulated and four down-regulated) proteins (by gene symbol): acetyl-Coenzyme A acyltransferase 2, ATP synthase, H^+ transporting, mitochondrial F1 complex, alpha subunit 1, ATP synthase, H^+ transporting, mitochondrial F1 complex, beta, ATP synthase, H^+ transporting, mitochondrial F1 complex, O subunit, DEAD (Asp-Glu-Ala-Asp) box polypeptide 5, enolase 2 (gamma, neuronal), enolase 3 (beta, muscle), GTPase activating protein (SH3 domain) binding protein 2, glutathione transferase zeta 1, hexokinase 1, high-mobility group box 2, high-mobility group box 1, hydroxysteroid (17-beta) dehydrogenase 10, lactate dehydrogenase A, microtubule-associated protein, RP/EB family, member 1, phospholipase C, gamma 1, and ubiquitin-conjugating enzyme E2L 3, including members of the glycolysis/gluconeogenesis pathway. This is also observed to an even greater extent in the low-dose SWNT exposure (Table VIII), where Carbohydrate Metabolism is part of the second-rated network (significance score of 20) along with Cancer and Genetic Disorder, and contains the following differentially expressed proteins: acyl-Coenzyme A binding domain containing 3, actin, alpha 1, aldolase A, fructose-bisphosphate, acidic (leucine-rich) nuclear phosphoprotein 32 family, member A, HLA-B associated transcript 1, ELAV (embryonic lethal, abnormal vision, Drosophila)-like 1 (Hu antigen R), enolase 1, (alpha), glyceraldehyde-3-phosphate dehydrogenase, glucose phosphate isomerase, heterogeneous nuclear ribonucleoprotein U (scaffold attachment factor A), lactate dehydrogenase A, myosin, heavy chain 9, non-muscle, nucleoside diphosphate kinase, phosphoglycerate kinase 1, ribosomal protein S5, talin 1, and triosephosphate isomerase 1. Again, glycolytic/gluconeogenic proteins are interacting broadly in this functional network and are implicated in the biological effects of CNPs in this regard. As mentioned earlier, such effects are absent at exposures where agglomeration is evident. The functional networks and pathways impacted by low-dose CNP exposure are thus likely to be nanoscale effects.

Other interaction networks and pathways presented in Tables VII and VIII are established in fundamentally the same manner as that described above. Only the specific protein components differ. For instance, fullerene exposure at 0.004 $\mu g/cm^2$ is associated with a predominant up-regulation in the expression of proteins in cell cycle, gene expression and cell death functional networks. These, and several other functional networks, appear in bold print in Table VII to emphasize the fact that these network components are similarly affected to some degree by all three CNPs studied, at the lowest two doses. Studies of bronchoalveolar cells in mice have demonstrated increased apoptosis and GI arrest after 14 and 28 days of C_{60} instillation (Park et al. 2010). That same study also showed that the expression of the tissue damage-related MMPs, Timp and Slpi gene, and the expression of oxidative stress related SOD gene were increased until day 28 after a single instillation. Protein changes related to cell death have also been reported by SWNT exposures by Cui in HEK293 cells (Cui et al. 2005), along with down-regulated cellular growth and proliferation. These changes were accompanied by a decrease of markers associated with G1 to S transition (e.g., cdk2, cdk4, and cyclin A, E, and D3) as well as markers associated with S, G2, and M phase and down-regulation of expression of adhesion proteins (laminin, fibronectin, cadherin FAK and collagen IV). The relevance of the changes we have observed to those alterations seen by others in various tissues will require additional studies.

Although we have no evidence of oxidative stress, as ROS-related protein alterations are otherwise absent from our data as is any other evidence of cytotoxic effect, the pathway analysis reported in Table VIII suggests the SWNT-mediated up-regulation of NRF-2 mediated oxidative stress response at 0.04 $\mu g/cm^2$ (in contrast to the decrease in this response at 40 $\mu g/cm^2$), is consistent with an overall trend observed in our study, that the CNPs have greater biological effect at lower as opposed to higher exposure levels.

Other pathways impacted by CNP exposure at very low levels include alteration in functional networks involved in inflammatory diseases and regulation of amino acid metabolism. Changes in the expression of components of various metabolic pathways may be particle specific as well as dose- and exposure time-dependent. These aspects require further investigation.

Conclusion

The present study has shown that CNP induced significant alterations in renal collecting duct cell function, and protein expression. At high doses, CNP suspensions cause an increased nuclear proliferation. At low, more physiologically relevant concentrations, the CNPs cause changes in epithelial barrier function as well as changes in protein expression that remain, for the moment, documented but difficult to characterize. The observed changes are subtle, not related to overt toxicity, and likely represent cellular alterations that would have physiological effects over a prolonged time-course.

Declaration of interest: These studies were supported by a grant from NIGMS (R01GM085218), NIEHS (RC2ES018810), and the IUPUI Undergraduate Research Opportunities Program. The authors gratefully acknowledge the technical support of Heather Ringham and Susana Ado Ntim, and sincerely thank Dr Alain Vandewalle (INSERM U478, Paris, France) for providing the $mpkCCD_{cl4}$ cell line. The authors report no conflicts of interest. The authors alone are responsible for the content and writing of the paper.

References

Amos AD, Witzmann FA, Chernoff EA, Hong D, Lai X, Ringham HN, Blazer-Yost BL. 2008. Changes in cell function and protein expression of mouse renal principal cells, mpkCCD, after carbon nanoparticle (CNP) exposure. FASEB J 22:942.

Bens M, Vallet V, Cluzeaud F, Pascual-Letallec L, Kahn A, Rafestin-Oblin ME, Rossier BC, Vandewalle A. 1999. Corticosteroid-dependent sodium transport in a novel immortalized mouse collecting duct principal cell line. J Am Soc Nephrol 10:923–934.

Bevort M, Leffers H. 2000. Down regulation of ribosomal protein mRNAs during neuronal differentiation of human NTERA2 cells. Differentiation 66:81–92.

Bolstad BM, Irizarry RA, Astrand M, Speed TP. 2003. A comparison of normalization methods for high density oligonucleotide array data based on variance and bias. Bioinformatics 19:185–193.

Borm PJ, Robbins D, Haubold S, Kuhlbusch T, Fissan H, Donaldson K, Schins R, Stone V, Kreyling W, Lademann J, Krutmann J, Warheit D, Oberdörster E. 2006. The potential risks of nanomaterials: A review carried out for ECETOC. Part Fibre Toxicol 3:11.

Bradford MM. 1976. A rapid and sensitive method for the quantitation of microgram quantities of protein utilizing the principle of protein-dye binding. Anal Biochem 72: 248–254.

Chen Z, Meng H, Xing G, Chen C, Zhao Y, Jia G, Wang T, Yuan H, Ye C, Zhao F. 2006. Acute toxicological effects of copper nanoparticles in vivo. Toxicol Lett 163:109–120.

Craig R, Beavis RC. 2004. TANDEM: Matching proteins with tandem mass spectra. Bioinformatics 20:1466–1467.

Cui DX, Tian FR, Ozkan CS, Wang M, Gao HJ. 2005. Effect of single wall carbon nanotubes on human HEK293 cells. Toxicol Lett 155:73–85.

Donaldson K, Aitken R, Tran L, Stone V, Duffin R, Forrest G, Alexander A. 2006. Carbon nanotubes: A review of their properties in relation to pulmonary toxicology and workplace safety. Toxicol Sci 92:5–22.

Eng JK, McCormack AL, Yates JR, 3rd. 1994. An approach to correlate tandem mass spectral data of peptides with amino acid sequences in protein database. J Am Soc Mass Spectrom 5: 976–989.

Fernandez-Capetillo O, Lee A, Nussenzweig M, Nussenzweig A. 2004. H2AX: The histone guardian of the genome. DNA Repair 3:959–967.

Guo L, Von Dem Bussche A, Buechner M, Yan A, Kane AB, Hurt RH. 2008. Adsorption of essential micronutrients by carbon nanotubes and the implications for nanotoxicity testing. Small 4:721–727.

Gupta AK, Gupta M. 2005. Cytotoxicity suppression and cellular uptake enhancement of surface modified magnetic nanoparticles. Biomaterials 26:1565–1573.

Hale JE, Butler JP, Gelfanova V, You JS, Knierman MD. 2004. A simplified procedure for the reduction and alkylation of cysteine residues in proteins prior to proteolytic digestion and mass spectral analysis. Anal Biochem 333:174–181.

Higgs RE, Knierman MD, Gelfanova V, Butler JP, Hale JE. 2005. Comprehensive label-free method for the relative quantification of proteins from biological samples. J Proteome Res 4:1442–1450.

Higgs RE, Knierman MD, Gelfanova V, Butler JP, Hale JE. 2008. Label-free LC-MS method for the identification of biomarkers. Methods Mol Biol 428:209–230.

Jia G, Wang H, Yan L, Wang X, Pei R, Yan T, Zhao Y, Guo X. 2005. Cytotoxicity of carbon nanomaterials: Single-wall nanotube, multi-wall nanotube, and fullerene. Environ Sci Technol 39:1378–1383.

Kane AB, Hurt RH. 2008. Nanotoxicology: The asbestos analogy revisited. Nat Nanotechnol 3:378–379.

Lacerda L, Herrero MA, Venner K, Bianco A, Prato M, Kostarelos K. 2008. Carbon-nanotube shape and individualization critical for renal excretion. Small 4:1130–1132.

Lam CW, James JT, McCluskey R, Arepalli S, Hunter RL. 2006. A review of carbon nanotube toxicity and assessment of potential occupational and environmental health risks. Crit Rev Toxicol 36:189–217.

Leussink BT, Baelde HJ, den Berg TMB-v, de Heer E, van der Voet GB, Slikkerveer A, Bruijn JA, de Wolff FA. 2003. Renal epithelial gene expression profile and bismuth-induced resistance against cisplatin nephrotoxicity. Human Experim Toxicol 22:535–540.

Mangum JB, Turpin EA, Antao-Menezes A, Cesta MF, Bermudez E, Bonner JC. 2006. Single-Walled Carbon Nanotube (SWCNT)-induced interstitial fibrosis in the lungs of rats is associated with increased levels of PDGF mRNA and the

formation of unique intercellular carbon structures that bridge alveolar macrophages in situ. Part Fibre Toxicol 3:15.

Maynard AD, Baron PA, Foley M, Shvedova AA, Kisin ER, Castranova V. 2004. Exposure to carbon nanotube material: Aerosol release during the handling of unrefined single-walled carbon nanotube material. J Toxicol Environ Health A 67: 87–107.

Muller J, Decordier I, Hoet PH, Lombaert N, Thomassen L, Huaux F, Lison D, Kirsch-Volders M. 2008. Clastogenic and aneugenic effects of multi-wall carbon nanotubes in epithelial cells. Carcinogenesis 29:427–433.

Muller J, Huaux F, Moreau N, Misson P, Heilier J-F, Delos M, Arras M, Fonseca A, Nagy JB, Lison D. 2005. Respiratory toxicity of multi-wall carbon nanotubes. Toxicol Appl Pharmacol 207:221–231.

Murr LE, Garza KM, Soto KF, Carrasco A, Powell TG, Ramirez DA, Guerrero PA, Lopez DA, Venzor J 3rd. 2005. Cytotoxicity assessment of some carbon nanotubes and related carbon nanoparticle aggregates and the implications for anthropogenic carbon nanotube aggregates in the environment. Int J Environ Res Public Health 2:31–42.

Park E-J, Kim H, Kim Y, Yi J, Choi K, Park K. 2010. Carbon fullerenes (C60s) can induce inflammatory responses in the lung of mice. Toxicol Applied Pharmacol 244: 226–233.

Park KH, Chhowalla M, Iqbal Z, Sesti F. 2003. Single-walled carbon nanotubes are a new class of ion channel blockers. J Biol Chem 278:50212–50216.

Poland CA, Duffin R, Kinloch I, Maynard A, Wallace WAH, Seaton A, Stone V, Brown S, MacNee W, Donaldson K. 2008. Carbon nanotubes introduced into the abdominal cavity of mice show asbestos-like pathogenicity in a pilot study. Nat Nano 3:423–428.

Reijnders L. 2006. Cleaner nanotechnology and hazard reduction of manufactured nanoparticles. J Cleaner Product 14:124–133.

Shane MA, Nofziger C, Blazer-Yost BL. 2006. Hormonal regulation of the epithelial Na+ channel: From amphibians to mammals. Gen Comp Endocrinol 147:85–92.

Svotelis A, Gevry N, Gaudreau L. 2009. Regulation of gene expression and cellular proliferation by histone H2A.Z. Biochem Cell Biol 87:179–188.

Wang M, You J, Bemis KG, Tegeler TJ, Brown DPG. 2008. Label-free mass spectrometry-based protein quantification technologies in proteomic analysis. Brief Funct Genomic Proteomic 7:329–339.

Warner JR, McIntosh KB. 2009. How common are extraribosomal functions of ribosomal proteins? Molec Cell 34:3–11.

Witzmann FA, Monteiro-Riviere NA. 2006. Multi-walled carbon nanotube exposure alters protein expression in human keratinocytes. Nanomedicine 2:158–168.

Supplementary material available online

Complete list of the detected proteins and their pertinent information.

CHAPTER 1. INTRODUCTION

1.1. Nanotechnology and Implications

The nanotechnology industry has considerable economic potential today as well as in future markets. Nanotechnology aims at fabrication of materials on the nanometer scale (<100 nm) that exhibit specific inherent unique structural and functional properties. These peculiar properties are a result of their nanoscale sizes that imparts them with greater surface area per unit mass. Benefits afforded by these novel entities called nanoparticles (NP) are significant in fields such as plastics, energy, electronics, aerospace, cosmetics and agriculture. In the biomedical area, engineered NP are being explored for molecular imaging, *in vitro* cell markers, contrast agents, biochemical sensors and drug delivery [1]. Apart from the unique physico-chemical properties, NPs exhibit ability to interact with the biological environment by redistributing, agglomerating, or self-functionalizing with biological macromolecules [2].

Potential occupational and environmental exposures due to manufacturing, usage, spillage, industrial waste management and recycling are the consequences that call for attention toward biological effects of these particles. NPs may be an emerging kind of environmental contaminant. In occupational settings, these NPs may be released into the surroundings in aerosol form. Due to their increased specific surface area, nanoparticles may present an increased hazard and risk to the health of humans and animals. Typically, biological reactivity increases with decrease in particle size [3] [4]. It has been suggested that nanoparticles less than 100 nm in diameter can enter the cells, those with diameter below 40 nm can enter the nucleus and those smaller than 35 nm can pass through the blood-brain barrier [5]. Oberdorster *et al.* [6] demonstrated the translocation of ultrafine particles to brain following inhalation, possibly reflecting translocation across the blood-brain barrier. CNPs have shown to bind to and aggregate the DNA during replication and to inhibit bacterial growth [7].

The flooding of the market with nanotechnology fabricated products without adequate assessment of potential adverse biological effects should be regarded as a serious violation of risk management practices. It is projected that the production of nanoparticles will increase from the estimated 2,300 tons produced in the year 2008 to 58,000 tons by the year 2020 (http://www.raeng.org/uk/policy/reports/nanoscience.htm) [8]. The increase in nanoparticle containing products that include some manufactured by leading brands (http://www.foe.org/camps/comm/nanotech/) and constant discovery of new applications of

nanoparticles, has made it very important to be aware of health effects of nanoparticle exposure.

Certain workplace conditions generate nanoparticles that can reach exposure concentrations of up to several hundred micrograms per cubic meter [9]. They deposit in the lungs [10], are translocated to the bloodstream [11], reach the gastrointestinal tract [12], follow dermal routes [13], reach central nervous system [6] and accumulate in kidney [14]. Looking at the nanoparticle production expansion, the bio-accumulation and potential bio-toxicity of nanoparticles, the analysis of these particles requires updated experimentation.

1.2. Carbon Nanoparticles

Carbon nanoparticles (CNP) are important components of the rapidly expanding nanotechnology field. CNPs are materials composed mainly of carbon; with one or more dimensions of 100 nm or less. Like other nanoparticles, due to their size, and unique physicochemical properties (light weight, high tensile strength, thermal/chemical stability and conductivity), they have found widespread application in biomedical, electronics, computer, aerospace, agriculture, pharmaceutical and other industries. The discovery of fullerenes in 1985 and of carbon nanotubes in 1991 opened a wide field of activity in nanocarbon research [15]. The three most widely used and well developed carbon nanoparticles are **fullerenes (C_{60}), single walled nanotubes (SWNT) and multi walled nanotubes (MWNT)** [16].

1.2.1. Fullerenes

Fullerenes (C_{60}), also called Buckyballs or Buckminsterfullerenes consist of 60 carbon atoms arranged symmetrically to yield a characteristic cage like structure with an average diameter of 0.72 nm (Figure 1c). Fullerenes occur naturally around us as a release from fuel combustion, volcanic eruptions and forest fires. Recently, due to industrial manufacturing of these particles and the particles produced as byproducts of various industrial manufacturing, there has been a tremendous increase in the amount of fullerenes in the environment and manufacturing sites.

Many studies have shown the adverse effects of fullerenes. For example, oxidative stress and depletion of glutathione following exposure to fullerenes in juvenile largemouth bass causing lipid peroxidation in brain has been observed [17]. Maternal intravenous injection of fullerenes in rats passes to the fetuses and if intraperitonealy injected results in death and morphological abnormalities in mouse embryos. Fullerenes also inhibited the differentiation of mouse midbrain cells [18]. C_{60} instillation induces an increase in G1 arrest in BAL (bronchoalveolar lavage) cells. This increase was also accompanied by secretion of cytokines

such as IL-1 (interleukin-1), TNF-α (tumor necrosis factor-alpha), and IL-6 (interleukin-6), Th1 (T-helper cells, type 1), IL-12 (interleukin-12) and IFN-r (interferon-r) in BAL fluid [19]. Recently, it was shown that fullerenes may act as blockers or modulators of a variety of K^+ channels and thus effectively hinder the function of K^+ channels and hence induce toxicity [20]. Further assessment of all of these potentially adverse effects on human and animal health thus becomes a matter of utmost importance.

1.2.2. Single Walled Nanotubes (SWNTs)

SWNTs can be visualized as rolled graphene sheets forming seamless cylinders with diameters in the nanometer range (Figure 1a). Carbon nanotubes (CNTs) have been brought under scrutiny due to their thin fiber like structures. Intraperitoneal administration of SWNTs, irrespective of their length or dose (50-1000 mg/kg b.w.) can form fiber like structures inside the body. It has been shown that aggregates persisted inside Swiss mice cells for up to 5 months after administration [21]. Following the lung instillation of rats with SWNTs, a series of multifocal granulomas, which were evidence of a foreign tissue body reaction, were observed by Warheit *et al.* [22]. In a separate study, the lungs of some animals instilled with SWNTs also revealed peribronchial inflammation and necrosis that extended into the alveolar septa [23]. In yet another study, an early inflammatory response with oxidative stress developed into multifocal granulomatous pneumonia and interstitial fibrosis after SWNT inhalation for 4 days [24]. In a lung fibroblast cell line exposed to SWNT, cytotoxicity tests showed loss of viability in a concentration and time dependent manner following induction of DNA damage [25]. Alteration of gene regulation induced by SWNT exposure was found in human embryonic kidney (HEK) cells [26]. SWNTs have also been shown to induce platelet activation *in vitro* and exert prothrombotic effects in the microcirculation *in vivo* [27].

1.2.3. Multi Walled Nanotubes (MWNTs)

These are synthetic carbon nanotubes comprised of many concentric graphite cylinders or SWNTs with a nanoscale diameter (Figure 1b). Due to their unique structure and size, they are highly desirable for use within the commercial, environmental and medical sectors. Because of their structural similarity to asbestos fibers, MWNTs are of special interest [28].

Exposure to MWNTs produced pulmonary inflammation and fibrosis in epithelial cells of Wistar rats [29]. Exposure to MWNTs in mice lungs by oropharyngeal aspiration lead to elevation of total cells and the number of polymorphonuclear leukocytes in BAL cells. BAL fluids showed significantly increased levels of total proteins, LDH (lactate dehydrogenase), TNFα, IL-1β, mucin, and surfactant protein-D and thus inducing cytotoxic and inflammatory response in the lungs of mice [30].

Cellular studies support the *in vivo* results. After media exposure, MWNT were found to be present within cytoplasmic vacuoles of HEK cells. The release of the proinflammatory cytokine, IL-8, was also observed in these cells [31]. Rat lung epithelial cells exposed to MWNTs lead to a dose- and time-dependent increase in the formation of free radicals, the accumulation of peroxidative products, the loss of cell viability, increase in the activity of caspases-3 and caspase-8 in cells and antioxidant depletion indicating apoptosis of the cells [32]. Toxicity of three doses (40, 200, 400 μg/mL) of MWNT was observed to cause massive loss of cell viability through DNA damage and programmed cell-death compared to control in normal human dermal fibroblast cells [33]. MWNTs have been shown to alter expression of genes for cellular transport, metabolism, cell cycle regulation, and stress responses [34].

1.3. Inhalation and Lung Effects

In addition to the experiments described above, numerous studies have associated ultrafine particles, comparable to nanoparticles, with lung inflammatory diseases [35] [36] [37]. Due to fiber like structures of CNTs, they have been compared to asbestos, raising alarming concerns that increasing use of CNTs may lead to mesothelioma, cancer of the lining of the lungs just like exposure to asbestos. Inflammation and the formation of lesions known as granulomas after exposing the mesothelial lining of the body cavity of mice to MWNTs correlates with asbestos-like, pathogenic behavior [28]. Since the lung cells produce surface mucoprotein, the nanoparticles may get trapped on the apical surface facilitating the destructive contact between the nanoparticle and the cell.

1.4. Kidney Effects after Translocation from Organs of Direct Exposure

Not only do nanoparticles affect lungs, but they are transported via blood to different organs such as liver, spleen, kidney and brain [37] [38] [39] [40] [41] [42]. Due to its waste management function in the body that involves concentration and excretion of toxins, the kidney is particularly susceptible to substances foreign to biological systems. Many studies have looked into the cellular effects of nanoparticles in renal cell lines. Alteration of gene regulation induced by SWNT exposure was found in HEK293 cells. [26]. In a separate study, MWNT-induced cytotoxicity using same cells was demonstrated by Reddy *et al*. Some of the effects seen were decreased cell viability and cell membrane damage in a concentration dependent manner, increased production of IL-8, increased TBARS (Thiobarbituric Acid Reactive Substances Assay), and decreased intracellular glutathione levels [43].

In addition to the cellular studies, *in vivo* studies have also indicated nanoparticles induced renal damage. For example, Wang *et al.* [44] demonstrated that TiO_2 nanoparticles induce protein in urine in the renal tubule and swelling in the renal glomerulus in female mice.

Protein in urine is an indicator of compromise of the glomerular filtration apparatus and/or in the barrier function of epithelial cells of the tubule. Bio-distribution studies also confirmed presence of nanoparticles in kidney after intravenous administration [45] [46]. In a separate study, the histology of post instilled MWNT in rats indicated that the particles reached the kidney and caused tubular necrosis and interstitial nephritis, the toxicity of which was further confirmed by the elevated levels of tissue damage biomarkers [47]. Thus, there is clear evidence of translocation of the nanoparticles to the kidney and the damage caused by them.

1.5. Hypothesis

We hypothesized that as-manufactured and non-functionalized carbon nanoparticles (CNPs), when exposed to barrier epithelia (lung and kidney), exert a biological effect that alters the cell function. Therefore, the ion transport and barrier functions that are characteristic of these cells may be altered.

1.6. Experimental Approach

An *in vitro* approach using cultured epithelial cell lines has been adopted for this study. Well characterized cell lines are excellent model systems that can be easily controlled and manipulated. In general, whole organ systems are quite complex and involve the interaction of several cell types. The final effect on the whole organ shows up after the damage to the cells has already been done. Therefore, whole organ or organ system studies can miss the subtle toxic or sub toxic cellular changes that add up to bigger pathological problems over time. The effects of CNPs on cellular viability, function, cellular uptake, and subcellular localization as well as mechanistic studies can best be tested in a cellular environment that is highly controlled. Once characterized, individual cell lines can be used to study the effects of CNPs in the context of all the functions exhibited by the cell line. For example, in the current experiments the effect of CNP exposure on the barrier function of high resistance epithelia has been studied in well characterized individual cell lines. In addition, various cell lines respond to hormonal stimuli with ion transport responses that mimic their counterparts *in vivo* and can be used to examine sub-toxic but important changes in normal cell functions after nanoparticle exposure.

1.6.1. Renal Cell Line (mpkCCD$_{cl4}$)

The mpkCCD$_{cl4}$ (mouse principal kidney cortical collecting duct, clone 4) cell line, isolated by Vandewalle, exhibits all the hormonal regulation associated with distal portion of cortical collecting duct of the kidney [48]. These cells form confluent monolayers on permeable supports

and develop high transepithelial resistances (≥1000 $\Omega.cm^2$). After forming a confluent monolayer, the cell line responds to hormones regulating ion transport in kidney, a function that is key to the renal regulation of electrolyte and fluid homeostasis in the body. The line responds to aldosterone, ADH (anti-diuretic hormone) and insulin [48] [49]. In response to ADH, there is a cAMP mediated increase in Cl^- secretion via CFTR (cystic fibrosis transmembrane regulator) and Na^+ absorption via ENaC (epithelial Na^+ channel) [49]. We have chosen to study the effects of ADH because this peptide hormone elicits a multi-phasic response consisting of both Cl^- secretion via CFTR and Na^+ absorption via ENaC.

1.6.2. Airway Cell Line (Calu-3)

The Calu-3 cell line is a human airway serous epithelial cell line that has all of the important features of ion transport of respiratory epithelium [50]. Calu-3 cells form sheets of cells held by tight junctions. These sheets form a fully functional epithelium that can transport ions and fluid. In addition, permeability data for small lipophilic molecules across Calu-3 monolayers suggested that the cell line is a suitable model to examine the transport of low molecular weight substances and xenobiotics [50]. Calu-3 cells form tight monolayers and give appreciable transepithelial electrical resistance (TEER) values in culture when grown under air-interface culture (AIC) conditions (Figure 2). Calu-3 cells have the highest level of natural CFTR expression of any known immortalized cell, even higher than some intestinal cell lines that once held the record (www.cfri.org/news/94fall/res294f.html). The cell line responds to hormones such as epinephrine and mediators such as isoproterenol, bradykinin, methacholine and histamine with an increase in transepithelial Cl^- secretion via apically located CFTR channel [51]. The Na^+ inhibitor amiloride failed to show the presence of ENaC in these cells [52].

1.7. Aim of the study

The current studies examine the effect of carbon nanoparticles on the function of the renal ($mpkCCD_{cl4}$) and airway (Calu-3) epithelial cells. Both these cell lines form confluent monolayers that simulate the barrier epithelial function and hormonal responsiveness found *in vivo* in renal distal tubules and collecting ducts [48] and airways [50] [53] respectively.

The importance of examining effects of physiologically relevant concentrations of CNPs, is underscored by the consequences of altered functionality of these cell types. Compromised barrier integrity of the epithelium in kidney can offset the equilibrium between the filtrate and interstitium and can have serious pathological consequences from inability to maintain salt and fluid homeostasis to renal failure. Changes in the hormonal responses of these cells can change the salt homeostasis resulting in changes in blood pressure. On the other hand, similar situations in airways can be serious too. Changes in barrier function are likely to have

physiological effects that can cause or exaggerate respiratory problems. Diminished hormonal responses may lead to the cystic fibrosis like condition of dehydrated airways with the inability to clear the passageways of inhaled foreign substances.

Experiments were conducted to determine the functional, structural and proteomic changes induced by CNP exposure on these barrier epithelial cells.

CHAPTER 2. MATERIALS AND METHODS

2.1. Materials

Dulbecco's minimal essential media (DMEM/F-12), glutamax, penicillin, streptomycin, sodium pyruvate (100 X), non-essential amino-acids (100 X) were purchased from Invitrogen (Carlsbad, CA). Fetal bovine serum was from Gemini Bioproducts, (West Sacramento, CA). Cell culture flasks, six well polystyrene plates and transwell cell culture plates (24 mm inserts, polycarbonate, 0.4 μm pore size) were obtained from Costar-Corning (Acton, MA). Cell Culture reagents including 10 X trypsin-EDTA solution (0.5 %), Hanks balanced salt solution (HBSS) and ciprofloxacin was obtained from Mediatech, Inc, (Herndon, VA). Transferrin, sodium selenite, triiodothyronine, rhodamine-phalloidin and mouse monoclonal PCNA (proliferating cell nuclear antigen) antibody were obtained from Sigma (St.Louis, MO). Goat anti-mouse Alexa fluor red 594 secondary antibody was obtained from Invitrogen-Molecular Probes (Eugene, OR).

NPPB (5-Nitro-2-(3-phenylpropylamino)-benzoic acid) and BAPTA-AM [1,2-*Bis*(2-aminophenoxy)ethane-*N*,*N*,*N*,*N*'-tetraacetic acid tetrakis(acetoxymethyl ester)] was obtained from Enzo Lifesciences (Plymouth, PA), ionomycin from Ascent Scientific (Princeton, NJ), CFTR inh 172 from Calbiochem (San Diego, CA) and tannic acid from Sigma Aldrich (St.Louis, MO).

2.2. CNP Preparation

CNPs were purchased from SES Research (Houston, TX) and used as supplied. As reported by the manufacturer, C_{60} (#600-9980) was 99.95+ %, ultra-pure and vacuum oven-dried; SWNT (#900-1301) (long) were purified singlewall nanotubes with an outer diameter <2 nm, length ranging from 5-15 μm, purity >90 % CNT (>50 % SWNT), ash <2 % wt and amorphous carbon <5 % wt; and purified MWNT (# 900-1203) with an outer diameter of 40-60 nm, length ranging from 5-15 μm, >95 % nanotubes vs amorphous carbon (<2 %), and ash content <0.2 %.

SWNT, MWNT, and C_{60} were prepared in fetal bovine serum at a concentration of 5 mg/mL. Serum acts as a surfactant to disperse hydrophobic nanoparticles via destabilization of the aggregates by serum proteins [54]. At low nanomaterial concentrations, the presence of proteins in cell culture media has been reported to generate small agglomerates of particles with small amount of size variations and improved the stability of the dispersions [55]. Samples were sonicated using a Branson Sonifier 450 at a duty cycle of 30 % and an output control of 3

for 20 seconds. Before sonication of each sample, the probe was cleaned with ethanol and coated for 10 seconds with serum. After sonication, the samples were autoclaved and diluted to a final concentration of nanoparticles in the media. Additional CNP-free FBS was added to a final concentration of 2 % and 15 % FBS-CNP in media for mpkCCD$_{cl4}$ and Calu-3 respectively. Control fetal bovine serum without nanoparticles was treated in an identical manner. The amount of CNP was regulated so as to obtain a desired final concentration of CNP in media when normal concentration of FBS was added to it. Since Calu-3 cells require 15 % of FBS in the culture media, only 2 % of the FBS was autoclaved with CNPs and the rest of the 13 % was added as such. On the other hand, mpkCCD$_{cl4}$ cells require only 2 % of FBS in the culture media so no additional FBS was added. The nanoparticles were added to the apical side of the cells after they developed a high resistance phenotype. Only 200 µl of CNP containing media was added to the apical side (5 cm^2) of Calu-3 cells to maintain the air liquid interface (Figure 2) of the cells.

The nanoparticle concentrations are shown as g/cm^2 to more accurately reflect the actual exposures. However all volumes were maintained in constant proportions so that the surface exposure can be converted into concentration per volume of media using the following formula: N g/cm^2 = 2.5N g/mL for mpkCCD$_{cl4}$ and N g/cm^2 = 25N g/mL for Calu-3 cells

2.3. Cell Culture

The mpkCCD$_{cl4}$ cell line was a gift from Alain Vandewalle (Inserm, Paris) and Calu-3 (ATCC no. HTB-55) cell line was purchased from ATCC (Manassas, VA) and started with passage 19. Cells were cultured in 75 cm^2 tissue culture flask using 10 ml and 15 ml (recommended by ATCC) of media for the respective cell line and were grown in humidified atmosphere of 5 % CO_2-95 % air at 37 °C. Both cell culture media were comprised of DMEM/F-12 (1:1) with 2.40 mg/L $NaHCO_3$ and 1 mM Glutamax. The media for mpkCCD$_{cl4}$ was supplemented with 2 % fetal bovine serum, 25,000 U/L penicillin, 25 g/L streptomycin, 12 mg/L ciprofloxacin, 5 mg/L transferrin, 20 µg/L sodium selenite, and 10^{-7} M triiodothyronine. The media for Calu-3 was supplemented with 15 % FBS, 100,000 U/L penicillin, 100 g/L streptomycin, 0.5 mM non-essential amino acids and 0.5 mM sodium pyruvate.

The media were replaced thrice a week and cells were passaged weekly at a split ratio of 1:10 and 1:4 for mpkCCD$_{cl4}$ and Calu-3 cell lines, respectively. For electrophysiology, the cells were seeded directly on the permeable filters of the transwell cell culture plates with media on the apical and basolateral sides. Two days after inoculation of the Calu-3 cells, the media was removed from the apical side and was replaced only on the basolateral side (AIC, Figure 2). The mpkCCD$_{cl4}$ cells were maintained with a usual 2 ml of media on the apical side of the transwell cultures. Cells grown as monolayers were used on 14th day after being seeded on the transwells, the time at which the cells show a high resistance phenotype.

2.4. Electrophysiology

Electrophysiological techniques (Figure 3) were used to monitor TEER as well as to observe changes in ion flux across the cellular monolayers in response to hormonal stimulation. Cells were grown to confluency on the transwell filters and exposed to CNPs for the times indicated in the figures. At the end of the incubation period, the filters were cut from the plastic inserts, mounted in a Ussing chamber that separates the apical (luminal) surface from basolateral. The Ussing chamber was connected to a DVC-1000 Voltage/Current Clamp (World Precision Instruments) with voltage and current electrodes on either side of the membrane. The spontaneous transepithelial potential difference was clamped to zero, and the resultant short-circuit current (SCC) was monitored continuously. SCC is a measure of net transepithelial ion flux. Typically, an increase in SCC is either due to cation absorption (apical to serosal transport) or anion secretion (serosal to apical transport). The cells were bathed in serum-free medium maintained at 37 °C via water-jacketed buffer chambers on either side of the filter. Medium was circulated and kept at constant pH using a 5 % CO_2 / 95 % O_2 gas lift. A voltage pulse of 2 mV was applied every 200 s and the resulting current displacement was used to determine TEER by using Ohm's law. After the basal current stabilized (time=0), hormones, ADH (100 µU/ml) and epinephrine (10^{-6} M) were added to the serosal bathing medium. Addition of inhibitors, amiloride (10^{-5} M) and NPPB, (100 µM) to the apical bathing medium were used to inhibit Na^+ or Cl^- secretion respectively. A 10 min pretreatment with CFTR inh 172 (100 µM) or tannic acid (100 µM) were used to inhibit the CFTR and calcium activated Cl^- channels (CaCCs) respectively.

2.5. Immunohistochemistry

For immunohistochemistry, cells were grown on polystyrene six well plates. After the cells formed confluent monolayers, they were washed with HBSS, fixed in 4 % paraformaldehyde, and permeabilized with 0.1 % triton X-100 in DI water. After rinsing with 4-(2-hydroxyethyl)-1-piperazineethanesulfonic acid (HEPES) buffer, cells were treated for 8 minutes with hot citric acid buffer, washed with HEPES and blocked with normal goat serum diluted [1:10] in blocking buffer (NGSBB; 0.75 g blocking reagent / 150 mL 1 X tris buffered saline with tween-20 (TBST)) for two hours at room temperature. Cells were then treated with mouse monoclonal PCNA antibody in NGSBB (1:3000) overnight at 4 °C. After washing with HEPES buffer, goat anti-mouse Alexafluor Red 594 secondary antibody in blocking buffer (1:1000) was added to the cells for 2 h at room temperature. The cells were washed again with HEPES buffer and treated with DAPI (4',6-diamidino-2-phenylindole). Cells were visualized using a Nikon Eclipse TE2000-U microscope fitted with a Nikon digital camera (DXM1200F).

For actin staining, the cells were grown till confluent on polystyrene six well plates, treated with rhodamine-phalloidin in HBSS (1:200) for 15 minutes, washed, and exposed to

DAPI. Cells were visualized using a Nikon Eclipse TE2000-U microscope fitted with a Nikon digital camera (DXM1200F).

2.6. Cytokine Assay

Mouse inflammation ELISA strip for profiling 8 cytokines kit (Signosis, Sunnyvale CA) was used for determining eight cytokines; IL-1a (interleukin-1a), IL-1b (interleukin-1b), G-CSF (granulocyte-colony stimulating factor), GM-CSF (granulocyte macrophage-colony stimulating factor), MCP-1 (monocyte chemotactic protein-1), MIP-1a (macrophage inflammatory protein-1 alpha), SCF (stem cell factor), and RANTES (regulated on activation, normal T expressed and secreted) in the apical and basolateral media from mpkCCD_{cl4} cell cultures.

Human inflammation ELISA strip for profiling 8 cytokines kit (Signosis, Sunnyvale CA) was used for determining eight cytokines: TNF-α, IFNr, G-CSF, GM-CSF, IL-1a, IL-8, IP-10 (Interferon inducible protein 10), and RANTES in the apical and basolateral media from Calu-3 cell cultures. The assay was done in triplicate according to the given protocol. Due to the large surface area of the nanoparticles, they have the ability to adsorb a wide variety of small organic solutes, indicator dyes or their reduction products [56]. Since this is a colorimetric assay, therefore, we carried out controls for this assay with addition of nanoparticles at the time of the assay.

2.7. Lactate Dehdrogenase (LDH) assay

LDH is an enzyme found in the cell cytoplasm. Decreases in cellular viability cause leakiness in the plasma membrane and therefore, release of LDH into the culture medium.

Media was collected from both apical and basolateral sides of exposed cells grown for electrophysiological studies and assayed for LDH. The LDH assay was performed using Promega CytoTox 96 non-radioactive cytotoxicity assay kit (Promega, Madison, WI) [57] [58] [59]. To avoid misinterpretations due to adsorption of the LDH protein on the particle surface, the cell supernatant was centrifuged to remove particle adsorbed proteins along with cell debris [60]. This is a colorimetric assay that quantitatively measures LDH, a stable cytosolic enzyme released upon cell lysis. The released LDH oxidizes lactate to pyruvate which promotes conversion of tetrazolium salt INT to formazan, a water soluble molecule with absorbance at 490 nm. The amount of LDH released is proportional to the number of cells damaged or lysed.

2.8. Scanning Electron Microscopy (SEM) and Energy Dispersive X-ray Spectroscopy (EDS)

Cell culture media containing all the three nanoparticles was sent to Dr Somenath Mitra, NJIT, NJ (New Jersey Institute of Technology, New Jersey) for SEM and EDS. In SEM, the sample is exposed to a very high energy electron beam. The electrons interact with the sample at the atomic level and provides signals of the sample surface topography. EDS relies on interaction of electromagnetic radiations with matter to analyze the elemental composition of a sample. The sample is exposed to charged particles in response to which it emits X-rays that are characteristic of the elements present in the sample.

SEM and EDS data were collected on a LEO 1530 VP Scanning Electron Microscope equipped with an energy-dispersive X-ray analyzer. A few drops of SWNT and MWNT dispersions in cell culture media were placed on silicon wafers and allowed to air-dry. The silicon wafers were then mounted on aluminum stubs for SEM and EDS analysis.

2.9. Dielectric Spectroscopy of Carbon Nanotubes in Media

The samples, the culture medium blank and CNPs dispersed in the medium at two different concentrations, (0.004 and 0.04 $\mu g/cm^2$) were collected for dielectric spectroscopy and sent to Dr Somenath Mitra, NJIT, NJ for the analysis. Dielectric spectroscopy measures the conductivity of the medium as a function of frequency, where frequency represents an external electric field and conductivity represents the dipole moment of the sample. Dielectric spectroscopy was carried out with a Novacontrol BDS-80 broadband dielectric spectrometer, using a liquid sample cell with the size of 11.04 X 6.6mm (diameter X thickness). The bias voltage was set at 1 volt, and the dielectric spectra were collected at room temperature in the frequency range 1-105 Hz. normalized, and compared for relative abundance. Significant differences in protein expression across dose groups were determined by analysis of variance (ANOVA). To eliminate technical bias, randomization of order of measurement and ‘quantile normalization’ was used [61] and data normalized using a log2 scale.

2.10. Atomic Force Microscopy (AFM)

The cells were seeded onto six well permeable supports and allowed to reach confluency. After confluency, the cells were exposed to the nanoparticles. The media was removed and frozen plates were sent to Dr Somenath Mitra, NJIT, NJ for the analysis. AFM measures the forces acting between a fine tip attached to a cantilever and the sample when the tip is brought close to the sample. Morphology of these surfaces was evaluated with tapping-mode AFM using a Digital Instrument Nanoscope II. In tapping mode AFM, the cantilever with

the fine tip is oscillated at its resonance frequency and decrease in the amplitude by various types of interactions in the sample is measured when the tip is brought closer to the sample.

2.11. Analysis of Particle Size and Zeta Potential of Nanoparticles in Media

Cell culture media containing SWNTs and MWNTs were analyzed by using a Zetasizer nano ZS90 (Malvern Instruments Ltd.). To mimic the normal cellular incubation conditions, the nanoparticle-containing media were prepared in the usual manner, incubated at 37 °C and measured after 1, 24, 48 hours. In this technique, particle size is the diameter of the sphere that diffuses at the same speed as the particle being measured [62] [63] [64]. The zetasizer system determines the size by first measuring the Brownian motion of the particles in a sample using dynamic light scattering (DLS) and then interpreting a size from this using established theories [65].

Since smaller particles move rapidly in a liquid than larger particles, the position of two images of the sample separated by a short interval of time is used to determine the displacement of the particle and therefore its relative size. A minimal displacement with similar particle positions indicate that the particles in the sample are large whereas larger displacements with different particle positions indicate that the particles in the sample are small. Using this principle and the relationship between diffusion speed and size, the relative sizes can be determined.

A potential that exists between the particle surface and the liquid in which it is dispersed and varies according to the distance from the particle surface is called the zeta potential. Zeta potential is measured using a combination of the measurement techniques: electrophoresis and laser doppler velocimetry, sometimes called laser doppler electrophoresis. This method measures how fast a particle moves in a liquid when an electrical field is applied i.e. its velocity. Once the velocity of the particle is determined and the electrical field applied, one can, by using two other known constants of the sample-viscosity and dielectric constant, determine the zeta potential.

2.12. Proteomics

The cells were grown in triplicate. While one of the triplicates was used for electrophysiology, the other two were sent to Dr Frank Witzmann, IUSM, IN (Indiana University School of Medicine, Indiana) for proteomic analysis.

mpkCCD$_{cl4}$ cell line: For mpkCCD$_{cl4}$ cells, this analysis was performed after 48 h exposures for all the three CNPs at three different concentrations-40, 0.4 and 0.004 μg/cm^2.

Cultured cell proteins were extracted using a lysis buffer containing 8 M urea and 10 mM dithiothreitol (DTT) and protein concentrations were determined by Bradford assay. The same lysis buffer was used as the background reference for the protein assay and for bovine serum albumin (BSA) protein standards. The resulting protein extracts were reduced and alkylated with triethylphosphine and iodoethanol. Protein mixtures were digested with trypsin and filtered through 0.45 µm spin filters before being applied to the high-performance liquid chromatography (HPLC) system.

Tryptic peptides (20 µg) were injected randomly onto a Surveyor HPLC system (Thermo-Finnigan) with a C18 microbore column (Zorbax 300SB-C18, 1 mm × 65 cm). Peptides were eluted with a linear gradient from 5 %-45 % acetonitrile developed over 120 minutes at a flow rate of 50 µL/min and the effluent was electro-sprayed into the linear trap quadrupole (LTQ) mass spectrometer (Thermo Fisher Scientific, Waltham, MA). Data were collected in the "Triple Play" (MS scan, Zoom scan, and MS/MS scan) mode.

The acquired data were filtered and analyzed by a proprietary algorithm licensed to Monarch Lifesciences LLC, Indianapolis IN. Database searches against the International Protein Index (IPI) mouse database and the non-redundant *Mus musculus* database (NCBI) were carried out using the X!Tandem and SEQUEST algorithms. Only those proteins identified with >90 % confidence were evaluated quantitatively. Briefly, when raw files were acquired from the LTQ mass spectrometer, all extracted ion chromatograms (XICs) were aligned by retention time. After alignment, area under the curve for each individually aligned peak from each sample was measured, normalized, and compared for relative abundance. Significant differences in protein expression across dose groups were determined by ANOVA. To eliminate technical bias, randomization of order of measurement and "quantile normalization" was used and data normalized using a log2 scale.

Calu-3 cells: For Calu-3 cells, analysis was done for SWNT and MWNT only since C_{60} did not show any effect in terms of changes in TEER or hormonal responses. The analysis was done for 24 h exposure only because we feel that 24 h is an optimum time period to study these short term effects. Exposure concentration of 0.4 µg/cm^2 and 4 ng/cm^2 representing a higher and lower concentrations of CNTs were used.

For Calu-3 cells, apical media from each transwell was collected. The adherent cells were briefly rinsed with ice-cold 250 mM sucrose. After aspiration, 500 µL of lysis buffer (8 M urea, 10 mM DTT freshly prepared) was added. Cells were incubated at 35 °C for 1 hour with agitation, transferred to an ultracentrifuge tube, briefly vortexed, and centrifuged at 100,000 × g for 20 min at 4 °C to remove the mucus gel and insoluble materials. The cell lysate was then transferred to an Ultrafree-MC Centrifugal Filter Unit and centrifuged at 3,500 x g for 8 min at room temperature for final cleanup. Fully solubilized cell protein samples were then stored at

80 °C until analysis. Protein concentration was determined by the Bradford Protein Assay using Bio-Rad protein assay dye reagent concentrate. A 100 µg aliquot of each sample was adjusted to 200 µL with 4 M urea and then reduced and alkylated by triethylphosphine and iodoethanol as described [66]. A 150 µL aliquot of a 20 µg/mL trypsin solution was added to the sample and incubated at 35 °C for 3 h, after which another 150 µL of trypsin was added, and the solution incubated at 35 °C for 3 h (n=5 per observation).

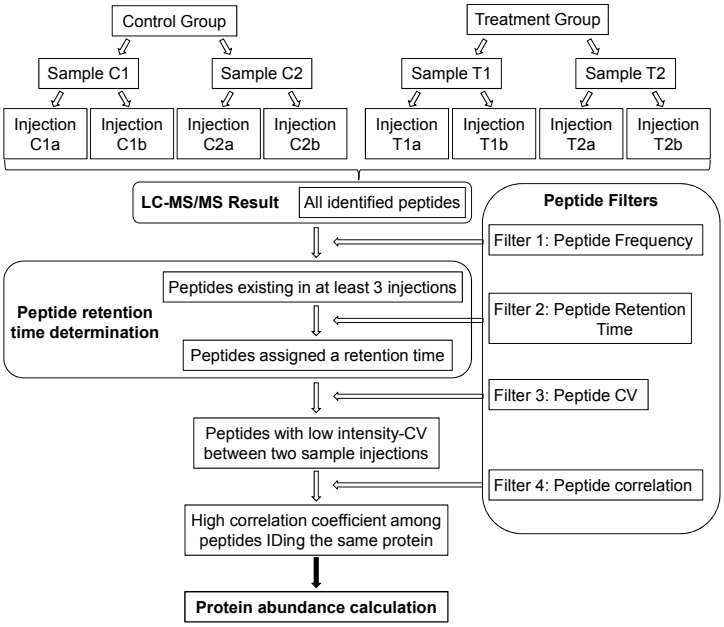

Work-flow of the IdentiQuantXL LFQMS platform for global protein profiling, depicting a hypothetical 2 sample experiment. The strength of this approach lies in the accurate determination of peptide peak retention time and subsequent filtering steps to eliminate peptides that are unqualified for quantitation. This leads to comprehensively accurate protein abundance calculation.

Exactly 20 µg of each tryptic digest sample were injected randomly as 2 technical replicates onto a C18 microbore RP column (Zorbax SB-C18, 1.0 mm x 150 mm) at a flow rate of 50 µL/min. The mobile phases A and B were 0.1 % formic acid in water and 50 % acetonitrile with 0.1 % formic acid in water, respectively. The gradient elution profile was as follows: 10 % B (90 % A) for 10 min and 10-100 % B (90-0 % A) for 170 min. The spectral data were collected in the "Data dependent MS/MS" mode with the ESI (electrospray ionization interface) using normalized collision energy of 35 %. Dynamic exclusion settings were set to repeat count 1, repeat duration 30 s, exclusion duration 120 s, and exclusion mass width 0.75 m/z (low) and 2.0 m/z (high). A blank was injected between each sample to clean and balance the column and eliminate carryover The acquired data was searched against the International Protein Index (IPI) database (ipi.HUMAN.v3.69) using SEQUEST (v. 28 rev. 12) algorithms in Bioworks (v. 3.3). Peptide and protein identifications ("hits") were validated by PeptideProphet [67] and ProteinProphet [68] in the Trans-Proteomic Pipeline (TPP, v. 3.3.0) (http://tools.proteomecenter.org/software.php). Only proteins and peptides with protein probability ≥0.9000 and peptide probability ≥0.8000 respectively, and peptide weight ≥0.5000 were used in the quantitative algorithm and are represented in the workflow diagram as "All identified peptides". Before clustering the retention time, peptide frequency was calculated and only peptides identified in at least three injections were included. To determine retention time, the retention time range of each filtered peptide from all scans from all injections were

calculated. For a peptide with a range ≤3 min, a weighted mean was calculated using Tukey's Biweight (bisquare) and used as the retention time for all injections. For a peptide with a range >3 min, all measured retention times were classified into three clusters based on elution patterns. The weighted mean retention time of each cluster was calculated and sorted from high to low as T1, T2, and T3. If T1-T3 ≤3 min, a weighted mean was calculated and used as the retention time for all injections. If T1-T3 >3 min, the frequency (F1, F2, and F3) and interquartile range (IQR1, 2, and 3) of each cluster was calculated and sorted. If a cluster with frequency (F)≤0.25, or 0.25<F≤ 0.50 with IQR>4, or 0.50<F≤0.75 with IQR>6, or 0.75<F ≤1.00 and IQR>8, it was excluded. If F1-F2>0.25, the cluster with F1 was chosen. If F1-F2<0.25 and F1-F3≥0.25, the cluster with a smaller retention time was chosen. If F1-F2<0.25 and F1-F3<0.25, the cluster with the smaller retention time was chosen. Peptides that do not meet these criteria were not assigned a retention time and were excluded from further analysis. After retention time determination, a weighted mean m/z of each peptide was calculated and a tab delimited file is created to extract peptide intensity using MASIC [69]. Peptides were then filtered according to intensity CV across all samples and intensity correlation, for those identifying a particular protein. Protein abundance was then calculated from all qualified corresponding peptides matched to that protein using the formula:

Protein abundance calculation

$$Ap = \sum_{i=1}^{n} \left(\frac{Ip}{Fp}\right) i$$

Where Ap = protein abundance
Ip = peptide intensity
Fp = frequency of peptide sharing

Because some tryptic peptides were shared by more than one protein, and sometimes several, the intensity of shared peptides was divided by the sharing frequency (e.g. the number of other proteins sharing the peptide). This strategy decreased the impact of shared peptides in protein quantitation, a unique feature of this platform.

Comparison of individual protein quantitation dose-group means generated by LFQMS was performed within the IdentiQuantXL platform using one-way ANOVA and Pairwise Multiple Comparisons (Holm-Sidak method). Critical F-ratio significance for ANOVA was set at p<0.001 and pairwise comparison at p<0.01, All p-values were transformed into q-values that estimate the False Discovery Rate (FDR) [70] using Q-value software (http://genomics.princeton.edu/storeylab/qvalue/).

For both the cell lines, to assist with interpretation of the numerous protein expression effects, we analyzed the differentially expressed protein data using Ingenuity Pathways Analysis (IPA) tools (Ingenuity Systems, Mountain View, CA; http://www.ingenuity.com/index.html), a web-delivered application that enables the discovery, visualization, and exploration of molecular interaction networks and canonical pathways in protein expression data. Lists of differentially expressed proteins were uploaded into the IPA system and proteins that were associated with a specific functional network or canonical pathway in the Ingenuity Pathways Knowledge Base were considered for evaluation. The IPA computes a score for each network according to the fit of the user's set of proteins of interest. The score is derived from a p value and indicates the likelihood that the selected proteins are categorized in a network due to random effects.

2.13. Cyclic AMP (cAMP) assay

The Calu-3 cells were treated apically with media containing FBS-CNPs for 48 h, followed by stimulation with or without epinephrine (10^{-5} M) for 10 seconds. The cells were washed twice with HBSS at 37 °C and incubated for 5 minutes with 1 % triton-X-100 in 0.1 M HCl at 37 °C. Permeabilized cells were scraped from the underlying supports and lysates were centrifuged for 1 min at 14,000 x g to remove cellular debris. The cAMP assay was done by using assay designs direct cyclic AMP EIA kit (Ann Arbor, MI) following the manufacturer's instructions.

Due to large surface area of the nanoparticles, they have the ability to adsorb a wide variety of small organic solutes, indicator dyes or their reduction products [56]. Therefore, we carried out controls for this assay with addition of nanoparticles to control at the time of the cyclic AMP assay.

2.14. Statistical Analysis

Line and bar graphs have been generated by using Sigma Plot 2007 software. The points in the line graphs and bar in the bar graphs represent means ±SEM. Students t-test has been used to analyze the experiments and differences were considered significant when $p \leq 0.05$. ANOVA was used to analyze the proteomics and $p \leq 0.001$ was considered significant.

CHAPTER 3. RESULTS

3.1. Characterization of Nanoparticles

Samples of all the three CNPs prepared in tissue culture media were sent to Dr Somenath Mitra, NJIT, NJ for characterization of nanoparticles in aqueous media. In addition frozen plates of treated cellular monolayers on permeable supports were sent to him for AFM analysis. The visual particle agglomeration and Zetasizer analysis of relative particle size and zeta potential studies were done at Indiana University-Purdue University Indianapolis, IN.

3.1.1. Characterization of Nanoparticles in Aqueous Media

Figure 4 shows the elemental composition of all the three CNPs and scanning electron micrographs (SEM) of SWNT and MWNT. Fullerenes (C_{60}) did not show presence of any elemental impurities such as iron, nickel and/or cobalt that are generally the byproducts of CNP manufacturing process. On the other hand, SWNTs and MWNTs did contain these elemental impurities. SEM showed that both SWNT and MWNT are free of amorphous carbon.

In tissue culture media, the nanotubes form visual agglomerates and precipitate out at the highest concentrations used in this study (40 and 4 $\mu g/cm^2$). These precipitates can be seen on the apical surfaces of the cellular monolayers when cells grown on the transwells are treated with them (Figure 5). Lower concentrations show no visible aggregates.

3.1.2. Atomic Force Microscopy (AFM)

AFM, also performed by Dr Mitra demonstrated that the roughness factor (Ra) of the NP on the cellular monolayers was high at higher concentrations (40 $\mu g/cm^2$) as compared to lower concentrations (0.4 $\mu g/cm^2$) at which the measured Ra was nearly the same as blank (Table 1). High Ra value at higher concentration suggests the presence of large agglomerated particles associated with the cellular surface. At a lower dose, Ra is very low, suggesting more dispersion of the particles in media and may, therefore, have greater potential for cellular interaction and biological activity. These data are in complete agreement with our visual studies (Figure 5) and particle size measurements determined in particle agglomeration assay below.

3.1.3. Dielectric Spectroscopy of CNPs in Media

Frequency dependence of AC conductivity of SWNTs and MWNTs dispersed in the media at two different concentrations (0.004 and 0.04 μg/cm^2) was done by using dielectric spectroscopy (DS), a technique used for characterization of colloidal suspensions (Figure 6). A blank that represents media with no ^{o}s has also been shown. As shown, conductivity of the blank and C_{60} dispersions are very low and underwent little change over the entire frequency range. On the other hand, the conductivity of media with CNTs was relatively high and was not stable throughout. This difference in conductivity of the medium and the CNT particles causes interfacial polarization resulting in movement of surface charges trapped at the interface of components of media.

The conductivity of SWNTs increases with increase in concentration and this increase plateaus at higher concentrations. This increase at higher concentration may be due to increase in finely dispersed CNTs at that concentration. The stagnation may be due to the fact that for these particles, polarization is not enough to change with further change in electric field.

In the case of MWNTs at lower concentration (0.004 μg/cm^2), conductivity was same as SWNTs at same concentration but plateaus at lower conductivity levels than SWNT media. The relation between concentration and conductivity was opposite than what was seen in the case of SWNT media. This may be due to higher agglomeration tendencies of MWNTs at higher concentrations than SWNTs that cause hindrance in the conduction path.

3.1.4. Particle sizing and Zeta Potential

The relative particle size measurements of different concentrations (4 μg/cm^2-4 pg/cm^2) of SWNTs and MWNTs in the Calu-3 culture media are shown Figures 7-12. Controls were prepared in culture media with the same serum as the nanoparticle solutions. Therefore, the predominate measured particles in the control are serum proteins and these would be expected to be in all solutions.

In both the CNTs there is a shift toward the lower size range when compared to their respective controls indicating the presence of individual or small agglomerates of only a few CNTs. At the highest concentration (4 μg/cm^2),we could see an increase in percentage of the particles in the smaller size range but could not see the particles in the higher size range. This may be due to the agglomeration of the particles at these concentrations resulting in the sedimentation of these particles and hence makes them unable to be detected.The observed sediments of CNTs in experimental solutions as compared to the clear solution of control corroborates this. The lowest concentration (4 pg/cm^2) graphs were very much similar to

control. This is likely due to the fact that at this diluted concentration, the relatively low number of CNTs cannot be detected in the presence of the larger concentration of proteins. There were a few anomalies in the data which may be attributed to the sedimentation of CNTs while doing the experiment. Since the machine works on the principle of dynamic scattering of light, sedimentation may cause the CNTs to settle down and hence makes them unable to be detected.

Dielectric conductivity of the CNPs in media showed electrical conductivity of all the three nanoparticles. These nanoparticles were subjeted to zeta potential measurements in the media to evaluate the surface charges. The zeta potentials of all the three nanoparticles in media at all the seven concentrations (4 $\mu g/cm^2$-4 pg/cm^2) studied came out to be negative. The average zeta potentials (n=7) ± SEM in the media for C_{60}, SWNT and MWNT was -8 ± 0.62, -7.59 ± 0.71 and -6.14 ± 0.63 respectively.

3.2. Effect of Carbon Nanoparticles on Renal Cells

Experiments were conducted to determine functional, structural, and proteomic changes induced by exposure of CNPs to the mpkCCD_{cl4} cell line. Electrophysiological studies were used to determine the effect of CNPs on TEER, a measure of barrier integrity, and SCC was used to monitor hormone responsiveness. Quantitative proteomic studies were conducted to correlate the observed structural and functional studies with CNP-induced changes in the cellular proteins.

3.2.1. Structural Effects of Nanoparticle Exposure

To visualize potential changes in the actin cytoskeleton as well as change in the cellular proliferative responses, both actin and PCNA staining was done on the CNP exposed cellular monolayer. At high concentrations, where agglomeration of particles is pronounced, an increase in cellular proliferation as well as an increase in filamentous actin was seen immediately around the agglomerates. This effect was not seen in C_{60} exposures and SWNT or MWNT concentrations $\leq$0.4 $\mu g/cm^2$ (Figures 13-14).

3.2.2. Functional Effects of Nanoparticle Exposure

The functional effects were studied in terms of effect on the barrier integrity of the cells and changes in hormonal responses. TEER is an effective measure of the barrier integrity of the cells and also serves as a very sensitive measurement of cellular viability. SCC measures the net movement of ions across the membrane in both directions (apical to serosal and *vice versa*).

A six order of magnitude dose response was studied with 48 hour of nanoparticle exposure. While incubation with multiwall nanotubes decreases the TEER of the renal cells equally over a six order of magnitude dose response range, SWNT and C_{60}, on the other hand, show an inverse dose response relationship with the lower concentrations showing a significant decrease in TEER. The higher concentrations were without effect (Figure 15).

In particle studies, dose is usually described as mass per unit volume (e.g. μg/ml) but it is practically impossible to get a stable suspension of nanoparticles due to agglomeration. At the highest concentrations, the agglomeration produces particles that are visible while smaller agglomerations are likely at lower concentrations. Therefore it is more appropriate to express dose in terms of mass per unit surface area of the culture well (e.g. $\mu g/cm^2$).

The cells were exposed to ADH/vasopressin. The hormone caused an immediate response that consists of a CFTR-mediated Cl^- secretory phase followed by an ENaC-mediated increase in Na^+ flux. Amiloride, a specific inhibitor of ENaC, was used to terminate the experiment at time t = 30 min. Figure 16 contains the data from control, 40 $\mu g/cm^2$ (highest dose) and 0.4 ng/cm^2 (lowest dose). Nanoparticle exposure did not alter either the Cl^- secretory or the Na^+ absorption response to ADH. The experiments were repeated at every concentration shown in figure 15 and all doses were without effect.

3.2.3. Lactate Dehydrogenase (LDH) and Cytokine Assay

The leakage of LDH reflects cellular membrane injury and hence cytotoxicity. An LDH assay (Table 3) showed that none of the doses, except the highest dose of MWNTs, altered the levels of LDH in the culture media as compared to control. This is in exact correlation to TEER studies, where also, MWCNTs exhibited the maximum decrease in TEER and at all the six concentrations studied. These data are also in agreement with the TEER changes as none of the exposed monolayers showed a decrease in TEER that was substantial enough to represent altered cell viability. However, another important observation here is the relatively lower values of LDH in basolateral side of the cells as compared to the apical sides. This shows that the CNPs may be affecting the cellular monolayer in different ways on these two sides

To determine more subtle effects on the cells we conducted cytokine release assay (Table 4). Cytokine assay indicated mild irritation to the cells by both the nanotubes as indicated by significantly different values of G-CSF, MCP-1 and SCF in case of SWNT (apically) and RANTES in case of MWNT (basolaterally).

3.2.4. Proteomics Effects of Nanoparticle Exposure

On an average, 1,878 proteins were identified, quantified and compared for three doses (40, 0.04 and 0.004 μg/cm^2) for all three CNPs. All the CNPs caused changes in protein expression as compared to control. The number of proteins whose expression was significantly altered decreased with increasing exposure doses (Table 5). The least effect was seen in case of C_{60} with SWNTs showing maximum effect.

Out of all differentially expressed proteins, none of the proteins was common to all three CNP exposure conditions. Neither was any altered protein common to all three doses within the same CNP exposure. Table 6 shows the altered expression of proteins that were affected at low doses (0.04 and 0.004 μg/cm^2).

There was no altered protein at 40 μg/cm^2 concentration, common to all three CNPs and only two proteins (Histone cluster 2 and H2ac) were altered by all CNPs at 0.04 μg/cm^2. Seven proteins were altered by all three CNPs at the lowest dose (0.004 μg/cm^2) as shown in Table 7.

Table 8 lists 26 proteins that were similarly affected by exposure to SWNT and MWNT at 0.004 μg/cm^2. At 0.04 μg/cm^2, members J and X of the H2A histone family (H2AJ and H2AX) and histone cluster 2 were altered. Only catenin, beta like 1 (cTNNBL1) was upregulated at 40 μg/cm^2 by both CNTs.

Table 9 and 10 list the significant (P≤0.001) functional networks and canonical pathway involving proteins altered by the CNP exposure.

Interestingly, most of the proteins affected by ROS or cellular toxicity were not affected at any of these doses. All Glutathione-S-transferases except GST mu-4 (upregulated 10.1 % by SWNT at 0.004 μg/cm^2), GST omega-1 (upregulated 10.7 % by fullerenes at 0.04 μg/cm^2 and down-regulated 10.6 % by SWNT at 0.004 μg/cm^2), glutathione reductase and formyl glutathione lyase (glyoxalase1) were normally expressed. Similarly superoxide dismutase Mn and Cu-Zn, stress proteins, proteins of cytochrome P450 family, proteins associated with perodoxin family of antioxidant enzymes and peroxisomes were unaffected.

3.3. Effect of Carbon Nanoparticles on Airway Cells

For the Calu-3 cell line, a well characterized model of airway epithelium, air interface cultures (AIC) show higher TEER and basal SCC than liquid covered cultures (LCC). In the present study, AIC demonstrated a maximum TEER of 881 Ω.cm^2 after 14 days which was higher than that demonstrated by LCC (387 Ω.cm^2) in the same time period. It has been shown by numerous

studies that AIC simulate *in vivo* conditions more efficiently than the more commonly used LCC [71] [72] [73].

The Calu-3 cells grown on permeable supports are mounted in Ussing chambers to measure basal and hormone stimulated ion flux. After mounting, the basal SCC stabilized to approximately 25-30 $\mu A/cm^2$ in few minutes. We have used epinephrine to stimulate these cells. Epinephrine is an endogenous hormone that binds α- and β-adrenergic receptors and increases cAMP levels [74]. The stimulation results in an average eight fold increase over the basal ion transport. This cell line has also been shown to exhibit an increase in basal ion transport within 1-2 minutes after exposure to mediators like isoproterenol, forskolin, bradykinin, methacholine, trypsin, histamine [51]. This sudden increase is followed by marked progressively dampening oscillations over time (Figure 17).

3.3.1. Characterization of Calu-3 Cells

To look at the contribution of Na^+ flux to the basal ion transport, amiloride (10^{-5}M), a specific inhibitor of ENaC, was added apically before the addition of epinephrine. Amiloride did not show any effect on the basal or hormone-stimulated ion transport indicating no contribution of Na^+ absorption (Figure 18). Pretreatment with NPPB (100 μM) however, not only significantly inhibited the basal ion transport but also inhibited the epinephrine stimulated peaks (Figure 19). This observation indicated that the basal ion transport in these cells and the epinephrine stimulated peaks are mostly due to Cl^- secretion.

CFTR inh 172 (100 μM), a selective CFTR Cl^- channel blocker [75], was used to pretreat the cells 10 minutes before the addition of epinephrine (Figure 20). Approximately, 59 % of the first epinephrine stimulated ion transport peak was inhibited by CFTR inh 172. The remaining transport indicates the presence of another Cl^- conducting element.

Tannic acid is an inhibitor of calcium activated chloride channels (CaCCs) [76] [77] [78] including the recently discovered transmembrane 16A channel (TMEM 16A). Tannic acid does not affect CFTR Cl^- channels [79]. When 100 μM tannic acid was used to pretreat the cells 10 min before adding epinephrine, the Cl^- peak was inhibited but to lesser extent (around 43 %) than what was inhibited by CFTR inh 172 (Figure 21 vs 20). The first Cl^- peak was thus the Cl^- secretion via CFTR and CaCC channels.

To substantiate the findings of the data shown in Figures 20 and 21, the cells were pretreated with both CFTR inh 172 and tannic acid, 10 min before the addition of epinephrine. As shown in Figure 22, the treatment not only inhibited the basal ion transport but also eliminated the epinephrine stimulated Cl^- flux further indicating that CFTR and CaCC are responsible for the hormone stimulated Cl^- secretion.

To further prove the presence of Ca^{+2} activated channels, we used ionomycin (0.1 μM), a selective calcium ionophore to elevate the Ca^{+2} concentration in these cells. As a result of 10 minutes of pretreatment, interestingly, the basal ion transport was elevated with an inhibition of the first peak and elevation of subsequent peaks indicating these peaks to be Ca^{+2} activated (Figure 23).

BAPTA-AM (1,2-Bis(2-aminophenoxy)ethane-N,N,N',N'-tetraacetic acid acetoxymethyl ester (100 μM), a cell permeable Ca^{+2} chelator however, seems to diminish all epinephrine stimulated ion flux (Figure 24). This provides a further indication of the importance of Ca^{+2} to epinephrine stimulated ion flux.

3.3.2. Functional Effects of Nanoparticle Exposure

After having characterized the basal and epinephrine-stimulated ion flux, experiments were conducted to determine functional changes induced by exposure of CNPs to these cells. To examine the effect of short-term vs long term incubation, Calu-3 cells were grown to confluency and treated with CNPs for 1, 24 or 48 hours over a concentration range of 4 $\mu g/cm^2$ - 4 pg/cm^2. For the 1 and 24 time points, the CNPs were added only to the apical bathing media to simulate a more acute exposure. For the 48 hour exposure, the CNPs were added to both the apical and basolateral bathing media.

Electrophysiological studies were used to determine the effect of CNPs on TEER, a measure of barrier integrity, and SCC, a measure of hormone responsiveness. Quantitative proteomic studies were conducted to correlate the observed functional studies with CNP-induced changes in the cellular proteins.

The results of these TEER studies are shown in Figure 25. All three carbon nanoparticles were without effect after an hour of exposure. Likewise, no significant reduction in TEER of the monolayer was observed in the case of fullerene exposures at any of the time points or concentrations studied. Conversely, 24 or 48 hours of nanotube (SWNT and MWNT) exposure over a wide range of concentrations caused a decrease in TEER. After 48 hours of exposure, the SWNTs demonstrated effects in the concentration range of 4 $\mu g/cm^2$ to 40 pg/cm^2 whereas MWNTs showed the effects in the range of 4 $\mu g/cm^2$ to 0.4 ng/cm^2. At 24 hrs, the resistance decreases were more variable with the overall effect roughly between the effects seen with 1 h and 48 h exposures. Interestingly, none of these concentrations were toxic to the cells and did not affect the monolayer viability as evidenced by the substantial remaining TEER. The maximal effects of the nanotubes is observed at concentrations that are orders of magnitude lower than previously reported effects.

To determine whether the nanoparticles induce changes in cellular function, response to epinephrine was studied. As already shown, epinephrine stimulates transepithelial Cl^- transport in a secretory direction (serosal to mucosal). The first peak represents the most robust response to epinephrine in these cells. For simplicity, only the magnitude of this initial Cl^- secretory response was measured to determine effects of nanoparticles as the secondary oscillations in SCC were not uniformly inhibited by nanoparticle exposure.

The response to epinephrine stimulation after 48, 24 or 1 hour of nanoparticle exposure are shown in Figures 26-28 respectively. During the 24 and 48 h treatments, no change in Cl^- secretion was observed after fullerene exposure. For simplicity only the highest and lowest fullerene concentrations are presented. However, exposure to either of the nanotubes caused a decrease in hormone-stimulated Cl^- transport over roughly the same concentration range as seen in the TEER measurements. For clarity, only the highest and lowest nanotube concentrations that have significant effects on Cl^- secretion are shown. All intermediate concentrations were assayed and exhibited similar patterns (data not shown).

After 1 hour of exposure, there were no nanoparticle-induced changes in epinephrine stimulated Cl^- secretion so only the highest and lowest concentrations are depicted although intermediate concentrations were assayed with similar results (Figure 28).

3.3.3. cAMP Assay

The initial increase in Cl^- secretion is predominately mediated by an increase in intracellular cAMP resulting in activation of PKA and consequently phosphorylation and activation of CFTR. For both SWNT and MWNT exposures, after epinephrine stimulation, the rise in cAMP was found to be the same in both nanotube exposed and control monolayers (Figures 29-30). These results suggest that the ion transport element affected by the nanoparticles lies beyond the basolateral membrane epinephrine receptor and intracellular cAMP production.

3.3.4. Cytokine Assay

Cytokines are extracellular signaling proteins that are major determinants of inflammatory responses. Profiling the expression of cytokines provides information about the underlying immunological mechanism. Eight different cytokines were profiled to assess the inflammatory responses of the Calu-3 cells on exposure to SWNTs and MWNTs (Figure 31). The cells failed to show cytokine release in any of the treatments.

3.3.5. Proteomics Analysis

Carbon nanotube treatment induced significant alterations in protein expression. Table 11 indicates, both CNTs (MWNT and SWNT) caused differences in protein expression compared to controls. The number of proteins whose expression was significantly altered was inversely proportional to the dose. Whereas higher dose (0.4 μg/cm^2) exposures caused a change in protein expression of 21 proteins (Table 12), 563 proteins in total were changed by lower dose (0.004 μg/cm^2) exposures of both CNTs. Out of 17 proteins that were altered at the higher dose (0.4 μg/cm^2), only 4 proteins were common to both CNTs (Table 13), whereas out of 332 proteins that were altered at the lower dose (0.004 μg/cm^2) (Table 16), 231 proteins were common to both SWNT and MWNT exposure (Table 17). Interestingly, the expression of the majority of the proteins were down-regulated.

To interpret the biological significance of the affected proteins, Ingenuity Pathways Analysis was used. This software database enables matching the differential protein expression data into its molecular interaction networks and canonical pathways based on known information integrated into the database. Tables 14 and 15 list the most significant ($P \leq 0.001$) functional networks and canonical pathways involving proteins altered by the CNT exposures.

CHAPTER 4. DISCUSSION

4.1. Size and Concentration of CNP

A great deal of attention has been paid on studying the functionalized nanoparticles because of their extensive utility in almost all industries. However, little to no attention has been paid to raw, non-functionalized nanoparticles that are produced in enormous quantities to provide the raw materials for the synthesis of these functionalized nanoparticles. Being the raw materials, these are likely to be produced in massive quantities and therefore, may contribute substantially to both environmental and occupational pollution.

As manufactured CNPs are highly hydrophobic so they have to be ultrasonically dispersed in FBS. The MWNT have been reported to have a strong tendency to aggregate into microscopic bundles which in turn agglomerate loosely into small clumps [80]. Kinetic analyses of a more flexible type of MWNT support its poorly soluble agglomerated carbonaceous particulate nature [81]. Likewise, L'Azou *et al.* [82] while analyzing the *in vitro* effect of carbon black and TiO_2 NPs on renal cells found that the particles do not retain their nano sizes in solutions as they tend to aggregate into larger complexes with many fold increased sizes compared to initial sizes of isolated particles. Ultrasonic dispersion in a protein-containing solution is the preferred method of increasing solubility and decreasing particle size. However, even this method does not fully solubilize the CNPs. At higher concentrations, there are visible aggregates and relative particle sizing indicates the presence of smaller multi-component aggregates.

In the current studies several methods were used to determine the relative particle size in order to correlate this parameter with functional assays. Results of AFM analysis (Table 1), particle size measurement (dynamic light scattering, Figures 7-12) and dielectric spectroscopy (Figure 6) in the present study corroborate the increased solubilization at lower concentrations. Also, at 40 and 4 $\mu g/cm^2$, significant agglomeration is evident while visible particles are absent below that level. Due to the agglomeration of nanoparticles at higher concentrations and better dispersion at lower concentrations, these particles may exhibit different effects at different levels of exposure-micro-effects due to exposure to agglomerated particles and nano-effects due to exposure to individual particles

Further characterization is provided by the zeta potential measuremnents of the CNPs in culture media. These measurements were performed across the entire dose range of CNPs. The

zeta potential came out to be negative for all the three CNPs which suggests that these particles have negative surface charge. The zeta potential of C_{60} at all the seven concentrations was almost the same except for 0.4 ng/cm^2 where the magnitude is small as compared to other concentrations. This anomaly can be accounted for by the experimental error due to sedimentation of the CNPs. The zeta potentials for both the nanotubes at different concentrations were different as the nanotubes used in this study had a range of lengths and zeta potentials can vary with the variable lengths.

Negative value of the zeta potential suggests that these particles should repel each other and agglomeration should be prevented. Since the thermal energy contained in a particle at room temperature corresponds to a voltage of 25 mV (http://physics.nist.gov/cuu/constants/index.html) and the measured zeta-potentials are clearly smaller than that, therefore other forces, such as attractive van der Waals forces can overcome the repulsive electrostatic forces between these particles. This causes them to agglomerate at particularly higher concentrations where the number of particles per ml of the media is much more as compared to the lower concentrations causing more agglomeration to take place at higher concentrations.

4.2. Effect of CNPs on Renal (mpkCCD$_{cl4}$) Cells

Previous studies have indicated that very high concentrations of nanoparticles are toxic to cultured cells. For example, toxicity of three doses (40, 200, 400 µg/mL) of MWNT was observed to cause massive loss of cell viability through DNA damage and programmed cell-death compared to control in normal human dermal fibroblast cells [33]. In agreement with the previous studies, a significant decrease in TEER of mpkCCD$_{cl4}$ cells on exposure to very high doses (200 µg/cm^2) has been reported previously by our laboratory [83]. The proteomic analysis confirmed changes in various junctional and cell adhesion related proteins at these very high concentrations. However, these concentrations do not represent doses that will be found in the environment, even in the manufacturing workplace. Therefore, the current experiments have been done using lower, more physiologically relevant doses of CNPs.

Some studies have reported carcinogenic effects of carbon nanoparticles at a concentration of 10 µg/ml [84]. MWNT have been specifically implicated due to their structural similarity to chrysotile asbestos that is widely accepted to cause carcinogenic responses in humans [85] [28]. Cui *et al.* [26], analysed five different concentrations of SWCNTs in the range of 25-200 µg/ml and showed that the HEK cells that were growing far from SWNT contact grew well as compared to cells in direct contact with SWNTs suggesting direct contact being necessary for cytotoxicity. This contact is indication of focal damage. By electron microscopy, Panessa-Warren *et al.* [2] found that both colon and lung cells showed focal damage to apical plasma membrane at the sites of carbolex (2 µl dose of 100 µM) nanoparticle attachment. An *in vitro*

exposure of lung fibroblasts to 0.24 μg/ml of dispersed SWNT has been shown to stimulate cell proliferation and induce collagen production with elevation of matrix metalloproteinases-9, which is known to be involved in lung fibrosis [86]. In our study, PCNA staining of confluent monolayers of mpkCCD_{cl4} after exposure to highest concentration (40 μg/cm^2) of nanotubes (SWNT and MWNT) also showed changes in cells surrounding agglomerates. Cells seemed to exhibit proliferating nuclei. Once confluent, untreated monolayers of polarized epithelial cells show contact inhibition and stop growing. The results with nanotubes indicate that the agglomeration is causing the cells to replicate abnormally, suggesting that hyperplasia is occurring. Despite elevated PCNA staining at agglomerant foci, PCNA expression as detected by proteomic analysis, remained unchanged at all doses analyzed.

Staining with rhodamine-phalloidin also revealed a general increase in expression of polymerized (filamentous) actin. Previously, such changes in actin expression have been shown to contribute to a changes in cellular functions including division [87]. Our observed trends in cell function and abnormal cellular replication seen via PCNA staining support this. However, the proteomic results do not support differential expression of total actin. These results suggest that the observed changes in filamentous (phalloidin-stained) actin are the result of changes in the filamentous-to-globular actin ratio and not the total actin.

In summary, the structural studies indicate that CNP exposure can influence important cellular functions including division in focal area of the monolayer. CNPs can cause the cells to replicate abnormally, suggesting hyperplasia is occuring. Since this study represented short term CNP exposures, study of long term exposures needs to be done in order to better understand these effects.

TEER is a measure of monolayer integrity and is also a very sensitive measure of cellular viability. As cellular viability decreases slightly, TEER falls significantly. In the experiments shown in figure 15, TEER was significantly decreased after treatment with all concentrations of MWNT from 40 μg/cm^2 down to 0.4 ng/cm^2. Interestingly, after incubation with fullerenes or SWNT, resistances were lowered only by exposure to concentrations below 0.4 μg/cm^2. It was interesting to note that even after the exposure to CNPs, the cells maintained their viability though the TEER decreased, which is an indication of subtle changes that may include cytoskeletal changes that directly influence junctional complexes or membrane alterations rather than toxicity causing cell death.

To further investigate nanotube-induced changes in cellular function in the renal cell line, the responses to ADH, a hormone to which these cells normally respond were assessed using the method of SCC, a measure of net ion transport. Interestingly, there were no alterations in the cellular response to ADH, a hormone known to regulate both Na^+ and Cl^- in the principal cells. These results are consistent with the maintenance of a viable monolayer, albeit one with reduced TEER.

The proteomic analysis showed an inverse relation between the dose and the number and fold changes of cellular proteins altered after exposure to CNPs. This may be due to the higher degree of agglomeration of CNPs at higher concentrations and therefore shifting from exhibiting nano effects to micro or no effect in this case. Size measurements of CNPs corroborate this.

None of the altered proteins indicated toxicity induced by CNPs which is in direct agreement with the lack of cell death in the TEER studies, LDH measurements and minimal cytokine secretion. Another important finding was absence of any junctional protein altered in response to CNP exposure except upregulated tight junction signaling proteins at 0.04 $\mu g/cm^2$ SWNT exposure.

The highest concentration of CNPs, i.e. 40 $\mu g/cm^2$, had little effect. Only 19 proteins were altered despite the decline in TEER observed in MWNT. However, at lower concentrations, differential protein expression was significantly greater and substantiated the functional change measured as a decline in TEER. This may be due to CNP agglomerates (at 40 $\mu g/cm^2$) exerting focal effects which are significant in foci, but are undetectable when all cells are examined together. This may also account for focal elevations of PCNA staining, but no significant change overall in PCNA as measured by proteomic changes.

As Table 6 indicates, the lowest two SWNT exposures resulted in a decreased expression of 6 ribosomal proteins that was not shown by C_{60} or MWNT. Ribosomal proteins are involved in protein synthesis and individual ribosomal proteins are known to play a role in regulating cell growth, transformation and death [88] and ribosomal protein gene expression has been shown to decrease in renal toxicity [89].

For the interpretation of the proteomic results, Ingenuity Pathways Analysis was used. One of the effects observed in all three CNP exposures at the 0.004 $\mu g/cm^2$ dose was an up-regulation of glycolysis/gluconeogenesis pathways. Guo *et al.* [90] reported a dose-dependent adsorption and depletion of nutrients from RPMI cell culture medium by purified SWNTs that contained 10 % Fe. HepG2 cells cultured in these depleted media showed significantly reduced viability that was restored by replenishment of folate. However, those effects occurred at doses of 10 µg/mL (corresponding to 25 $\mu g/cm^2$) and above, higher than the doses used in the present study. Alternatively, one can view the increased glycolysis/gluconeogenesis pathway as a generalized response to stress. Systemically, such phenomena are usually manifested in a fight or flight response. However, the stimuli for a more subtle, analogous change at a tissue or molecular level are not well documented.

Fullerene exposure at 0.004 $\mu g/cm^2$ is associated with a predominant up-regulation in the expression of proteins in cell cycle, gene expression and cell death functional networks. Studies of bronchoalveolar cells in mice have demonstrated increased apoptosis and GI arrest after 14 and 28 days of C_{60} instillation [19]. That same study also showed that the expression of

the tissue damage-related MMPs, Timp and Slpi gene, and the expression of oxidative stress related SOD gene were increased until day 28 after a single instillation. Alteration of gene regulation induced by SWNT exposure was found in human embryonic kidney cells [26]. Decreased cell proliferation and adhesion, upregulation of cell cycle associated genes, down-regulation of signal transduction genes and adhesion proteins such as laminin, fibronectin, cadherin, FAK and collagen IV, GI arrest of cells and apoptosis was also observed [26]. The relevance of the changes we have observed to those alterations seen by others in various tissues will require additional studies.

No ROS-related protein alterations or cytotoxic effect have been seen at 40 μg/cm^2. The upregulation of NRF-2 mediated oxidative stress response at 0.04 μg/cm^2 (in contrast to the decrease in this response at 40 μg/cm^2), however further suggests, that the CNPs have greater biological effect at lower exposure levels.

Other pathways impacted by CNP exposure at very low levels include alteration in functional networks involved in inflammatory diseases and regulation of amino acid metabolism. Changes in the expression of components of various metabolic pathways may be particle specific as well as dose- and exposure time-dependent. These aspects require further investigation.

There is little overlap among the three nanoparticle types in terms of the types of proteins, molecular interaction networks and pathways, suggesting the physicochemically distinct particles act differently at the biochemical and molecular level, with respect to effects on the proteome.

Important alterations in cell structure, function and protein expression has been induced by CNPs in mpkCCD$_{cl4}$ cells representing renal collecting ducts. The exposure times simulated in this study represent short term effects and observed changes are subtle but these effects may be additive over time in long term or chronic exposures resulting in major cellular changes with serious pathological implications.

4.3. Characterization of Calu-3 Cell Line

Calu-3 cells form an ion transporting cell line representative of the serous cell type in the airways. The presence of CFTR, a cAMP mediated Cl^- secreting channel in Calu-3 cell line has long been established [91]. Our studies however showed that CFTR inhibitor 172 was able to inhibit the Cl^- current by 59 % only. This indicated the presence of another Cl^- transporting element in these cells.

Many studies have shown the presence of calcium dependent responses in these cells. Our studies are in agreement with those of Fisher *et al.* [92] who showed that the CFTR

inhibitor, CFTR inh 172, abolished 60 % of the basal Cl^- secretions. These investigators found that FFA (flufenamic acid), an inhibitor of CaCC lead to approximately 20 % inhibition in these cells indicating the presence of calcium activated chloride secreting channel. Ito *et al.* [93] found evidence that the 4,4'-Diisothiocyanatostilbene-2,2'-disulfonate (DIDS), when added basolateraly, induced Cl^- secretion in Calu-3 cells that involves Ca^{2+}-dependent component that is interrupted by BAPTA/AM, a Ca^{+2} chelator. Therefore, testing for CaCC was relevant to this study.

Tannic acid is an inhibitor of recently discovered CaCCs including TMEM16A channel. The inhibition of the remaining of the Cl^- secretion response of epinephrine stimulation by tannic acid suggests the presence of calcium activated chloride channel in Calu-3 cells. TMEM16A is highly expressed in secretory epithelial tissues where it has been implicated to play a key role in calcium-dependent Cl^- secretion [76] [78] [94] [95]. It has been shown that TMEM16A knockout mice die soon after birth because of tracheomalacia [96]. In another study by the same group, CaCC current measurements in these mice suggested a major role of TMEM16A in epithelial Cl^- secretion in the airways [95]. Therefore, Calu-3 cells have two different mediators of Cl^- secretion. This has also been shown by others that at least two kinds of second messengers, cAMP and Ca^{2+}, are implicated in Cl^- transport in Calu-3 cells [72].

The elevation in the baseline on pretreatment with ionomycin indicates the role of calcium activated chloride channel along with CFTR in maintaining basal ion transport. Robust CaCC current in TMEM16A-transfected cells vs no currents in the non-transfected cells in response to ionomycin have been reported [97]. Pretreatment with both CFTR inh 172 and tannic acid indicates that the epinephrine stimulated Cl^- secretion is predominately mediated by these two channels.

Pretreatment with the Ca^{+2} ion chelator, BAPTA AM inhibits all the Cl^- secretion in these cells. This suggests that Cl^- secretion via CFTR may be dependent on CaCCs. CFTR and CaCC have been shown to be functionally coupled through a direct channel-channel interaction [98] [99].

Despite the importance of Na^+ absorption in airway secretory events, we were not able to find any ENaC in these cells. Many studies in the past have shown that ENaC and CFTR functionally interact with each other and the high levels of CFTR down-regulate ENaC below the level of detection [100] [101] [102] [103]. The mechanism by which CFTR modulates the function of ENaC proteins is still obscure and somewhat controversial and needs further investigation.

In conclusion, consistent with previous reports, we find that confluent Calu-3 cells express two types of Cl^- secretory channels, CFTR and a CaCC and that both contribute significantly to Cl^- secretion. Understanding this cell line was very important to study the effects of CNPs on respiratory epithelium. Since this epithelium is first line of defense against inhaled foreign material and is involved in important functions such as mucociliary clearance, any compromise due to effects of CNPs can have serious respiratory consequences.

4.4. Effect of CNPs on Airway Epithelial (Calu-3) cells

While both SWNT and MWNT impair the barrier function of Calu-3 monolayers measured as TEER, the change in TEER is not consistent with an altered viability of the cells. These results are consistent with our findings in the renal cell line. Others have also examined the TEER of the airway cells and have found similar results although no studies have utilized the low concentrations of the current experiments. Rotoli *et al.* [104] demonstrated a significant decrease in TEER of Calu-3 monolayers exposed to 100 µg/ml of MWNTs and SWNTs. The decrease in TEER was also accompanied by an increase in permeability shown by mannitol permeability experiments with no significant alteration in monolayer viability.

The observed changes in resistances indicate subtle changes associated with membrane, cytoskeleton or junctional complexes. This is also corroborated by cytokine release and proteomics studies. The absence of cytokine release indicate lack of inflammation or irritation in these cells. Proteomics analysis results also failed to show the upregulation of any stress response protein. Rather down-regulation of junctional complex proteins like CDH1 [cadherin1, type 1, E-cadherin (epithelial)], CTNNA1 (catenin alpha-1), CTNNBL1 (catenin, beta like 1), ITGB1 (integrin beta 1A and 1C), JUP (junction plakoglobin) and ITGAE (Integrin alpha-E) by both CNTs were observed

Both SWNTs and MWNTs inhibited the epinephrine stimulated chloride transport in these cells at 48h and 24 h exposure times. Many studies, particularly those in the cystic fibrosis field, have demonstrated the importance of Cl^- transport and the accompanying water flux in keeping the viscous secretions of the airways and lungs hydrated. The inhibition of stimulated Cl^- transport during chronic nanotube exposure may have pathological implications resulting from a decreased mucociliary clearance. While cystic fibrosis has a genetic basis, our studies indicate a toxicological basis for the impairment of the function of CFTR channel.

As demonstrated, Calu-3 cells express two different Cl^- channels one of which is CFTR, a channel activated via the adenylyl cyclase/cAMP/PKA pathway [105] [51]. The initial peak in response to epinephrine is partially cAMP-PKA mediated Cl^- secretion via CFTR channels [74]. The absence of nanoparticle induced change in cAMP levels after epinephrine stimulation at the concentrations studied rules out any basolateral ion transport element being affected by nanoparticles. This also suggests that many of the intracellular mediators are not changed, strongly suggesting an apical membrane effect or at least an effect after cAMP generation.

The time points in the present study represent short term exposure to the cells. Serious pathological implications may be the future outcome of longer term exposures. It is also worth reiterating that the concentrations used in the current study are, to our knowledge, several orders of magnitude lower than most previously published results. Workplace exposures to nanotubes are difficult to assess and, using currently available methods, different groups have applied different approaches in assessing the workplace concentrations of nanoparticles [106]

[107] [108]. Maynard *et al.* [109] estimated the air borne concentration of nanotubes material generated during handling and suggested that the concentrations were lower than 53 $\mu g/m^3$ However, effects of these nanoparticles in the picogram/cm^2 range suggest that workplace levels, particularly during chronic exposures, are likely to have physiological effects that can cause or exacerbate respiratory problems.

In the renal cells, higher concentrations of nanoparticles (40 $\mu g/cm^2$-0.4 $\mu g/cm^2$) were without effect on TEER while lower concentrations (0.04 $\mu g/cm^2$-0.4 ng/cm^2), similar to the levels used with Calu-3 cells, significantly decreased TEER. Unlike the renal cells that showed no nanoparticle-induced change in hormonal response, in the airway cells there are decreases in epinephrine stimulated Cl^- secretion in addition to the changes in barrier properties of the epithelial monolayer. Thus the effects of nanoparticles may be cell specific.

The effects on the protein expression in the airway cells are also inversely related to doses. The change in 21 proteins at higher dose (0.4 $\mu g/cm^2$) are insignificant when compared to the number of proteins (543) whose expression changed at low dose (0.004 $\mu g/cm^2$). This is also true for the proteomics results of the renal cells examined in the present study. As suggested above, this may correspond to the characterization studies that suggests that the CNPs agglomerate at higher concentrations and therefore no longer fall under the 'nano' particle sizes. Therefore the effect they exhibit is not a nanoparticle effect. It is however a microparticle effect. Functional studies however show that TEER is affected by higher concentrations too. The decrease in TEER at higher concentrations may be due to the particles that are not agglomerated and remain dispersed inside the culture media. The expression of the majority of the proteins was down-regulated with only a few showing upregulation.

Although the typical marker proteins of junctional complexes like ZO-1 (zona occludens) and TJP2 (tight junction protein 2) were not altered, many others were differentially expressed. These proteins included CDH1 (cadherin1, type 1, E-cadherin (epithelial)), CTNNA1 (catenin alpha-1), CTNNBL1 (catenin, beta like 1), ITGB1 (integrin beta 1A and 1C), JUP (junction plakoglobin) and ITGAE (integrin alpha-E). All these proteins were down-regulated by both the CNTs at lower dose. The down-regulation of these proteins is consistent with the reduction in TEER observed at 24 h for these doses as a direct relationship between the amount of expressed junctional proteins and barrier TEER has been previously established [110]. Evidences are there that junctional complex proteins are also involved in basic cellular processes like the regulation of cell growth and differentiation [111] [112] and the recovery from toxic injury [113]. CDH1 is a key member of cadherin family of cell adhesion molecules required for intracellular adhesion. Altered E-cadherin expression has been related to various types of carcinomas [114]. The intracellular domain of E-cadherin binds to actin filaments via alpha and beta catenins that have also been down-regulated. Loss of expression of alpha-catenin has been found in several cancer cell lines [115] and beta-catenin has an important role to play in cellular differentiation and proliferation [116]. Therefore, the down-regulation of all these proteins can not only disrupt the

normal epithelial tissue architecture but could have a chain effect down onto actin cytoskeleton and hence could affect the normal proliferation of these epithelial cells.

This is also evident from the down-regulation of actin cytoskeleton signaling with down-regulation of various actin cytoskeleton related proteins like PFN2 (profilin 2), EZR (ezrin), CFL1 (cofilin1), GSN (gelsolin), PLS 1and 3 (plastin 1 and 3), ANXA1 (annexin 1) and ADD1 (alpha-adducin 1). Actin binding proteins in addition to junctional complex proteins, may play a role in maintenance of junctional complex. The actin cytoskeleton signaling is essential for cells to maintain their shape and perform essential functions such as force generation, motility, and division. Witzmann *et al.* [34] observed decrease in expression of actin interacting and related proteins (Aip 1 and Arp 1) and other cytoskeleton-associated chaperones in human epidermal keratinocytes when exposed to MWCNTs. Holt *et al.* [87] demonstrated that SWCNTs do not induce acute cell death, but cell proliferation is greatly reduced in SWCNT-treated cells with an increase in actin-related division defects in purified model actin systems. The actin staining in renal cells in the present study also indicated reorganization of actin around nanotube agglomerates. The down-regulation of actin related proteins was also accompanied by down-regulation of intermediate filament KRT7 (Keratin, type II cytoskeletal 7) and KRT1 (Keratin, type II cytoskeletal 7). Overall, these results might suggest the subcellular rearrangement of cytoskeletal proteins and possible phenotypic changes of the cells. While the present study simulates short term effects related to actin reorganization, long term exposures can lead to serious cellular division defects.

Down-regulation of cytoskeletal signaling is also evident from the down-regulation of 14-3-3 proteins theta (YWHAQ) as decreased 14-3-3 proteins can destabilize cytoskeletal structure because of its regulatory activity on actin dynamics. Also, 14-3-3 can regulate actin dynamic through the actin-binding protein cofilin 5 [117], which was also down-regulated. Actin cytoskeleton functions in the generation and maintenance of cell morphology and polarity [118] and the changes in junctional complex proteins point towards the changes in cellular polarity. It has been reported that 14-3-3 can also block apoptosis [119]. Therefore, its down-regulation could potentially exert its roles in anti-apoptosis in CNT-treated cells through further down-regulation of 14-3-3-cofilin-actin pathway. Evidence for this is provided by down-regulation of proteins like NOD1 (Nucleotide-binding oligomerization domain-containing protein 1), AKR1C2 (Aldo-keto reductase family 1 member C2), PYCARD (Isoform 1 of Apoptosis-associated speck-like protein containing a CARD) that are associated with caspase related apoptosis and xenobiotic metabolism. This may be manifested as an abnormal growth of these cells over time. This is further supported by the down-regulation of cofilin-1 that is an actin regulatory protein shown to have a key role in the apoptotic process [120]. Overall, they did reflect changes in the proteome of the cells that can prove to be pathologically serious in long term exposures.

Heat shock proteins function as molecular chaperones to mediate many cellular processes such as formation and function of the cell cytoskeleton [121]. Down-regulation of

HSP90AA1, HSPA2, HSPA4, HSPA1A, HSPA1B, HSPA7 also points towards disorganization of cytoskeleton and hence alter morphology and polarity of cells. Heat-shock proteins also monitor the cellular proteins by carrying proteins to proteasomes for degradation and help folding of newly synthesized proteins. The down-regulation of these proteins along with the ribosomal proteins and proteasomal proteins may indicate down-regulation of protein turnover in the cells. The ribosomal and proteasomal proteins that were down-regulated were RPS10 (ribosomal protein S10), RPLP0 (ribosomal protein P0, acidic), RPS3A (ribosomal protein S3A), RPS28 (ribosomal protein S28), RPL32 (ribosomal protein L32) RRBP1 (ribosome binding proteins 1, isoform 3) and PSMD9 (proteasome 26S subunit, non-ATPase, 9), PSMC2 (proteasome 26S subunit, non-ATPase, 2), PSMB3 (proteasome subunit, beta type-3), PSMD13 (proteasome 26S subunit, non-ATPase, 13), PSMA4 (proteasome subunit, alpha type-4. Dong *et al.* [122] has shown altered expression of genes related to ribosomes and proteasomal pathway in response to acid functionalized SWNTs in murine monocytic cell line-RAW264.7. The down-regulation of proteasomal proteins may target the quality control system of the cell as these are responsible for degradation of misfolded or damaged proteins [123] and major degenerative diseases have been reported to be caused due to intranuclear accumulation of proteins for ex: polyglutamine (polyQ)-containing proteins [124].

Another important component of efficient protein turnover in the cell is ubiquitination. Down-regulation of protein ubiquitination pathway has been seen in case of lower concentration in both the CNTs. Ubiquitation is involved in many intracellular pathways and is important in protein trafficking, particularly endocytosis and targeting of proteins to recycling or degradative pathways. One potentially important aspect of the altered activity of protein ubiquitination pathway determines increased susceptibility to tumors. For example, beta-catenin interacts with the tumor suppressor protein that regulates its intracellular level. Down-regulation of degradation of beta-catenin leads to its stabilization, accumulation and oncogenic activation [125]. Therefore, CNT exposure may long term exhibit oncogenic properties.

One of the common effects seen in the case of low dose exposure of both CNTs is down-regulation of RAN signaling (Table 16). RAN is a Ras-like GTPase that regulates the nucleocytoplasmic transport of proteins. Miyamoto *et al.* (2004) have shown that the classical RAN mediated nuclear import pathway is down-regulated in response to stress [126]. In this regard, exposure to nanotubes mimic cellular stress. However the expression of typical cellular stress related proteins such as SOD (superoxide dismutase) and GST (glutathione-S-transferase) were not changed. This may be a depiction of cellular response that follows the initial injury.

This is also true for all other proteins associated typically with ROS production, cellular stress or toxicity. Among the proteins that were analyzed and were not differentially expressed was macrophage migration inhibitory factor (MIF), whose expression has been reported to change with exposure to NPs in several studies [127] [128] [129]. MIF is a typical inflammatory cytokine and mediates multiple functions in innate and acquired immunity [130]. This is in direct

agreement with cytokine assay that did not point to any type of irritation or inflammation in these cells. The expression of MAPK (mitogen-activated protein kinase), an initiator of inflammation through activation of pro-inflammatory signaling cascades was also analyzed but was not altered. Other proteins whose expression did not change were GLYR1 (putative oxidoreductase GLYR1), HYOU1 (hypoxia up-regulated protein 1), IKBKG (NF-kappa-B essential modulator), IL-18 (interleukin-18), ILF-2 and 3 (interleukin enhancer-binding factor 2 and 3), GSTM 2, 3 and 4 (glutathione-S-transferase Mu 2, 3 and 4), GSTO1 (glutathione-S-transferase-omega 1), PRDX 6, 4 and 2 (peroxiredoxin-6, 4 and 2), CSF1 (macrophage colony stimulating factor 1), SOD 1 and 2 (superoxide dismutase 1 and 2), TXN and TXNRD2 (thioredoxin and thioredoxin reductase 2), OXR 1 (oxidation resistance protein 1), CAT (catalase) and GSS (glutathione synthetase). This supports the TEER studies as none of the treatment in these experiments killed the cells. The TEER was altered while the cells were still viable.

The cellular processes affected by CNT exposure in this study were similar to those affected by *in vitro* exposure of human monoblastic leukemia cells to 10 mg/ml MWCNT by Haniu *et al.* [121]. Haniu *et al.* reported altered cellular processes like general metabolism (lipid and protein metabolic processes, catalytic process, biosynthetic process, and carbohydrate metabolic process), translation, cell cycle (cell death, cell proliferation, cell differentiation) and signaling. With the exception of lipid metabolic process and response to stress, all these cellular processes were also observed to be affected by both CNT treatments in our study. The results are also similar to *in vivo* study done by Teeguarden *et al*. where pulmonary response of C57BL/6 mice to repeated exposures (pharyngeal aspiration, 40 µg, twice a week for three weeks) to SWCNTs was proteomically studied [131]. The majority of the cellular processes were nonspecific, including general metabolism (lipid and protein metabolic processes, catalytic process, biosynthetic process, and carbohydrate metabolic process), regulation (transcription and translation), cell cycle (cell death, cell proliferation, cell differentiation, and multicellular organismal development), and signaling (signal transduction/cell communication). Since the concentrations used in this study are first to be used as per our knowledge, there are a limited number of proteomic-based studies to compare with.

Many investigators have found that there is a dose and exposure time requirement for carbon nanoparticles to produce damage in living biological cells and tissues. Our studies add an important aspect to this. Using physiologically relevant concentrations of nanoparticles which are very low as compared to most of the concentrations used in similar studies is very important in understanding the effects of these nanoscale materials. Also, the duration of exposure may be even more predictive of damage done by the CNPs as demonstrated in 48 h, 24 h and 1 h exposure study in Calu-3 cells. More studies need to be done to characterize the biological reactivity profile and toxicity of nanoscale materials.

TABLES

Table 1 Results of AFM – Roughness (Ra) Values on Cell Surface

CNP	Ra values
Blank	147.5
SWNT 0.4 μg/cm^2	113.5
MWNT 0.4 μg/cm^2	160.1
C_{60} 40 μg/cm^2	622.2
SWNT 40 μg/cm^2	432.2
MWNT 40 μg/cm^2	214.0

Table 2 Zeta Potential (mV) of the CNPs in media

Zeta potential of the control=-4.74 mV

	C60	SWNT	MWNT
4 μg/cm^2	-7.02	-8.88	-3.00
0.4 μg/cm^2	-9.16	-8.54	-6.71
0.04 μg/cm^2	-9.66	-5.00	-7.24
4 ng/cm^2	-8.20	-5.48	-6.98
0.4 ng/cm^2	-4.83	-9.94	-4.62
0.04 ng/cm^2	-8.01	-6.67	-7.25
4 pg/cm^2	-9.10	-8.62	-7.20

Table 3 Lactate Dehydrogenase Measurements and response to 48 h CNT exposure

CNT dose	C (A)	C (B)	C60 (A)	C60 (B)	SW (A)	SW (B)	MW (A)	MW (B)
0.4 µg/cm^2	1.87	0.27	1.47	0.28	1.63	0.49	1.53	0.33
4 µg/cm^2	2.02	0.22	2.13	0.36	1.71	0.21	2.00	0.45
40 µg/cm^2	2.10	0.36	1.94	0.33	1.62	0.38	2.48	0.34

(A)=apical, (B)=basolateral. Values are mean optical densities, Apical MW 40 µg/cm^2 is significantly different from other doses, $P<0.001$, via ANOVA

Table 4 Inflammatory Cytokine Measurements and Response to 40 µg/cm^2 of CNT Exposure for 48 h

	C (A)	C (B)	C60 (A)	C60 (B)	SW (A)	SW (B)	MW (A)	MW (B)
IL-1A	0.273	0.342	0.298	0.297	0.369	0.370	0.334	0.344
IL-1B	0.406	0.429	0.448	0.388	0.419	0.452	0.432	0.422
G-CSF	2.262	1.329	2.150	1.561	2.429	1.031	2.190	1.694
GM-CSF	0.401	0.405	0.513	0.377	0.541	0.394	0.500	0.422
MCP-1	0.305	0.323	0.308	0.310	0.368	0.335	0.318	0.349
MIP-1A	0.354	0.324	0.3709	0.3253	0.350	0.341	0.413	0.397
SCF	0.301	0.351	0.3283	0.3045	0.375	0.364	0.303	0.334
RANTES	1.318	1.513	0.988	1.795	1.079	1.292	0.927	2.766

(A)=apical, (B)=basolateral. Values are mean optical densities, values in red are significantly different from corresponding control, P<0.01 via ANOVA and multiple range test

Table 5 Number of Proteins Altered ($P \leq 0.01$) by CNP Exposure in mpkCCD_{cl4} cells

CNP	CNP Dose (µg/cm^2)		
	0.004	0.04	40
C_{60}	61	16	5
SWNT	116	29	12
MWNT	105	17	10

Table 6 mpkCCD$_{cl4}$ Cell Proteins Altered in both Low Dose Exposures (0.004 and 0.04 μg/cm^2) in Response to Specific CNP

CNP	Gene ID	Protein name
C_{60}	CPPED1	calcineurin-like phosphoesterase domain containing 1 ▲,▼
SWNT	ACBD3	acyl-Coenzyme A binding domain containing 3 ▲,▲
	GAPDHS	glyceraldehyde-3-phosphate dehydrogenase ▲,▲
	H2AFX	histone family, member X ▲,▲
	MIF	macrophage migration inhibitory factor (glycosylation-inhibiting factor) ▲,▲
	RPL17	ribosomal protein L17 ▼,▼
	RPL27	ribosomal protein L27 ▼,▼
	EG237361	ribosomal protein L27a ▼,▼
	RPS8	ribosomal protein S8 ▼,▼
	GM5121	ribosomal protein S8 isoform 1 ▼,▼
	RPS17	ribosomal protein S17 ▼,▼
	SECTM1B	secreted and transmembrane 1B ▼,▼
MWNT	H2AFJ	H2A histone family, member J ▲,▼
	H2AFX	H2A histone family, member X ▲,▼
	H2AFY	H2A histone family, member Y ▲,▼
	HIST2H2AC	histone cluster 2, H2ac ▲,▼
	HADH	hydroxyacyl-Coenzyme A dehydrogenase ▼,▲
	SHMT2	serine hydroxymethyltransferase 2 (mitochondrial) ▼,▲

In each row, the first arrow refers to change associated with the 0.004 μg/cm^2 exposure; the second arrow refers to change associated with the 0.04 μg/cm^2 exposure.

Table 7 mpkCCD$_{cl4}$ Cell Proteins Altered by all CNPs (C_{60}, SWNT, MWNT) at the Lowest Dose (0.004 μg/cm^2)

Gene ID	Protein name
HIST1H2BF	histone cluster 1, H2bf ▲,▲,▼
HNRNPU	heterogeneous nuclear ribonucleoprotein U ▼,▼,▼
LHX9	LIM homeobox 9 ▼,▼,▼
MYBBP1A	MYB binding protein (P160) 1a ▼,▼,▼
PDE2A	phosphodiesterase 2A, cGMP-stimulated ▲,▲,▲
PIWIL1	piwi-like 1 (Drosophila) ▼,▲,▼
TMPO	thymopoietin ▼,▼,▼

In each row, the first arrow refers to the effect of C_{60}; the second arrow refers to the effect of SWNT; and the third arrow refers to the effect of MWNT.

Table 8 mpkCCD$_{cl4}$ Cell Proteins Altered by both SWNT and MWNT Exposures at the Lowest Dose (0.004 μg/cm^2)

Gene ID	Protein name
ACBD3	acyl-Coenzyme A binding domain containing 3 ▲,▼
AHNAK	AHNAK nucleoprotein ▼,▼
DNAHC9	dynein, axonemal, heavy chain 9 ▲,▼
GAPDH	glyceraldehyde-3-phosphate dehydrogenase ▲,▼
H2AFX	H2A histone family, member X ▲,▼
H2AFY	H2A histone family, member Y ▲,▼
HIST1H2BF	histone cluster 1, H2bf ▲,▼
HNRNPU	heterogeneous nuclear ribonucleoprotein U (scaffold attachment factor A) ▼,▼
KCNN3	K+ intermediate/small conductance Ca++-activated channel, subfamily N, member 3 ▲,▼
LHX9	LIM homeobox 9 ▼,▼
ABCG3	similar to ATP-binding cassette transporter ▲,▼
MAT2B	methionine adenosyltransferase II, beta ▼,▲
MIF	macrophage migration inhibitory factor (glycosylation-inhibiting factor)
MYBBP1A	MYB binding protein (P160) 1a ▼,▼
OIP5	Opa interacting protein 5 ▲,▼
PDE2A	phosphodiesterase 2A, cGMP-stimulated ▲,▲
PFN1	profilin 1 ▼,▲
PIWIL1	piwi-like 1 (Drosophila) ▲,▼
PPIL1	peptidylprolyl isomerase (cyclophilin)-like 1 ▼,▼
RDH5	retinol dehydrogenase 5 (11-cis/9-cis) ▲,▼
RPS5	ribosomal protein S5 ▼,▼
SHMT1	serine hydroxymethyltransferase 1 (soluble) ▼,▲
SHMT2	serine hydroxymethyltransferase 2 (mitochondrial) ▼,▲
SLC39A10	solute carrier family 39 (zinc transporter), member 10 ▲,▼
TLN1	talin 1 ▼,▲
TMPO	thymopoietin ▼,▼

In each row, the first arrow refers to the effect of SWNT; the second arrow refers to the effect of MWNT

Table 9 Functional Networks in mpkCCD$_{cl4}$ Cells Impacted by CNP Exposure (P≤0.001)

CNP	Protein name
Fullerene 0.004 μg/cm^2 (34▲; 27▼)	Gene Expression, Cell Death, Energy Production (13▲; 4▼) Cancer, Cellular Growth & Proliferation, Cell Cycle (6▲; 6▼)
Fullerene 0.04 μg/cm^2 (11▲; 5▼)	No significant relationship to networks
Fullerene 40 μg/cm^2 (4▲; 1▼)	No significant relationship to networks
SWNT 0.004 μg/cm^2 (57▲; 59▼)	Protein Synthesis, Gene Expression, Cellular Growth & Proliferation (4▲; 14▼) Carbohydrate Metabolism, Cancer, Genetic Disorder (13▲; 4▼) Cell Movement, Connective Tissue Development & Function (8▲; 5▼)
SWNT 0.04 μg/cm^2 (14▲; 15▼)	Cancer, Cell Death, Cellular Growth & Proliferation (7▲; 6▼)
SWNT 40 μg/cm^2 (7▲; 5▼)	No significant relationship to networks
MWNT 0.004 μg/cm^2 (45▲; 60▼)	Cancer, Cell Cycle, Cell Death (7▲; 8▼) Inflam. Disease, CT Disorders, Skeletal & Muscular Disorders (9▲; 7▼) Cell Death, Neurological Disease, Connective Tissue Disorders (10▲; 4▼) Endocrine Disorders, Cellular Movement, Metabolic Disease (9▲; 7▼)
MWNT 0.04 μg/cm^2 (10▲; 7▼)	DNA Replication, Recombination & Repair, Cancer, Genetic Disorder (3▲; 2▼)
MWNT 40 μg/cm^2 (3▲; 7▼)	No significant relationship to networks

Numbers in parentheses indicate proteins whose abundance increased ▲ and decreased ▼

Table 10 Canonical Pathways in mpkCCD$_{cl4}$ cells Impacted by CNP Exposure (only ≥3 proteins) (P<0.001)

CNP	Canonical Pathway
C_{60} 0.004 μg/cm^2	Fatty Acid Elongation in Mitochondria ▲ Glycolysis/Gluconeogenesis ▲▼ Mitochondrial Dysfunction ▲ Methane Metabolism ▲ Phenylalanine, Tyrosine and Tryptophan Biosynthesis ▲
C_{60} 0.04 μg/cm^2	No multiprotein pathways
C_{60} 40 μg/cm^2	No multiprotein pathways
SWNT 0.004 μg/cm^2	Glycolysis/Gluconeogenesis ▲ Pentose Phosphate Pathway ▲ Galactose Metabolism ▲ Fructose and Mannose Metabolism ▲ Methane Metabolism ▼
SWNT 0.04 μg/cm^2	Tight Junction Signaling ▲ NRF2-mediated Oxidative Stress Response ▲
SWNT 40 μg/cm^2	Xenobiotic Metabolism Signaling ▼ NRF2-mediated Oxidative Stress Response
MWNT 0.004 μg/cm^2	Glycolysis/Gluconeogenesis ▲ Methane Metabolism ▲ One Carbon Pool by Folate ▲ Glycine, Serine and Threonine Metabolism ▲ Cellular Effects of Sildenafil
MWNT 0.04 μg/cm^2	Lysine Degradation ▼
MWNT 40 μg/cm^2	No multiprotein pathways

Arrows indicate whether proteins in those pathways increased ▲ or decreased ▼or both ▲▼;Shaded areas emphasize pathways common to all 3 CNPs

Table 11 Number of Proteins Altered (P≤0.01) by CNT Exposure in Calu-3 Cells

CNP	CNP dose (μg/cm^2)	
	0.4	0.004
SWNT	13	281
MWNT	8	282

Table 12 Number of Calu-3 Proteins Altered in High Dose (0.4 μg/cm^2) Exposures (p<.01)

▼=Decrease, ▲=Increase

CNP	Gene name	Protein name
MWNT	GGH	Gamma-glutamyl hydrolase▼
	HINT1	Histidine triad nucleotide-binding protein 1▼
	-	cDNA FLJ43348 fis, clone NT2RI3008974, Probable transposase▼
	VARSL	Valyl-tRNA synthetase like▼
	HIBADH	3-hydroxyisobutyrate dehydrogenase▼
	COX5A	Cytochrome c oxidase subunit 5A, mitochondrial▲
	FH	Fumarate hydratase, mitochondrial▲
	IDH2	Isocitrate dehydrogenase [NADP], mitochondrial▲
SWNT	GGH	Gamma-glutamyl hydrolase▼
	HINT1	Histidine triad nucleotide-binding protein 1▼
	DF4	DF4▲
	ERO1L	ERO1-like protein alpha▼
	-	cDNA FLJ43348 fis, clone NT2RI3008974, Probable transposase▼
	PDCD6IP	Programmed cell death 6-interacting protein▼
	VARSL	Valyl-tRNA synthetase like▼
	RCN1	Reticulocalbin-1▼
	RPS3	Ribosomal protein S3▼
	MTPN	Myotrophin▼
	SUMF2	Sulfatase modifying factor 2 isoform d precursor▼
	EPRS	Glutamyl-prolyl-tRNA synthetase ▲
	ERP29	Endoplasmic reticulum resident protein 29▼

Table 13 Number of Calu-3 Proteins Altered in both SWNT and MWNT at High Dose (0.4 μg/cm^2) exposures (p<.01)

First▼=decrease for SWNT, Second▼=decrease for MWNT

Gene name	Protein name
GGH	Gamma-glutamyl hydrolase▼▼
HINT1	Histidine triad nucleotide-binding protein 1▼▼
-	cDNA FLJ43348 fis, clone NT2RI3008974, Probable transposase▼▼
VARSL	Valyl-tRNA synthetase like▼▼

Table 14 Functional Networks in Calu-3 Cells Impacted by CNP Exposure (p≤0.001)

CNP	Functional networks
SWCNT 0.004 μg/cm^2	RNA post transcriptional modification, Molecular Transport, Protein Trafficking (1▲; 29▼) Protein Synthesis, Cell Signaling, Infection Mechanism (0▲;31▼) Cancer, Gastrointestinal Disease, Inflammatory Disease (0▲;27▼) Cell-To-Cell Signaling and Interaction, Hematological System Development and Function, Immune Cell Trafficking (0▲;23▼) Gene Expression, Nucleic Acid Metabolism, Small Molecule Biochemistry (0▲;22▼)
MWCNT 0.004 μg/cm^2	Cell-To-Cell Signaling and Interaction, Hair and Skin Development and Function, Tissue Development (0▲;29▼) RNA Post-Transcriptional Modification, Cell Signaling, DNA Replication, Recombination, and Repair (0▲;28▼) Nucleic Acid Metabolism, Small Molecule Biochemistry, DNA Replication, Recombination, and Repair (0▲;31▼) Cell Morphology, Cellular Development, Cancer (0▲;23▼)
SWCNT 0.4 μg/cm^2	Endocrine System Disorders, Gastrointestinal Disease, Inflammatory Disease (1▲;8▼) Cell Death, Liver Necrosis/Cell Death, Cell-mediated Immune Response (0▲;2▼)
MWCNT 0.4 μg/cm^2	Cancer, Carbohydrate Metabolism, Cellular Development (4▲;4▼)
SWCNT 0.004 μg/cm^2 & MWCNT 0.004 μg/cm^2	RNA Post-Transcriptional Modification, Cell Morphology, Cellular Function and Maintenance (0▲;32▼) Cell-To-Cell Signaling and Interaction, Hair and Skin Development and Function, Tissue Development (0▲;25▼) Cellular Assembly and Organization, Cellular Function and Maintenance, Cancer (0▲;28▼) Post-Translational Modification, Protein Synthesis, Carbohydrate Metabolism (0▲;23▼) Lipid Metabolism, Small Molecule Biochemistry, Molecular Transport (0▲;20▼)

Numbers in parentheses indicate proteins whose abundance increased ▲and decreased ▼

Table 15 Canonical Pathways in Calu-3 Cells Impacted by CNP Exposure (P≤0.001)

CNP	Canonical pathway
SWCNT 0.004 μg/cm^2	RAN Signaling ▼ Aminoacyl-tRNA Biosynthesis ▼ Caveolar-mediated Endocytosis Signaling ▼ Actin Cytoskeleton Signaling ▼ Protein Ubiquitination Pathway ▼
MWCNT 0.004 μg/cm^2	Protein Ubiquitination Pathway ▼ RAN Signaling ▼ Huntington's Disease Signaling ▼ Starch and Sucrose Metabolism ▼ Mitochondrial Dysfunction ▼
SWCNT 0.4 μg/cm^2	Aminoacyl-tRNA Biosynthesis ▼▲ Valine, Leucine and Isoleucine Biosynthesis ▼ Folate Biosynthesis ▼ Glutamate Metabolism ▲ Mechanisms of Viral Exit from Host Cells ▼
MWCNT 0.4 μg/cm^2	Citrate Cycle ▲ Valine, Leucine and Isoleucine Biosynthesis ▲ Folate Biosynthesis ▼ Pentose Phosphate Pathway ▼ Aminoacyl-tRNA Biosynthesis ▼
SWCNT 0.004 μg/cm^2 & MWCNT 0.004 μg/cm^2	RAN Signaling ▼ Actin Cytoskeleton Signaling ▼ Protein Ubiquitination Pathway ▼ Aminoacyl-tRNA Biosynthesis RhoA Signaling ▼

Arrows indicate whether proteins in those pathways increased ▲ or decreased ▼, or both

Table 16 Number of Calu-3 Proteins Altered in Low Dose (0.004 μg/cm^2) Exposures=563 (p<.01)

▼=Decrease, ▲=Increase

CNP	Gene name	Protein name
MWNT	PFKL	Phosphofructokinase, liver ▼
	PSMA4	Proteasome (prosome, macropain) subunit, alpha type, 4 ▼
	SH3BGRL	SH3 domain-binding glutamic acid-rich-like protein ▼
	ARF1	ADP-ribosylation factor 1 ▼
	N4BP2L2	NEDD4-binding protein 2-like 2, Isoform 1 ▼
	C1orf198	C1orf198 ▼
	PPP1R11	Protein phosphatase 1 regulatory subunit 11 ▼
	MCM10	Minichromosome maintenance complex component 10 ▼
	GSN	Gelsolin, Isoform 1 ▼
	PFKP	Phosphofructokinase, platelet ▼
	GSN	Gelsolin ▼
	ITGB1	Integrin, beta 1C ▼
	RPS28	Ribosomal protein S28 ▼
	HEXA	Hexosaminidase A (alpha polypeptide) ▼
	AHNAK	AHNAK nucleoprotein ▼
	C19orf10	C19orf10 (Stromal cell-derived growth factor SF20) ▼
	RPS10	Ribosomal protein S10 ▼
	PSMD13	Proteasome (prosome, macropain) 26S subunit, non-ATPase, 13 ▼
	TARDBP	TAR DNA-binding protein 43, Isoform 2 ▼
	CTSC	Cathepsin C ▼
	XRCC6	X-ray repair cross-complementing protein 6 ▼
	MTAP	Methylthioadenosine phosphorylase ▼
	ITGB1	Integrin, beta 1A ▼
	RRBP1	Ribosome-binding protein 1, Isoform 3 ▼
	HSP90AA1	Heat shock protein HSP 90-alpha, Isoform 2 ▼
	IPO5	Importin 5, Isoform 1 ▼
	EZR	Ezrin ▼
	FLOT1	Flotillin 1 ▼
	GMPS	Guanine monphosphate synthetase ▼
	XRCC6	X-ray repair cross-complementing protein 6 ▼
	DHX9	DEAH (Asp-Glu-Ala-His) box polypeptide 9 ▼
	PPP2R1A	Protein phosphatase 2, regulatory subunit A, alpha ▼
	PSMC2	Proteasome (prosome, macropain) 26S subunit, ATPase, 2 ▼

PFKL	Desmoplakin Ia▼
PSMA4	Serpin peptidase inhibitor, clade B (ovalbumin), member 6▼
SH3BGRL	Growth factor receptor-bound protein 7, Isoform 1▼
ARF1	Heat shock-related 70 kDa protein 2▼
N4BP2L2	Thioredoxin▼
C1orf198	Cathepsin D ▼
PPP1R11	X-ray repair cross-complementing protein 5▼
MCM10	X-ray repair cross-complementing protein 6▼
GSN	Poteasome (prosome, macropain) 26S subunit, non-ATPase, 9▼
PFKP	Phosphatidylinositol transfer protein beta isoform 1▼
GSN	Ropporin, rhophilin associated protein 1, Isoform 2▼
ITGB1	Capping protein (actin filament) muscle Z-line, alpha 2▼
RPS28	
HEXA	UDP-glucose 6-dehydrogenase▼
AHNAK	Actin related protein 2/3 complex, subunit 2▼
C19orf10	RNA binding motif protein, X-linked-like 1▼
RPS10	Proteasome (prosome, macropain) 26S subunit, non-ATPase, 2▼
PSMD13	Heterogeneous nuclear ribonucleoprotein H▼
TARDBP	Transmembrane emp24 domain-containing protein 10▼
CTSC	
XRCC6	X-ray repair cross-complementing protein 6▼
MTAP	Aldo-keto reductase family 1, member C2▼
ITGB1	Protein phosphatase 2, regulatory subunit A, alpha▼
RRBP1	Heterogeneous nuclear ribonucleoprotein G isoform 2▼
HSP90AA1	
IPO5	Profilin 2▼
EZR	Guanine nucleotide binding protein (G protein), beta polypeptide 2▼
FLOT1	
GMPS	Apolipoprotein A-I▼
XRCC6	Solute carrier family 9 (sodium/hydrogen exchanger), member 3 regulator 1▼
DHX9	
PPP2R1A	Guanine nucleotide-binding protein subunit beta-2-like 1▼
PSMC2	
	Importin subunit alpha-2▼
DSP	Hydroxysteroid (17-beta) dehydrogenase 4▼
SERPINB6	Interferon-induced GTP-binding protein Mx1▼
	Lysophospholipase II▼
GRB7	Histone H2B type 1-B▼
HSPA2	Staphylococcal nuclease domain-containing protein 1▼
TXN	
CTSD	Tumor protein, translationally-controlled 1▼
XRCC5	Desmoplakin, Isoform DPII▼
XRCC6	Heterogeneous nuclear ribonucleoprotein U, Isoform

CTNNA1	Catenin alpha-1▼
MVP	Major vault protein▼
CAPZA2	Capping protein (actin filament) muscle Z-line, alpha 2▼
TRPM7	Transient receptor potential cation channel, subfamily M, member 7▼
EEF1A1	Eukaryotic translation elongation factor 1 alpha 1▼
DSP	Desmoplakin, Isoform DPI▼
TMPO	Lamina-associated polypeptide 2, isoform alpha (thymopoietin)
XPO1	Exportin 1▼
CDH1	Cadherin 1, type 1, E-cadherin (epithelial) ▼
KRT7	Keratin, type II cytoskeletal 7▼
HNRNPH1	Heterogeneous nuclear ribonucleoprotein H▼
PFKP	Phosphofructokinase, platelet▼
GAA	Glucosidase, alpha; acid, lysosomal▼
CTNNBL1	Catenin, beta like 1, Isoform 2▼
LAP3	Leucine aminopeptidase 3, Isoform 2▼
HNRNPD	Heterogeneous nuclear ribonucleoprotein D▼
RBMX	Heterogeneous nuclear ribonucleoprotein G▼
HNRNPD	Heterogeneous nuclear ribonucleoprotein D▼
RPS3A	Ribosomal protein S3a▼
MYH9	Myosin 9, Isoform 1▼
MYL6B	Myosin, light chain 6B, alkali, smooth muscle and non-muscle▼
RBMXL1	RNA binding motif protein, X-linked-like 1▼
EIF4A2	Eukaryotic initiation factor 4A-II, Isoform 1▼
RPLP0	Ribosomal protein P0, acidic▼
RPLP0	Ribosomal protein P0, acidic▼
MAPRE2	Microtubule-associated protein RP/EB family member 2▼
EHD1	EH domain-containing protein 1▼
RPL32	Ribosomal protein L32▼
PRDM8	PR domain zinc finger protein 8, Isoform 1▼
PDIA6	Protein disulfide-isomerase A6, Isoform 2▼
JUP	Junction plakoglobin▼
HNRNPAB	Isoform 4 of Heterogeneous nuclear ribonucleoprotein A/B▼
SPR	Sepiapterin reductase▼
CTNNA1	Catenin alpha-1, Isoform 2▼
LYPLA2	Lysophospholipase II▼
GALNT2	UDP-N-acetyl-alpha-D-galactosamine:polypeptide N-acetylgalactosaminyltransferase 2 (GalNAc-T2) ▼
EIF3B	Eukaryotic translation initiation factor 3 subunit B, Isoform 1▼
GRB7	Growth factor receptor-bound protein 7▼

LAP3	Leucine aminopeptidase 3▼
STIP1	Stress-induced-phosphoprotein 1▼
PDIA4	Protein disulfide-isomerase A4▼
MYH14	myosin-14 isoform 1▼
TYMP	Thymidine phosphorylase▼
EEF2	Elongation factor 2▼
CLTC	Isoform 1 of Clathrin heavy chain 1▼
ATP1A1	Isoform Long of Sodium/potassium-transporting ATPase subunit alpha-1▼
PYCARD	Isoform 1 of Apoptosis-associated speck-like protein containing a CARD▼
HARS	cDNA FLJ58554, highly similar to Histidyl-tRNA synthetase▼
ELAVL1	cDNA FLJ60076, highly similar to ELAV-like protein 1▼
SRRM1	cDNA FLJ61739, highly similar to Serine/arginine repetitive matrix protein 1▼
SUN2	Unc-84 homolog B▼
CHD4	Isoform 1 of Chromodomain-helicase-DNA-binding protein 4▼
LGALS3BP	cDNA FLJ53509, highly similar to Galectin-3-binding protein▼
KPNB1	Importin subunit beta-1▼
ASAH1	cDNA FLJ40980 fis, clone UTERU2014464, highly similar to ACID CERAMIDASE▼
HARS	Histidyl-tRNA synthetase, cytoplasmic▼
PSAP	Isoform Sap-mu-0 of Proactivator polypeptide▼
HSD17B10	Hydroxysteroid (17-beta) dehydrogenase 10▼
HEXB	Beta-hexosaminidase subunit beta▼
HEXB	ENC-1AS▼
CDV3 hCG_14782	CDV3 homolog (Mouse), isoform CRA_a▼
FLJ44635	TPT1-like protein▼
HNRNPR	heterogeneous nuclear ribonucleoprotein R isoform 3▼
ATP1A3	Sodium/potassium-transporting ATPase subunit alpha-3▼
CAND1	Isoform 1 of Cullin-associated NEDD8-dissociated
PARK7	protein 1▼
-	Protein DJ-1▼
ASH2L	Isoform 1 of Set1/Ash2 histone methyltransferase complex subunit ASH2▼
CHCHD2	Coiled-coil-helix-coiled-coil-helix domain-containing protein 2, mitochondrial▼
CS	Citrate synthase, mitochondrial▼
S100A13	S100 calcium binding protein A13▼
REXO2	Oligoribonuclease, mitochondrial, Isoform 1▼
OLA1	Obg-like ATPase 1▼

EIF3L	Eukaryotic translation initiation factor 3 subunit 6-interacting protein▼
ARF1	ADP-ribosylation factor 1▼
PPL	Periplakin▼
UNC80	Unc-80 homolog, Isoform 1▼
PDHB	Pyruvate dehydrogenase E1 component subunit beta, mitochondrial▼
PLS3	plastin 3, Isoform 2▼
ANXA1	Annexin A1▼
G3BP1	GTPase activating protein (SH3 domain) binding protein 1▼
USP5	Isoform Long of Ubiquitin carboxyl-terminal hydrolase 5▼
SEPT9	septin-9 isoform e▼
ADD1	Isoform 1 of Alpha-adducin▼
GMPS	GMP synthase [glutamine-hydrolyzing] ▼
CAD	CAD protein▼
OLA1	Isoform 3 of Obg-like ATPase 1▼
NOD1	Nucleotide-binding oligomerization domain-containing protein 1▼
FANCI	Isoform 1 of Fanconi anemia group I protein▼
HNRNPR	Isoform 1 of Heterogeneous nuclear ribonucleoprotein R▼
PCBP2	cDNA FLJ54752, highly similar to Poly(rC)-binding protein 2▼
ATP5B	ATP synthase subunit beta, mitochondrial▼
MVP	cDNA FLJ53437, highly similar to Major vault protein▼
AKR7A2	Aflatoxin B1 aldehyde reductase member 2▼
HSPA4	Heat shock 70 kDa protein 4▼
YARS	Tyrosyl-tRNA synthetase, cytoplasmic▼
HNRNPAB	Isoform 2 of Heterogeneous nuclear ribonucleoprotein A/B▼
PYGB	Glycogen phosphorylase, brain form▼
SFPQ	Isoform Long of Splicing factor, proline- and glutamine-rich▼
YWHAQ	14-3-3 protein theta▼
CAND1	Isoform 2 of Cullin-associated NEDD8-dissociated protein 1▼
HNRNPD	Isoform 1 of Heterogeneous nuclear ribonucleoprotein D0▼
CAPZB	Capping protein (Actin filament) muscle Z-line, beta▼
LOC652147	similar to U5 snRNP-specific 200kD protein, partial▼
MYOF	Uncharacterized protein▼
PLS1	Plastin-1▼
LMNA	Isoform A of Prelamin-A/C▼
PTGES3	Prostaglandin E synthase 3▼

TPT1	Tumor protein, translationally-controlled 1▼
ARCN1	Coatomer subunit delta variant 2▼
TPT1	cDNA FLJ57738, highly similar to Translationally-controlled tumor protein▼
GGCT	Isoform 1 of Gamma-glutamylcyclotransferase▼
MDH2	Malate dehydrogenase, mitochondrial▼
ESYT1	Isoform 1 of Extended synaptotagmin-1▼
NME1-NME2	Isoform 1 of Nucleoside diphosphate kinase A▼
RAB1A	Ras-related protein Rab-1A, Isoform 3▼
PSMB3	Proteasome subunit beta type-3▼
HDGF	Hepatoma-derived growth factor▼
OLA1	Obg-like ATPase 1▼
MTAP	Methylthioadenosine phosphorylase ▼
P4HB	Prolyl 4-hydroxylase, beta polypeptide▼
BZW2	Basic leucine zipper and W2 domain-containing protein 2▼
UQCRFSL1	Ubiquinol-cytochrome c reductase, Rieske iron-sulfur polypeptide-like 1▼
ATP5A1	ATP synthase subunit alpha, mitochondrial▼
PLS3	Plastin 3▼
NDUFS3	NADH dehydrogenase [ubiquinone] iron-sulfur protein 3, mitochondrial▼
-	cDNA FLJ56734, moderately similar to Sepiapterin reductase
SEPT9	septin-9 isoform a▼
IKZF3	Isoform 1 of Zinc finger protein Aiolos▼
IL18	Interleukin-18▼
STAT1	Isoform Alpha of Signal transducer and activator of transcription 1-alpha/beta▼
PCBP2	poly(rC)-binding protein 2 isoform c▼
PSMC1	26S protease regulatory subunit 4▼
HNRNPA2B1	heterogeneous nuclear ribonucleoprotein A2/B1▼
EIF3I	Eukaryotic translation initiation factor 3 subunit I▼
BAT3	cDNA FLJ60983, highly similar to Large proline-rich protein BAT3▼
HSPA1A;HSPA1B	Heat shock 70 kDa protein 1A/1B▼
AGRN	Agrin▼
MYOF	Isoform 1 of Myoferlin▼
AKR1C2	Aldo-keto reductase family 1 member C2▼
PFN2	Profilin 2▼
CETN2	Centrin-2▼
SLC44A4	Solute carrier family 44, member 4▼
SCP2	Sterol carrier protein 2, Isoform 2▼
PIN1	Peptidyl-prolyl cis-trans isomerase (Putative uncharacterized protein) ▼
SPTBN1	Spectrin beta chain, Isoform Long▼

ITGAE	Integrin alpha-E▼
CFL1	Cofilin-1▼
-	cDNA FLJ53754, highly similar to Transmembrane emp24 domain-containing protein 10▲
SF3B1	Splicing factor 3B subunit 1▼
DYNLL1	Dynein light chain 1, cytoplasmic▼
MYH14	Isoform 1 of Myosin-14▼
LAMP1	Lysosome-associated membrane glycoprotein 1▼
KRT1	Keratin, type II cytoskeletal 1▼
RNH1	Ribonuclease inhibitor▼
HNRNPA2B1	Isoform B1 of Heterogeneous nuclear ribonucleoproteins A2/B1▼
SERPINA1	Isoform 1 of Alpha-1-antitrypsin▼
NAP1L1	Nucleosome assembly protein 1-like 1▼
IGF2BP2	Isoform 1 of Insulin-like growth factor 2 mRNA-binding protein 2▼
ARF4	ADP-ribosylation factor 4▼
RASA1	Isoform 1 of Ras GTPase-activating protein 1▼
ETF1	Eukaryotic peptide chain release factor subunit 1▼
MPST	3-mercaptopyruvate sulfurtransferase▼
NCL	Nucleolin▼
ETF1	Uncharacterized protein▼
RAB1A	Ras-related protein Rab-1A, Isoform 2▼
BOP1	Ribosome biogenesis protein block of proliferation 1▼
RAB1A	Ras-related protein Rab-1A, Isoform 1▼
CHURC1	Full-length cDNA clone CS0DC015YK16 of Neuroblastoma of Homo sapiens (Fragment) ▼
ATP5C1	Isoform Heart of ATP synthase subunit gamma, mitochondrial▼
PECI	peroxisomal 3,2-trans-enoyl-CoA isomerase isoform 1▼
C10orf79	C10orf79▼
GNB2	Guanine nucleotide binding protein (G protein), beta polypeptide 2▼
CAP1	CAP, adenylate cyclase-associated protein 1▼
SAMHD1	Isoform 1 of SAM domain and HD domain-containing protein 1▼
U2AF2	Isoform 1 of Splicing factor U2AF 65 kDa subunit▼
PPIH	Peptidyl-prolyl cis-trans isomerase H▼
MAPRE1	Microtubule-associated protein RP/EB family member 1▼
PABPC4	Poly(A) binding protein, cytoplasmic 4 (inducible form) ▼
SAE1	SUMO-activating enzyme subunit 1▼
MCM7	PNAS-146▼
CDV3	Uncharacterized protein▼

	WDR1	WD repeat-containing protein 1▼
	NCSTN	Nicastrin, Isoform 1▼
	SCP2	Sterol carrier protein 2▼
	ACAT2	Acetyl-CoA acetyltransferase, cytosolic▼
	HLA-B	MHC class I antigen (Fragment) ▼
	IRF3	Interferon regulatory factor 3▼
	OSBPL2	Isoform 1 of Oxysterol-binding protein-related protein 2▼
	PABPC4	Isoform 1 of Polyadenylate-binding protein 4▼
	GNB1	Guanine nucleotide-binding protein G(I)/G(S)/G(T) subunit beta-1▼
	ETFA	Electron transfer flavoprotein subunit alpha, mitochondrial▼
	PAPSS2	Isoform A of Bifunctional 3'-phosphoadenosine 5'-phosphosulfate synthase 2▼
	RPL5;SNORD21	Ribosomal protein L5▼
	-	cDNA FLJ60546, highly similar to Homo sapiens bridging integrator 1 (BIN1), transcript variant 3, mRNA▼
	MAPK14	Isoform CSBP2 of Mitogen-activated protein kinase 14▼
	CPVL	Probable serine carboxypeptidase CPVL▼
	SUMF2	sulfatase modifying factor 2 isoform e precursor▼
	SMAP1	Isoform 1 of Stromal membrane-associated protein 1▼
	SAR1A	GTP-binding protein SAR1a▼
	LTA4H	Leukotriene A-4 hydrolase, Isoform 1▼
	C3	Complement C3▼
	GCN1L1	Translational activator GCN1▼
	PAFAH1B1	Isoform 1 of Platelet-activating factor acetylhydrolase IB subunit alpha▼
	HSPA7	Putative heat shock 70 kDa protein 7▼
	MCCC2	Isoform 1 of Methylcrotonoyl-CoA carboxylase beta chain, mitochondrial▼
	MLEC	Malectin▼
	ITIH1	Inter-alpha-trypsin inhibitor heavy chain H1▼
	NEUROD6	cDNA FLJ56829, highly similar to Neurogenic differentiation factor 6▼
	CUTA	Uncharacterized protein▼
SWNT	PFKL	phosphofructokinase, liver ▼
	PSMA4	Proteasome (prosome, macropain) subunit, alpha type, 4 ▼
	SH3BGRL	SH3 domain-binding glutamic acid-rich-like protein▼
	ARF1	ADP-ribosylation factor 1▼
	N4BP2L2	NEDD4-binding protein 2-like 2, Isoform 1▼
	H2AFV	Histone H2A.V▼

PFKL	C1orf198▼
PSMA4	Protein phosphatase 1 regulatory subunit 11▼
SH3BGRL	Minichromosome maintenance complex component 10 ▼
ARF1	Gelsolin, Isoform 1▼
N4BP2L2	Phosphofructokinase, platelet▼
H2AFV	Gelsolin▼
C1orf198	Integrin, beta 1C▼
PPP1R11	Ribosomal protein S28▼
MCM10	Hexosaminidase A (alpha polypeptide) ▼
GSN	AHNAK nucleoprotein▼
PFKP	Signal transducer and activator of transcription 3 (acute-phase response factor) ▼
GSN	Coatomer protein complex, subunit gamma▼
ITGB1	C19orf10 (Stromal cell-derived growth factor SF20) ▼
RPS28	Ribosomal protein S10▼
HEXA	Proteasome (prosome, macropain) 26S subunit, non-
AHNAK	ATPase, 13▼
STAT3	TAR DNA-binding protein 43, Isoform 2▼
COPG	Cathepsin C▼
C19orf10	X-ray repair cross-complementing protein 6▼
RPS10	Methylthioadenosine phosphorylase▼
PSMD13	Integrin, beta 1A▼
TARDBP	Ribosome-binding protein 1, Isoform 3▼
CTSC	Heat shock protein HSP 90-alpha, Isoform 2▼
XRCC6	Importin 5, Isoform 1▼
MTAP	Ezrin▼
ITGB1	Flotillin 1▼
RRBP1	Guanine monphosphate synthetase▼
HSP90AA1	X-ray repair cross-complementing protein 6▼
IPO5	Nicotinate phosphoribosyltransferase domain containing 1▼
EZR	DEAH (Asp-Glu-Ala-His) box polypeptide 9▼
FLOT1	Protein phosphatase 2, regulatory subunit A, alpha▼
GMPS	Proteasome (prosome, macropain) 26S subunit, ATPase, 2▼
XRCC6	Proteasome (prosome, macropain) subunit, alpha
NAPRT1	type, 4 ▼
DHX9	Desmoplakin Ia▼
PPP2R1A	Serpin peptidase inhibitor, clade B (ovalbumin), member 6▼
PSMC2	Growth factor receptor-bound protein 7, Isoform 1▼
PSMA4	Hexosaminidase A (alpha polypeptide) ▼
DSP	Ribosomal protein L3▼
	Heat shock-related 70 kDa protein 2▼
	Thioredoxin▼

CTSD	Cathepsin D ▼
XRCC5	X-ray repair cross-complementing protein 5▼
XRCC6	X-ray repair cross-complementing protein 6▼
PSMD9	Poteasome (prosome, macropain) 26S subunit, non-ATPase, 9▼
AIP	Aryl hydrocarbon receptor interacting protein▼
PITPNB	Phosphatidylinositol transfer protein beta isoform 1▼
ROPN1	Ropporin, rhophilin associated protein 1, Isoform 2▼
CAPZA2	Capping protein (actin filament) muscle Z-line, alpha 2▼
UGDH	UDP-glucose 6-dehydrogenase▼
ARPC2	Actin related protein 2/3 complex, subunit 2▼
RBMXL1	RNA binding motif protein, X-linked-like 1▼
ATP1A2	Sodium/potassium-transporting ATPase subunit alpha-2▼
PSMD2	Proteasome (prosome, macropain) 26S subunit, non-ATPase, 2▼
HNRNPH1	Heterogeneous nuclear ribonucleoprotein H▼
TMED10	Transmembrane emp24 domain-containing protein 10▼
XRCC6	X-ray repair cross-complementing protein 6▼
AKR1C2	Aldo-keto reductase family 1, member C2▼
PPP2R1A	Protein phosphatase 2, regulatory subunit A, alpha▼
RBMX	Heterogeneous nuclear ribonucleoprotein G isoform 2▼
PLS3	Plastin 3 ▼
PFN2	Profilin 2▼
GNB2	Guanine nucleotide binding protein (G protein), beta polypeptide 2▼
APOA1	Apolipoprotein A-I▼
SLC9A3R1	Solute carrier family 9 (sodium/hydrogen exchanger), member 3 regulator 1▼
GNB2L1	Guanine nucleotide-binding protein subunit beta-2-like 1▼
KPNA2	Importin subunit alpha-2▼
HSD17B4	Hydroxysteroid (17-beta) dehydrogenase 4▼
MX1	Interferon-induced GTP-binding protein Mx1▼
LYPLA2	Lysophospholipase II▼
HIST1H2BB	Histone H2B type 1-B▼
SND1	Staphylococcal nuclease domain-containing protein 1▼
TPT1	Tumor protein, translationally-controlled 1▼
DSP	Desmoplakin, Isoform DPII▼
HNRNPU	Heterogeneous nuclear ribonucleoprotein U, Isoform Short▼
CCT6A	Chaperonin containing TCP1, subunit 6A (zeta 1) ▼

RARS	Arginyl-tRNA synthetase, cytoplasmic, Isoform Complexed▼
CTNNA1	Catenin alpha-1▼
MVP	Major vault protein▼
CAPZA2	Capping protein (actin filament) muscle Z-line, alpha 2▼
TRPM7	Transient receptor potential cation channel, subfamily M, member 7▼
EEF1A1	Eukaryotic translation elongation factor 1 alpha 1▼
DSP	Desmoplakin, Isoform DPI▼
TMPO	Lamina-associated polypeptide 2, isoform alpha (thymopoietin) ▼
XPO1	Exportin 1▼
CDH1	Cadherin 1, type 1, E-cadherin (epithelial) ▼
KRT7	Keratin, type II cytoskeletal 7▼
HNRNPH1	Heterogeneous nuclear ribonucleoprotein H▼
PFKP	Phosphofructokinase, platelet▼
GAA	Glucosidase, alpha; acid, lysosomal▼
CTNNBL1	Catenin, beta like 1, Isoform 2▼
LAP3	Leucine aminopeptidase 3, Isoform 2▼
HNRNPD	Heterogeneous nuclear ribonucleoprotein D▼
RBMX	Heterogeneous nuclear ribonucleoprotein G▼
HNRNPD	Heterogeneous nuclear ribonucleoprotein D▼
RPS3A	Ribosomal protein S3a▼
MYH9	Myosin 9, Isoform 1▼
MYL6B	Myosin, light chain 6B, alkali, smooth muscle and non-muscle▼
RBMXL1	RNA binding motif protein, X-linked-like 1▼
EIF4A2	Eukaryotic initiation factor 4A-II, Isoform 1▼
RPLP0	Ribosomal protein P0, acidic▼
RPLP0	Ribosomal protein P0, acidic▼
MAPRE2	Microtubule-associated protein RP/EB family member 2▼
PTGES3	Prostaglandin E synthase 3▼
RPS7	Ribosomal protein S7▼
CUL4B	Cullin-4B, Isoform 2▼
TPM3	Tropomyosin 3▼
RBM14	RNA-binding protein 14▲
SFN	Stratifin ▼
SND1	Staphylococcal nuclease domain-containing protein 1▼
EHD1	EH domain-containing protein 1▼
RPL32	Ribosomal protein L32▼
PRDM8	PR domain zinc finger protein 8, Isoform 1▼
PDIA6	Protein disulfide-isomerase A6, Isoform 2▼
JUP	Junction plakoglobin▼

HNRNPAB	Isoform 4 of Heterogeneous nuclear ribonucleoprotein A/B▼
SPR	Sepiapterin reductase▼
CTNNA1	Catenin alpha-1, Isoform 2▼
LYPLA2	Lysophospholipase II▼
GALNT2	UDP-N-acetyl-alpha-D-galactosamine:polypeptide N-acetylgalactosaminyltransferase 2 (GalNAc-T2) ▼
EIF3B	Eukaryotic translation initiation factor 3 subunit B, Isoform 1▼
GRB7	Growth factor receptor-bound protein 7▼
LAP3	Leucine aminopeptidase 3▼
STIP1	Stress-induced-phosphoprotein 1▼
PDIA4	Protein disulfide-isomerase A4▼
MYH14	myosin-14 isoform 1▼
TYMP	Thymidine phosphorylase▼
EEF2	Elongation factor 2▼
CLTC	Isoform 1 of Clathrin heavy chain 1▼
ATP1A1	Isoform Long of Sodium/potassium-transporting ATPase subunit alpha-1▼
PYCARD	Isoform 1 of Apoptosis-associated speck-like protein containing a CARD▼
HARS	cDNA FLJ58554, highly similar to Histidyl-tRNA synthetase▼
ELAVL1	cDNA FLJ60076, highly similar to ELAV-like protein 1▼
SRRM1	cDNA FLJ61739, highly similar to Serine/arginine repetitive matrix protein 1▼
SUN2	Unc-84 homolog B▼
CHD4	Isoform 1 of Chromodomain-helicase-DNA-binding protein 4▼
LGALS3BP	cDNA FLJ53509, highly similar to Galectin-3-binding protein▼
KPNB1	Importin subunit beta-1▼
ASAH1	cDNA FLJ40980 fis, clone UTERU2014464, highly similar to ACID CERAMIDASE▼
HARS	Histidyl-tRNA synthetase, cytoplasmic▼
PSAP	Isoform Sap-mu-0 of Proactivator polypeptide▼
HSD17B10	Hydroxysteroid (17-beta) dehydrogenase 10▼
HEXB	Beta-hexosaminidase subunit beta▼
HEXB	ENC-1AS▼
CDV3 hCG_14782	CDV3 homolog (Mouse), isoform CRA_a▼
FLJ44635	TPT1-like protein▼
HNRNPR	heterogeneous nuclear ribonucleoprotein R isoform 3▼
ATP1A3	Sodium/potassium-transporting ATPase subunit alpha-3▼
CAND1	Isoform 1 of Cullin-associated NEDD8-dissociated

	protein 1▼
PARK7	Protein DJ-1▼
ASH2L	Isoform 1 of Set1/Ash2 histone methyltransferase complex subunit ASH2▼
CHCHD2	Coiled-coil-helix-coiled-coil-helix domain-containing protein 2, mitochondrial▼
CS	Citrate synthase, mitochondrial▼
-	Chaperonin Cpn60/TCP-1 family protein▼
EEF1G;TUT1	Elongation factor 1-gamma▼
CNDP2	Isoform 1 of Cytosolic non-specific dipeptidase▼
TLN1	Talin-1▼
GSR	Glutathion reductase delta8 alternative splicing variant▼
RNPEP	Uncharacterized protein▼
RAB7A	Ras-related protein Rab-7a▼
ATP1A3	cDNA FLJ59513, highly similar to Sodium/potassium-transporting ATPase alpha-3 chain▼
STAT1	22 kDa protein▼
BANF1	Barrier-to-autointegration factor▼
BTF3	Isoform 1 of Transcription factor BTF3▼
S100A13	S100 calcium binding protein A13▼
REXO2	Oligoribonuclease, mitochondrial, Isoform 1▼
OLA1	Obg-like ATPase 1▼
EIF3L	Eukaryotic translation initiation factor 3 subunit 6-interacting protein▼
ARF1	ADP-ribosylation factor 1▼
PPL	Periplakin▼
UNC80	Unc-80 homolog, Isoform 1▼
PDHB	Pyruvate dehydrogenase E1 component subunit beta, mitochondrial▼
PLS3	plastin 3, Isoform 2▼
ANXA1	Annexin A1▼
G3BP1	GTPase activating protein (SH3 domain) binding protein 1▼
USP5	Isoform Long of Ubiquitin carboxyl-terminal hydrolase 5▼
SEPT9	septin-9 isoform e▼
ADD1	Isoform 1 of Alpha-adducin▼
GMPS	GMP synthase [glutamine-hydrolyzing] ▼
CAD	CAD protein▼
OLA1	Isoform 3 of Obg-like ATPase 1▼
NOD1	Nucleotide-binding oligomerization domain-containing protein 1▼
FANCI	Isoform 1 of Fanconi anemia group I protein▼
HNRNPR	Isoform 1 of Heterogeneous nuclear ribonucleoprotein R▼

PCBP2	cDNA FLJ54752, highly similar to Poly(rC)-binding protein 2▼
ATP5B	ATP synthase subunit beta, mitochondrial▼
MVP	cDNA FLJ53437, highly similar to Major vault protein▼
AKR7A2	Aflatoxin B1 aldehyde reductase member 2▼
HSPA4	Heat shock 70 kDa protein 4▼
YARS	Tyrosyl-tRNA synthetase, cytoplasmic▼
HNRNPAB	Isoform 2 of Heterogeneous nuclear ribonucleoprotein A/B▼
PYGB	Glycogen phosphorylase, brain form▼
SFPQ	Isoform Long of Splicing factor, proline- and glutamine-rich▼
YWHAQ	14-3-3 protein theta▼
CAND1	Isoform 2 of Cullin-associated NEDD8-dissociated protein 1▼
HNRNPD	Isoform 1 of Heterogeneous nuclear ribonucleoprotein D0▼
CAPZB	Capping protein (Actin filament) muscle Z-line, beta▼
LOC652147	similar to U5 snRNP-specific 200kD protein, partial▼
MYOF	Uncharacterized protein▼
PLS1	Plastin-1▼
LMNA	Isoform A of Prelamin-A/C▼
PTGES3	Prostaglandin E synthase 3▼
TPT1	Tumor protein, translationally-controlled 1▼
ARCN1	Coatomer subunit delta variant 2▼
TPT1	cDNA FLJ57738, highly similar to Translationally-controlled tumor protein▼
GGCT	Isoform 1 of Gamma-glutamylcyclotransferase▼
MDH2	Malate dehydrogenase, mitochondrial▼
ESYT1	Isoform 1 of Extended synaptotagmin-1▼
NME1;NME2;NME1-NME2	Isoform 1 of Nucleoside diphosphate kinase A▼
HADHA	Trifunctional enzyme subunit alpha, mitochondrial▼
STIP1	STIP1 protein▼
SNHG4;MATR3	Uncharacterized protein▼
G6PD	Isoform Short of Glucose-6-phosphate 1-dehydrogenase▼
SSH3	Isoform 2 of Protein phosphatase Slingshot homolog 3▼
RAB1A	Ras-related protein Rab-1A, Isoform 3▼
PSMB3	Proteasome subunit beta type-3▼
HDGF	Hepatoma-derived growth factor▼
OLA1	Obg-like ATPase 1▼
MTAP	Methylthioadenosine phosphorylase ▼
P4HB	Prolyl 4-hydroxylase, beta polypeptide ▼
BZW2	Basic leucine zipper and W2 domain-containing

	protein 2▼
UQCRFSL1	Ubiquinol-cytochrome c reductase, Rieske iron-sulfur polypeptide-like 1▼
ATP5A1	ATP synthase subunit alpha, mitochondrial▼
PLS3	Plastin 3▼
NDUFS3	NADH dehydrogenase [ubiquinone] iron-sulfur protein 3, mitochondrial▼
-	cDNA FLJ56734, moderately similar to Sepiapterin reductase▼
SEPT9	septin-9 isoform a▼
IKZF3	Isoform 1 of Zinc finger protein Aiolos▼
IL18	Interleukin-18▼
STAT1	Isoform Alpha of Signal transducer and activator of transcription 1-alpha/beta▼
PCBP2	poly(rC)-binding protein 2 isoform c▼
PSMC1	26S protease regulatory subunit 4▼
HNRNPA2B1	heterogeneous nuclear ribonucleoprotein A2/B1 ▼
EIF3I	Eukaryotic translation initiation factor 3 subunit I▼
BAT3	cDNA FLJ60983, highly similar to Large proline-rich protein BAT3▼
HSPA1A;HSPA1B	Heat shock 70 kDa protein 1A/1B▼
AGRN	Agrin▼
MYOF	Isoform 1 of Myoferlin▼
AKR1C2	Aldo-keto reductase family 1 member C2▼
HARS2	Probable histidyl-tRNA synthetase, mitochondrial▼
APRT	Adenine phosphoribosyltransferase▼
APRT	adenine phosphoribosyltransferase isoform b▼
RRBP1	Isoform 2 of Ribosome-binding protein 1▼
PSMC1	26S protease regulatory subunit 4▼
GPD2	Isoform 1 of Glycerol-3-phosphate dehydrogenase, mitochondrial▼
EPDR1	Isoform 1 of Mammalian ependymin-related protein 1▼
RAB7A	Uncharacterized protein▼
-	61 kDa protein▼
RPLP2	60S acidic ribosomal protein P2▼
PFN2	Profilin 2▼
CETN2	Centrin-2▼
SLC44A4	Solute carrier family 44, member 4▼
SCP2	Sterol carrier protein 2, Isoform 2▼
PIN1	Peptidyl-prolyl cis-trans isomerase (Putative uncharacterized protein) ▼
SPTBN1	Spectrin beta chain, Isoform Long▼
ITGAE	Integrin alpha-E▼
EPRS	cDNA FLJ56021, highly similar to Bifunctional aminoacyl-tRNA synthetase[Includes: Glutamyl-tRNA

	synthetase (Fragment) ▼
CFL1	Cofilin-1▼
-	cDNA FLJ53754, highly similar to Transmembrane emp24 domain-containing protein 10▼
SF3B1	Splicing factor 3B subunit 1▼
DYNLL1	Dynein light chain 1, cytoplasmic▼
MYH14	Isoform 1 of Myosin-14▼
LAMP1	Lysosome-associated membrane glycoprotein 1▼
KRT1	Keratin, type II cytoskeletal 1▼
RNH1	Ribonuclease inhibitor▼
HNRNPA2B1	Isoform B1 of Heterogeneous nuclear ribonucleoproteins A2/B1▼
SERPINA1	Isoform 1 of Alpha-1-antitrypsin▼
NAP1L1	Nucleosome assembly protein 1-like 1▼
IGF2BP2	Isoform 1 of Insulin-like growth factor 2 mRNA-binding protein 2▼
FLNB	Isoform 1 of Filamin-B▼
MTAP	cDNA FLJ59758, highly similar to S-methyl-5-thioadenosine phosphorylase▼
HNRNPM	Isoform 1 of Heterogeneous nuclear ribonucleoprotein M▼
SPTBN1	Isoform Short of Spectrin beta chain, brain 1▼
ARCN1	coatomer subunit delta isoform 2▼
GALE	UDP-galactose-4-epimerasev▼
MAT2A	S-adenosylmethionine synthase isoform type-2▼

Table 17 Number of Calu-3 Proteins Altered in both SWNT and MWNT Low Dose (0.004 μg/cm^2) Exposures=231

First ▼=Decrease for SWNT, Second ▼= Decrease for MWNT

Gene name	Protein name
MVP	Major vault protein▼▼
CDH1	Cadherin 1, type 1, E-cadherin (epithelial) ▼▼
CHD	Isoform 1 of Chromodomain-helicase-DNA-binding protein 4▼▼
KPNB1	Importin subunit beta-1▼▼
PYCARD	Apoptosis-associated speck-like protein containing a CARD▼▼
KPNA2	Importin subunit alpha-2▼▼
HSPA4	Heat shock 70 kDa protein 4▼▼
SLC9A3R1	Solute carrier family 9 (sodium/hydrogen exchanger), member 3 regulator 1▼▼
PDHB	Pyruvate dehydrogenase E1 component subunit beta, mitochondrial▼▼
PYGB	Glycogen phosphorylase, brain form▼▼
RARS	Arginyl-tRNA synthetase, cytoplasmic, Isoform Complexed▼▼
SPTBN1	Spectrin beta chain, Isoform Long▼▼
AKR1C2	Aldo-keto reductase family 1 member C2▼▼
NOD1	Nucleotide-binding oligomerization domain-containing protein 1▼▼
ATP1A1	Isoform Long of Sodium/potassium-transporting ATPase subunit alpha-1▼▼
YARS	Tyrosyl-tRNA synthetase, cytoplasmic▼▼
N4BP2L2	NEDD4-binding protein 2-like 2, Isoform 1▼▼
ITGAE	Integrin alpha-E▼▼
CHCHD2	Coiled-coil-helix-coiled-coil-helix domain-containing protein 2, mitochondrial▼▼
HSPA2	Heat shock-related 70 kDa protein 2▼▼
RPS10	Ribosomal protein S10▼▼
RPLP0	Ribosomal protein P0, acidic▼▼
PFKP	Phosphofructokinase, platelet▼▼
PDA4	Protein disulfide-isomerase A4▼▼
TPT1	Tumor protein, translationally-controlled 1▼▼
SFPQ	Isoform Long of Splicing factor, proline- and glutamine-rich▼▼
P4HB	Prolyl 4-hydroxylase, beta polypeptide ▼▼
SM9	Poteasome (prosome, macropain) 26S subunit, non-ATPase, 9▼▼

CFL1	Cofilin-1▼▼
NME1	Nucleoside diphosphate kinase A, Isoform 1▼▼
HNRNPR	Isoform 1 of Heterogeneous nuclear ribonucleoprotein R▼▼
PSMD2	Proteasome (prosome, macropain) 26S subunit, non-ATPase, 2▼▼
G3BP1	GTPase activating protein (SH3 domain) binding protein 1▼▼
PSAP	Proactivator polypeptide, Isoform Sap-mu-0▼▼
HEXB	Beta-hexosaminidase subunit beta▼▼
EIF3I	Eukaryotic translation initiation factor 3 subunit I▼▼
HNRNPH1	Heterogeneous nuclear ribonucleoprotein H▼▼
C1orf198	C1orf198▼▼
DSP	Desmoplakin, Isoform DPI▼▼
PTGES3	Prostaglandin E synthase 3▼▼
S100A13	S100 calcium binding protein A13▼▼
EHD1	EH domain-containing protein 1▼▼
SPR	Sepiapterin reductase▼▼
YWHAQ	14-3-3 protein theta▼▼
IKZF3	Zinc finger protein Aiolos▼▼
DYNLL1	Dynein light chain 1, cytoplasmic▼▼
FANCI	Isoform 1 of Fanconi anemia group I protein▼▼
MYH9	Myosin 9, Isoform 1▼▼
ADD1	Alpha-adducin, Isoform 1▼▼
HSD17B4	Hydroxysteroid (17-beta) dehydrogenase 4▼▼
HDGF	Hepatoma-derived growth factor▼▼
MYOF	Isoform 1 of Myoferlin▼▼
LMNA	Isoform A of Prelamin-A/C▼▼
PSMC2	Proteasome (prosome, macropain) 26S subunit, ATPase, 2▼▼
HARS	Histidyl-tRNA synthetase, cytoplasmic▼▼
AHNAK	AHNAK nucleoprotein▼▼
APOA1	Apolipoprotein A-I▼▼
ESYT1	Isoform 1 of Extended synaptotagmin-1▼▼
BZW2	Basic leucine zipper and W2 domain-containing protein 2▼▼
CTSC	Cathepsin C▼▼
NAP1L1	Nucleosome assembly protein 1-like 1▼▼
CLTC	Isoform 1 of Clathrin heavy chain 1▼▼
USP5	Isoform Long of Ubiquitin carboxyl-terminal hydrolase 5▼▼
SH3BGRL	SH3 domain-binding glutamic acid-rich-like protein▼▼
CS	Citrate synthase, mitochondrial▼▼
NDUFS3	NADH dehydrogenase [ubiquinone] iron-sulfur protein 3, mitochondrial▼▼
TARDBP	TAR DNA-binding protein 43, Isoform 2▼▼
SF3B1	Splicing factor 3B subunit 1▼▼

CAPZA2	Capping protein (actin filament) muscle Z-line, alpha 2▼▼
GSN	Gelsolin, Isoform 1▼▼
LYPLA2	Lysophospholipase II▼▼
CCT6A	Chaperonin containing TCP1, subunit 6A (zeta 1) ▼▼
PSMB3	Proteasome subunit beta type-3▼▼
TMED10	Transmembrane emp24 domain-containing protein 10▼▼
HNRNPD	Heterogeneous nuclear ribonucleoprotein D0, Isoform 1▼▼
GMPS	GMP synthase [glutamine-hydrolyzing] ▼▼
PPP1R11	Protein phosphatase 1 regulatory subunit 11▼▼
STAT1	Isoform Alpha of Signal transducer and activator of transcription 1-alpha/beta▼▼
GGCT	Isoform 1 of Gamma-glutamylcyclotransferase▼▼
PLS1	Plastin-1▼▼
REXO2	Oligoribonuclease, mitochondrial, Isoform 1▼▼
C19orf10	C19orf10 (Stromal cell-derived growth factor SF20) ▼▼
RBMXL1	RNA binding motif protein, X-linked-like 1▼▼
CAND1	Isoform 1 of Cullin-associated NEDD8-dissociated protein 1▼▼
HNRNPAB	Isoform 4 of Heterogeneous nuclear ribonucleoprotein A/B▼▼
PFN2	Profilin 2▼▼
MCM10	Minichromosome maintenance complex component 10 ▼▼
MX1	Interferon-induced GTP-binding protein Mx1▼▼
IGF2BP2	Isoform 1 of Insulin-like growth factor 2 mRNA-binding protein 2▼▼
RAB1A	Ras-related protein Rab-1A, Isoform 3▼▼
EEF2	Elongation factor 2▼▼
RRBP1	Ribosome-binding protein 1, Isoform 3▼▼
ARF1	ADP-ribosylation factor 1▼▼
CETN2	Centrin-2▼▼
CTNNA1	Catenin alpha-1▼▼
OLA1	Isoform 3 of Obg-like ATPase 1▼▼
TMPO	Lamina-associated polypeptide 2, isoform alpha (thymopoietin) ▼▼
MYOF	Myoferlin▼▼
TXN	Thioredoxin▼▼
PLS3	Plastin 3▼▼
DSP	Desmoplakin, Isoform DPII▼▼
ITGB1	Integrin, beta 1C▼▼
ITGB1	Integrin, beta 1A▼▼
ANXA1	Annexin A1▼▼
KRT1	Keratin, type II cytoskeletal 1▼▼
HIST1H2BB	Histone H2B type 1-B▼▼
XRCC5	X-ray repair cross-complementing protein 5▼▼

TRPM7	Transient receptor potential cation channel, subfamily M, member 7▼▼
IL18	Interleukin-18▼▼
OLA1	Obg-like ATPase 1▼▼
MDH2	Malate dehydrogenase, mitochondrial▼▼
TYMP	Thymidine phosphorylase▼
GAA	Glucosidase, alpha; acid, lysosomal▼▼
PPL	Periplakin▼▼
ARCN1	Coatomer subunit delta variant 2▼▼
PARK7	Protein DJ-1▼▼
XPO1	Exportin 1▼▼
PDIA6	Protein disulfide-isomerase A6, Isoform 2▼▼
CAD	CAD protein▼▼
ELAVL1	ELAV (embryonic lethal, abnormal vision, Drosophila)-like 1 (Hu antigen R) ▼▼
ATP1A3	Sodium/potassium-transporting ATPase subunit alpha-3▼▼
ATP5B	ATP synthase subunit beta, mitochondrial▼▼
RBMX	Heterogeneous nuclear ribonucleoprotein G▼▼
HSPA1A;HS1B	Heat shock 70 kDa protein 1A/1B▼▼
AKR7A2	Aflatoxin B1 aldehyde reductase member 2▼▼
KRT7	Keratin, type II cytoskeletal 7▼▼
SRRM1	cDNA FLJ61739, highly similar to Serine/arginine repetitive matrix protein 1▼▼
EIF4A2	Eukaryotic initiation factor 4A-II, Isoform 1▼▼
ASH2L	Isoform 1 of Set1/Ash2 histone methyltransferase complex subunit ASH2▼▼
PFKL	Phosphofructokinase, liver ▼▼
HNRNPAB	Isoform 2 of Heterogeneous nuclear ribonucleoprotein A/B▼▼
PITPNB	Phosphatidylinositol transfer protein beta isoform 1▼▼
MYH14	Myosin-14, Isoform 1▼▼
AGRN	Agrin▼▼
PSMD13	Proteasome (prosome, macropain) 26S subunit, non-ATPase, 13▼▼
HSP90AA1	Heat shock protein HSP 90-alpha, Isoform 2▼▼
MTAP	Methylthioadenosine phosphorylase▼▼
ROPN1	Ropporin, rhophilin associated protein 1, Isoform 2▼▼
TPT1	Tumor protein, translationally-controlled 1▼▼
UNC80	Unc-80 homolog, Isoform 1▼▼
EIF3B	Eukaryotic translation initiation factor 3 subunit B, Isoform 1▼▼
HNRNPA2B1	Isoform B1 of Heterogeneous nuclear ribonucleoproteins A2/B1▼▼
EEF1A1	Eukaryotic translation elongation factor 1 alpha 1▼▼
FLJ44635	TPT1-like protein▼▼

SERPINB6	Serpin peptidase inhibitor, clade B (ovalbumin), member 6▼▼
LAP3	Leucine aminopeptidase 3, Isoform 2▼▼
ATP5A1	ATP synthase subunit alpha, mitochondrial▼▼
SEPT9	Septin-9 isoform e▼▼
PCBP2	poly(rC)-binding protein 2 isoform c▼▼
RPS3A	Ribosomal protein S3a▼▼
CTNNBL1	Catenin, beta like 1, Isoform 2▼▼
CTNNA1	Catenin alpha-1, Isoform 2▼▼
HNRNPU	Heterogeneous nuclear ribonucleoprotein U, Isoform Short▼▼
SCP2	Sterol carrier protein 2, Isoform 2▼▼
LYPLA2	Lysophospholipase II▼▼
RNH1	Ribonuclease inhibitor▼▼
SLC44A4	Solute carrier family 44, member 4▼▼
RBMX	Heterogeneous nuclear ribonucleoprotein G isoform 2▼▼
SERPINA1	Isoform 1 of Alpha-1-antitrypsin▼▼
JUP	Junction plakoglobin▼▼
PPP2R1A	Protein phosphatase 2, regulatory subunit A, alpha▼▼
CAND1	Cullin-associated NEDD8-dissociated protein 1, Isoform 2▼▼
MYH14	myosin-14 isoform 1▼▼
HSD17B10	Hydroxysteroid (17-beta) dehydrogenase 10▼▼
BAT3	cDNA FLJ60983, highly similar to Large proline-rich protein BAT3▼▼
PFKP	Phosphofructokinase, platelet▼▼
RBMXL1	RNA binding motif protein, X-linked-like 1▼▼
XRCC6	X-ray repair cross-complementing protein 6▼▼
CAPZB	Capping protein (Actin filament) muscle Z-line, beta▼▼
RPS28	Ribosomal protein S28▼▼
LOC652147	similar to U5 snRNP-specific 200kD protein, partial▼▼
SEPT9	Septin-9 isoform a▼▼
PIN1	Peptidyl-prolyl cis-trans isomerase (Putative uncharacterized protein) ▼▼
PCBP2	cDNA FLJ54752, highly similar to Poly(rC)-binding protein 2▼▼
FLOT1	Flotillin 1▼▼
PSMA4	Proteasome (prosome, macropain) subunit, alpha type, 4 ▼▼
IPO5	Importin 5, Isoform 1▼▼
CDV3	Protein CDV3 homolog (Mouse), isoform CRA_a▼▼
GSN	Gelsolin▼▼
MYL6B	Myosin, light chain 6B, alkali, smooth muscle and non-muscle▼▼
AKR1C2	Aldo-keto reductase family 1, member C2▼▼
EZR	Ezrin▼▼
DHX9	DEAH (Asp-Glu-Ala-His) box polypeptide 9▼▼

-	33 kDa protein▼▼
GNB2L1	Guanine nucleotide-binding protein subunit beta-2-like 1▼▼
CTSD	Cathepsin D ▼▼
HNRNPR	heterogeneous nuclear ribonucleoprotein R isoform 3▼▼
RPLP0	Ribosomal protein P0, acidic▼▼
PRDM8	PR domain zinc finger protein 8, Isoform 1▼▼
RPL32	Ribosomal protein L32▼▼
SUN2	Unc-84 homolog B▼▼
LAMP1	Lysosome-associated membrane glycoprotein 1▼▼
UQCRFSL1	Ubiquinol-cytochrome c reductase, Rieske iron-sulfur polypeptide-like 1▼▼
XRCC6	X-ray repair cross-complementing protein 6▼▼
GRB7	Growth factor receptor-bound protein 7▼▼
MAPRE2	Microtubule-associated protein RP/EB family member 2▼▼
CAPZA2	Capping protein (actin filament) muscle Z-line, alpha 2▼▼
STIP1	Stress-induced-phosphoprotein 1▼▼
PPP2R1A	Protein phosphatase 2, regulatory subunit A, alpha▼▼
TPT1	cDNA FLJ57738, highly similar to Translationally-controlled tumor protein▼▼
LGALS3BP	cDNA FLJ53509, highly similar to Galectin-3-binding protein▼▼
HARS	Histidyl-tRNA synthetase▼▼
HNRNPH1	Heterogeneous nuclear ribonucleoprotein H▼▼
SPR	Sepiapterin reductase▼▼
EPRS	Glutamyl-prolyl-tRNA synthetase▼▼
HEXA	Hexosaminidase A (alpha polypeptide) ▼▼
MVP	cDNA FLJ53437, highly similar to Major vault protein▼▼
LAP3	Leucine aminopeptidase 3▼▼
SND1	Staphylococcal nuclease domain-containing protein 1▼▼
EIF3L	Eukaryotic translation initiation factor 3 subunit 6-interacting protein▼▼
ARF1	ADP-ribosylation factor 1▼▼
TMED10	Transmembrane emp24 domain-containing protein 10▼▼
MTAP	Methylthioadenosine phosphorylase ▼▼
OLA1	Obg-like ATPase 1▼▼
HNRNPA2B1	Uncharacterized protein▼▼
GALNT2	UDP-N-acetyl-alpha-D-galactosamine:polypeptide N-acetylgalactosaminyltransferase 2 (GalNAc-T2) ▼▼
GNB2	Guanine nucleotide binding protein (G protein), beta polypeptide 2▼▼
ARPC2	Actin related protein 2/3 complex, subunit 2▼▼
GRB7	Growth factor receptor-bound protein 7, Isoform 1▼▼
ASAH1	N-acylsphingosine amidohydrolase (acid ceramidase) 1▼▼

GMPS	Guanine monphosphate synthetase▼▼
PFN2	Profilin 2▼▼
PLS3	plastin 3, Isoform 2▼▼
HNRNPD	Heterogeneous nuclear ribonucleoprotein D▼▼
UGDH	UDP-glucose 6-dehydrogenase▼▼
HEXB	Beta-hexosaminidase subunit beta▼▼
HNRNPD	Heterogeneous nuclear ribonucleoprotein D▼▼
DSP	Desmoplakin Ia▼▼

FIGURES

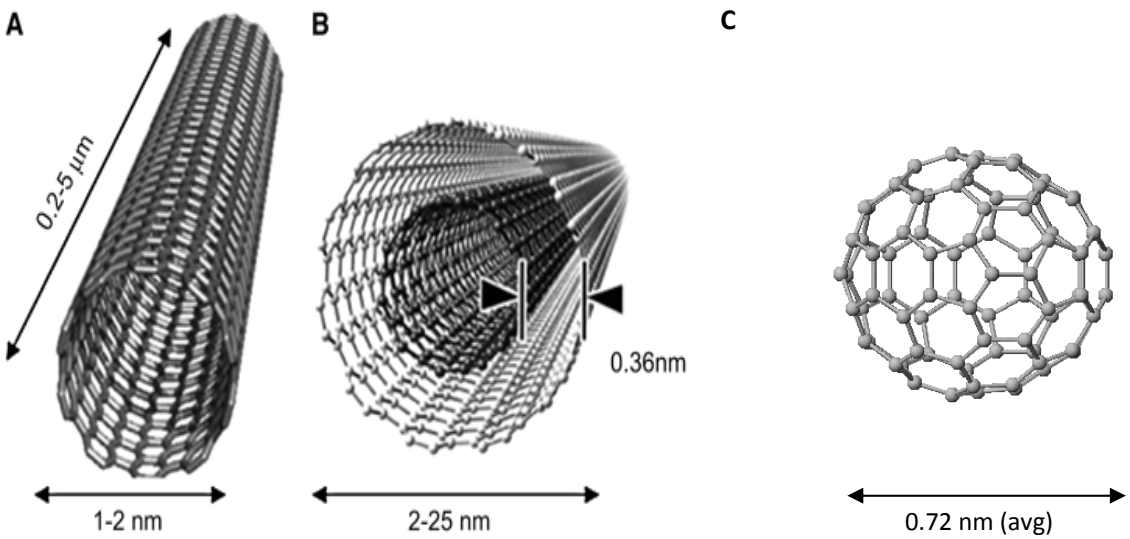

Figure 1 Conceptual Diagram of Carbon Nanoparticles

(A) Single walled nanotube (B) Multi walled nanotube (C) Fullerenes (C_{60}) (Adapted from jnm.snmjournals.org and www.ch.ic.ac.uk).

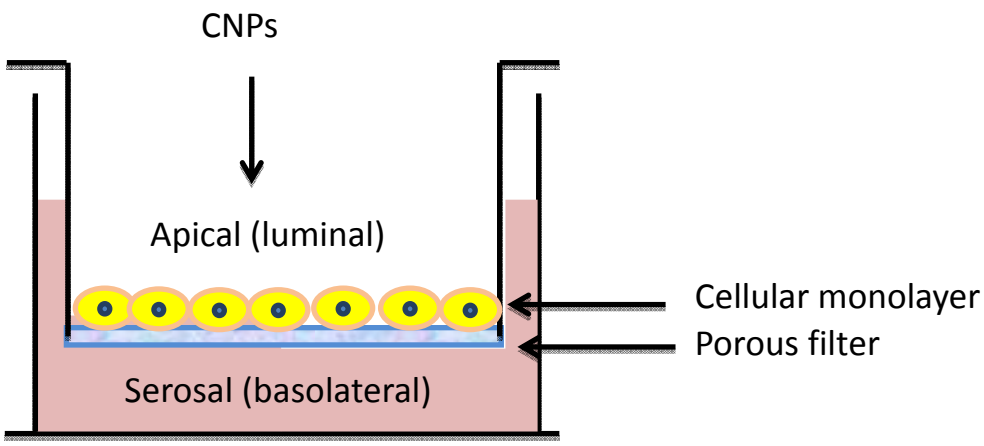

Figure 2 Air-Interface Culture (AIC)

Cells were seeded on the permeable filters of the transwell cell culture plates with media on the apical and basolateral sides. Two days after inoculation of the Calu-3 cells, the media was removed from the apical side and was replaced only on the basolateral side until the 14th day, the time at which the cells show a high resistance phenotype.

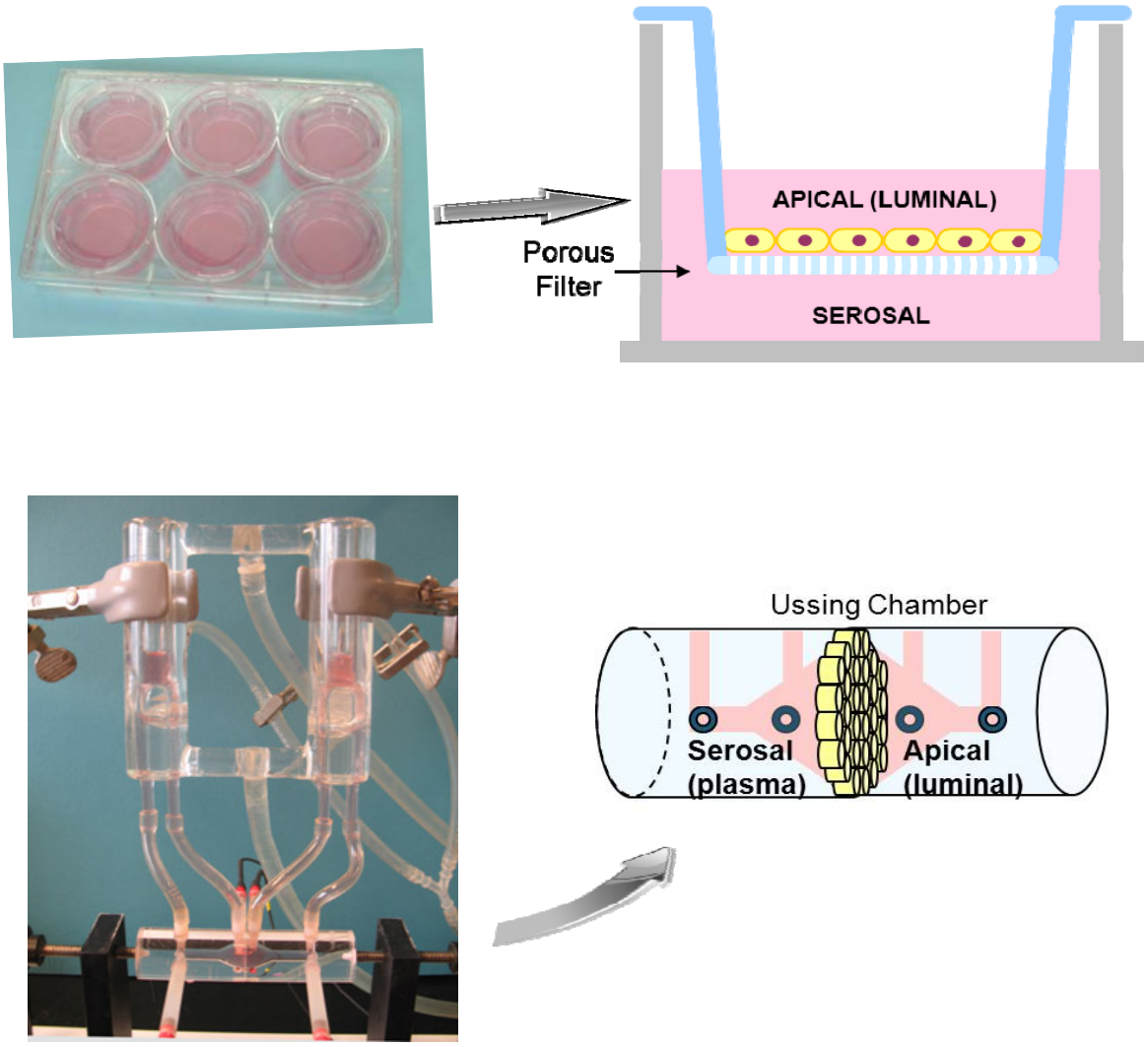

Figure 3 Short Circuit Current (SCC) Electrophysiology

Filters containing confluent cellular monolayers were cut from the plastic inserts, mounted in a Ussing chamber that separates the apical (luminal) surface from basolateral. The Ussing chamber is connected to a DVC-1000 Voltage/Current Clamp with voltage and current electrodes on either side of the membrane. The spontaneous transepithelial potential difference was clamped to zero, and the resultant SCC, a measure of net transepithelial ion flux, was monitored continuously. The cells were bathed in serum-free medium maintained at 37 °C via water-jacketed buffer on either side of the filter.

Element	C60 % Wt.	SWNT %	MWNT % Wt.
C	73.7	95.3	92.2
O	26.3	3.1	3.7
Fe	-	0.4	-
Ni	-	1.0	0.3
Co	-	0.2	4.3

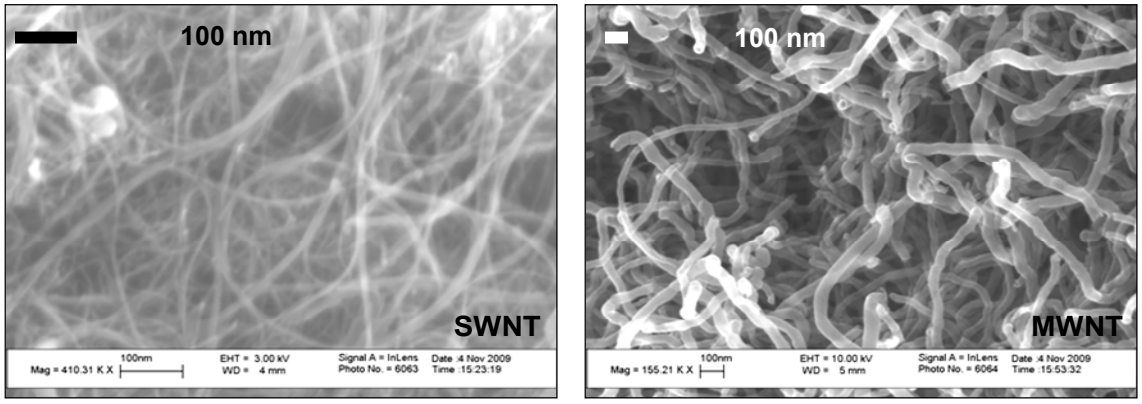

Figure 4 CNP Analysis

Elemental analysis of CNPs determined by energy dispersive X-ray spectroscopy (top) and scanning electron microscopy of SWNT and MWNT (bottom).

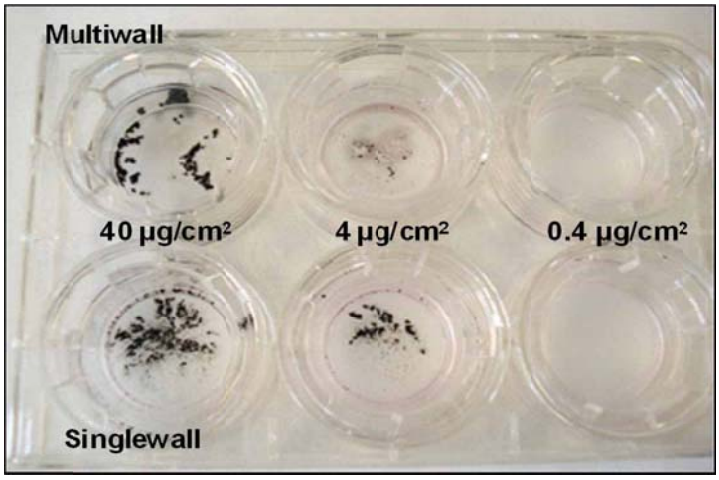

Figure 5 CNP Agglomeration

CNTs (SWNT and MWNT) solutions in media were added to the cellular monolayer grown on transwell in concentrations as indicated and incubated at 37 °C for 48 h. The media was removed. The figure shows the agglomerated particles deposited on the apical side of the cellular monolayer.

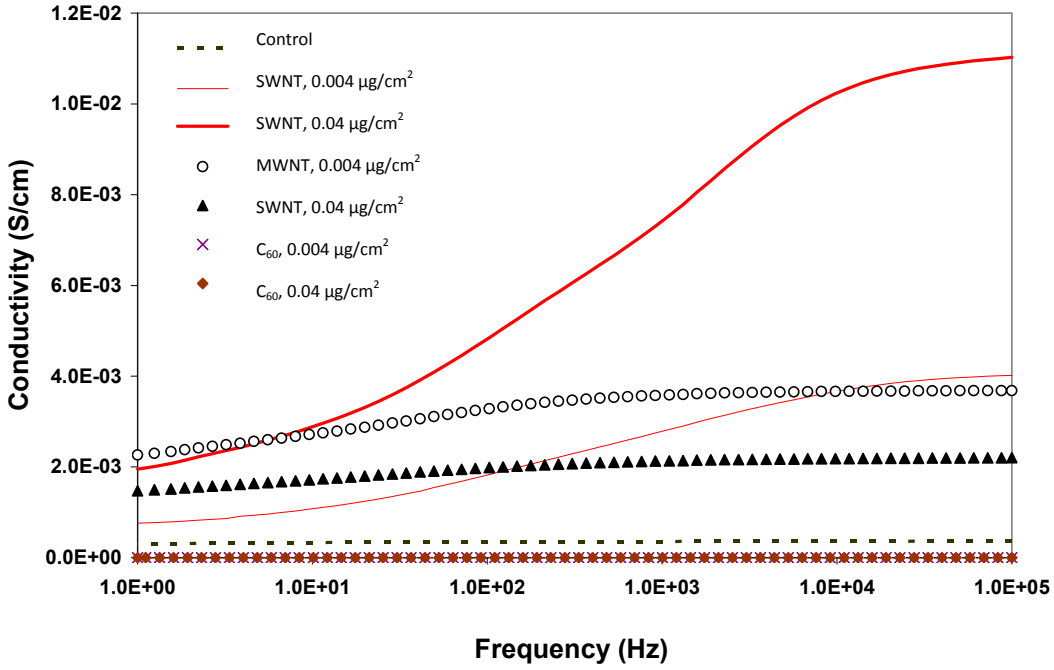

Figure 6 Frequency Dependency of AC Conductivity for a Culture Medium with CNPs

Frequency dependency of AC conductivity for a culture medium (dashed line), and the media with 0.004 µg/cm^2 (thin solid line) or 0.04 µg/cm^2 (thick solid line) of SWNT, the media with 0.004 µg/cm^2 (open circle) or 0.04 µg/cm^2 (filled triangle) of MWNT, and the media with 0.004 µg/cm^2 (pink cross) or 0.04 µg/cm^2 (red filled diamond) of C_{60}.

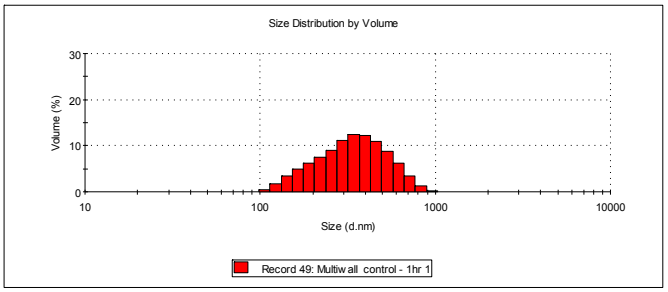

Control

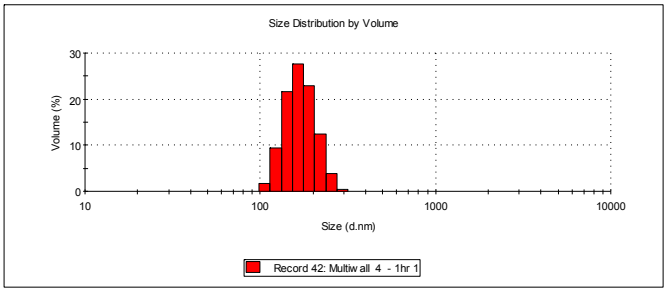

4 µg/cm^2

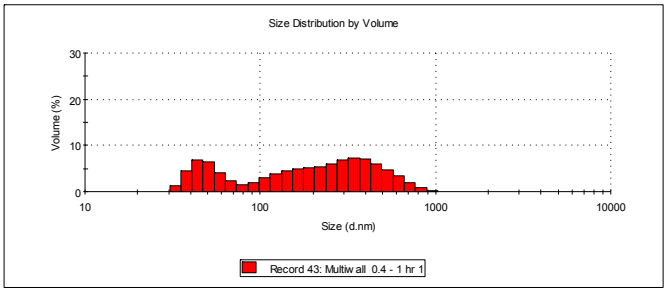

0.4 µg/cm^2

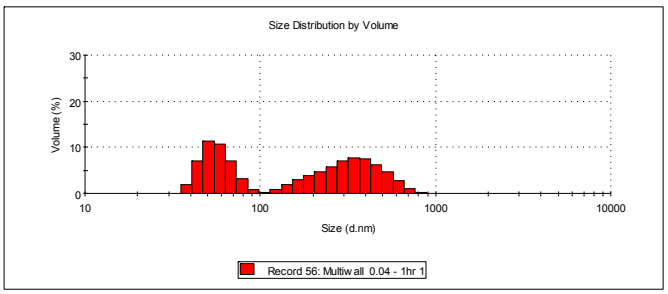

0.04 µg/cm^2

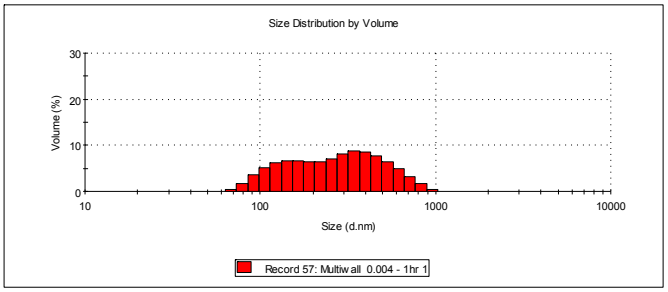

4 ng/cm^2

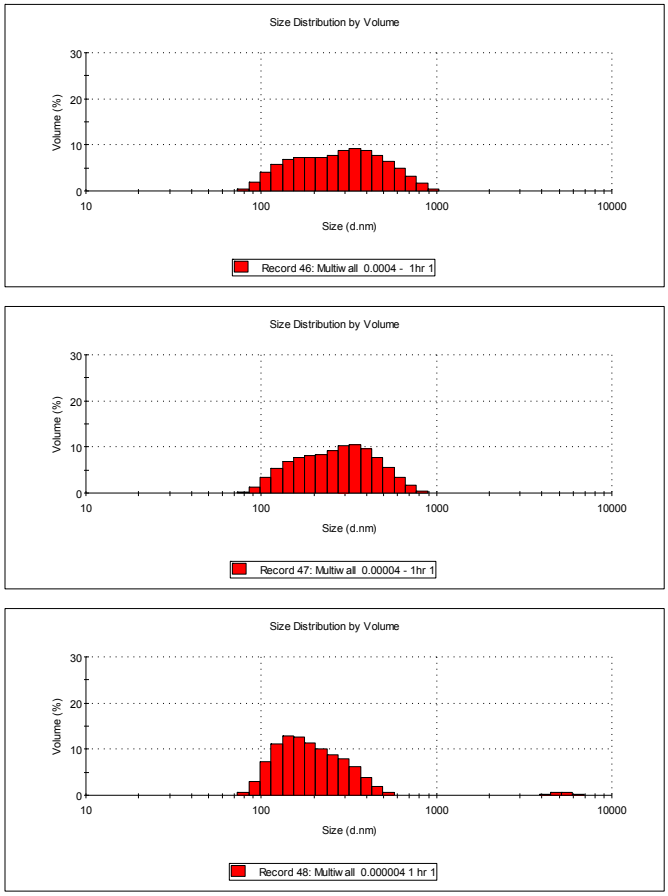

0.4 ng/cm^2

0.04 ng/cm^2

4 pg/cm^2

Figure 7 Particle Size Measurement of MWNTs at 1h

The culture media containing different concentrations (4 µg/cm^2-4 pg/cm^2) of MWNTs was prepared in the same way as it was prepared for exposure to the cells and incubated at 37 °C for 1 h. The particle sizes were measured by using Zetasizer nano ZS90. A control that was prepared in the same way was also included.

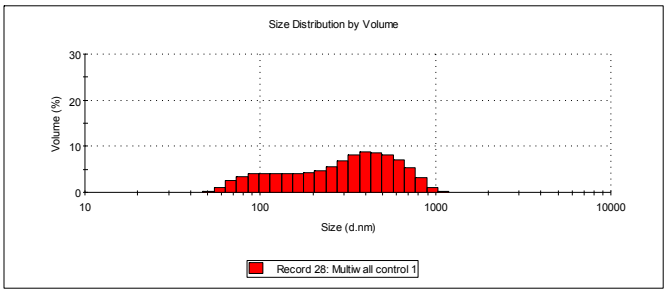

Control

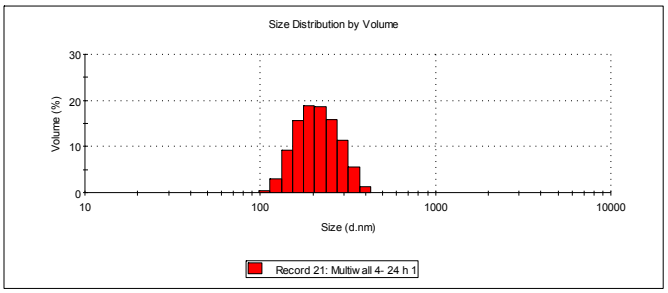

4 µg/cm^2

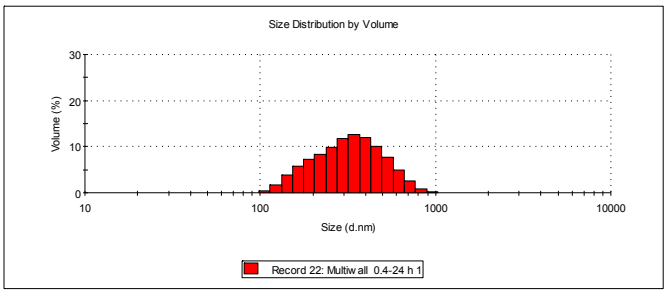

0.4 µg/cm^2

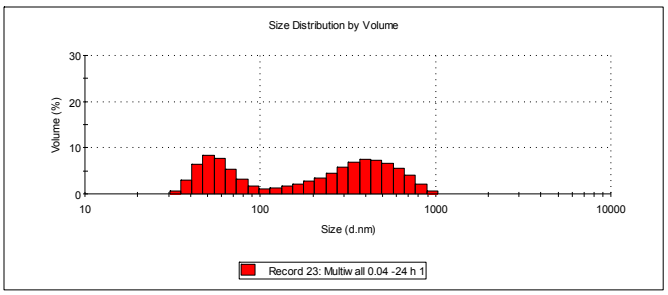

0.04 µg/cm^2

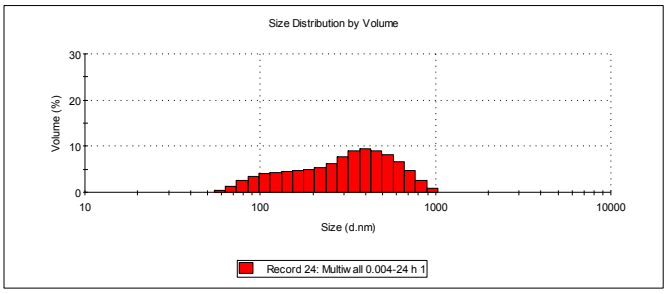

4 ng/cm^2

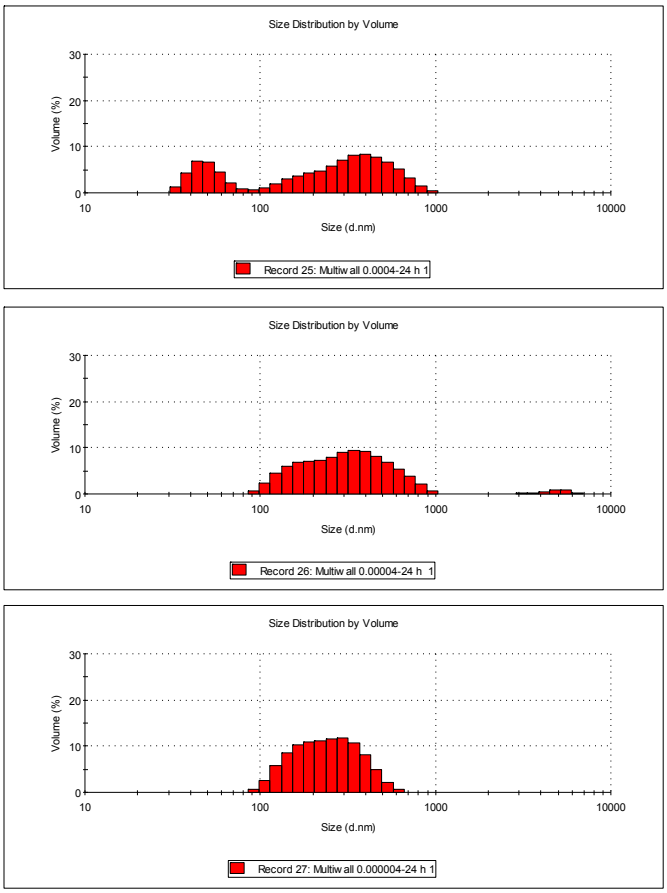

0.4 ng/cm^2

0.04 ng/cm^2

4 pg/cm^2

Figure 8 Particle Size Measurement of MWNTs at 24 h

The culture media containing different concentrations (4 µg/cm^2-4 pg/cm^2) of MWNTs was prepared in the same way as it was prepared for exposure to the cells and incubated at 37 °C for 24 h. The particle sizes were measured by using Zetasizer nano ZS90. A control that was prepared in the same way was also included.

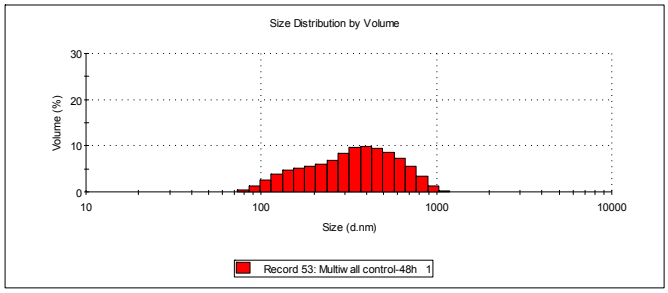

Control

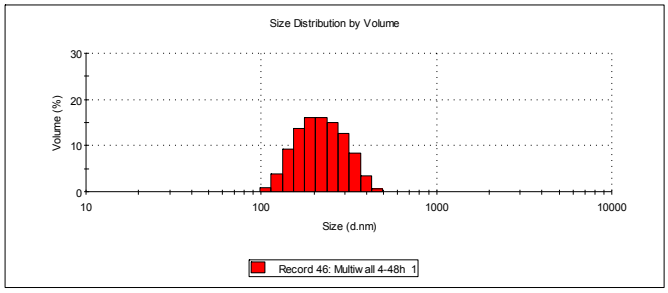

4 µg/cm^2

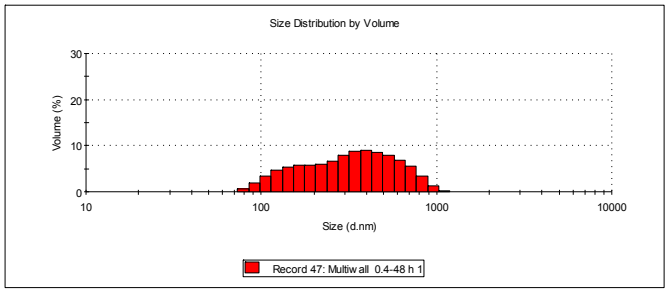

0.4 µg/cm^2

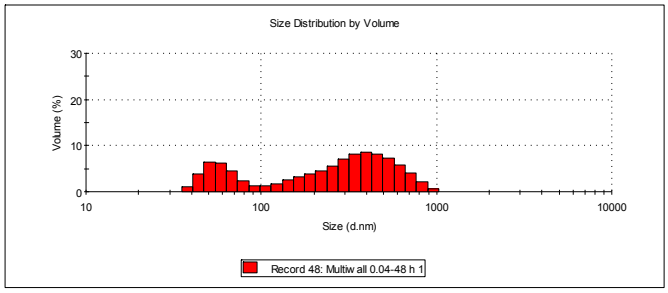

0.04 µg/cm^2

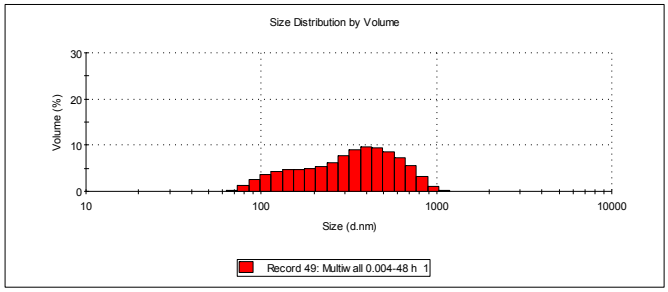

4 ng/cm^2

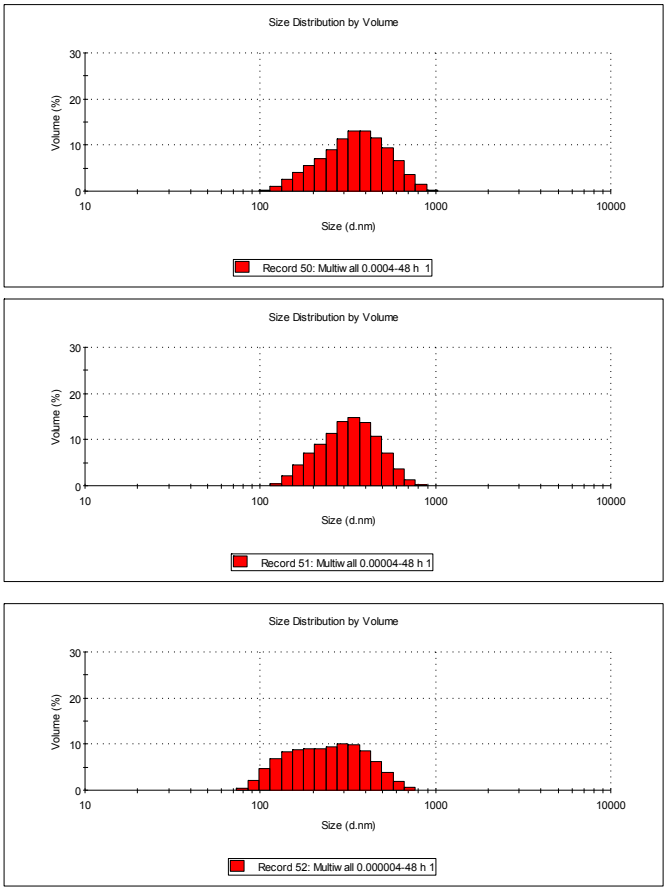

0.4 ng/cm^2

0.04 ng/cm^2

4 pg/cm^2

Figure 9 Particle Size Measurement of MWNTs at 48 h

The culture media containing different concentrations (4 µg/cm^2-4 pg/cm^2) of MWNTs was prepared in the same way as it was prepared for exposure to the cells and incubated at 37 °C for 48 h. The particle sizes were measured by using Zetasizer nano ZS90. A control that was prepared in the same way was also included.

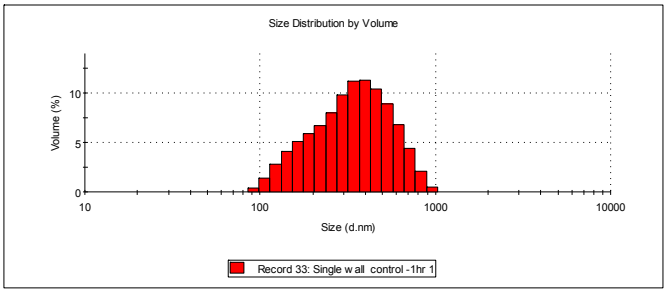

Control

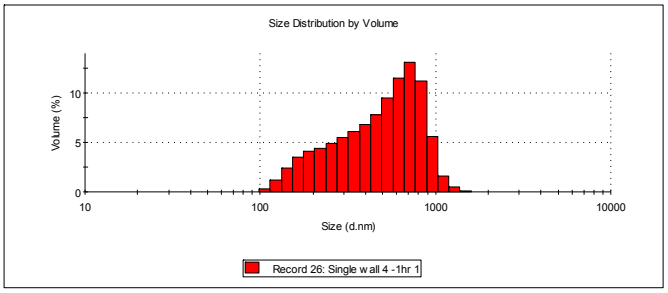

4 µg/cm^2

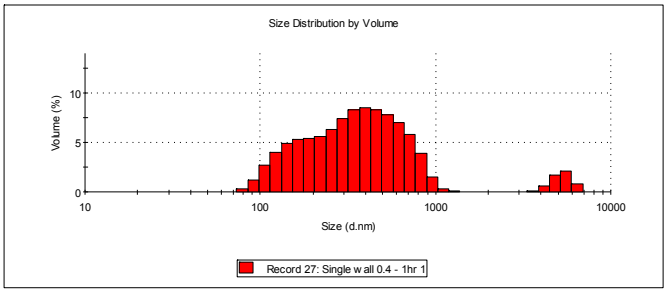

0.4 µg/cm^2

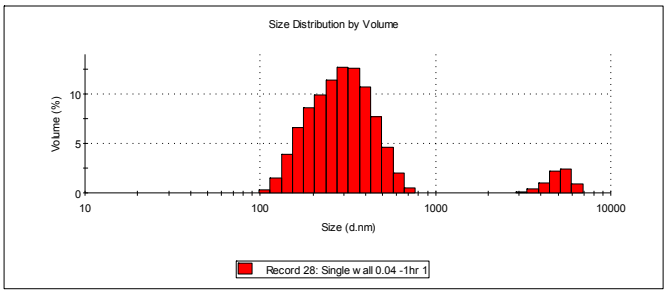

0.04 µg/cm^2

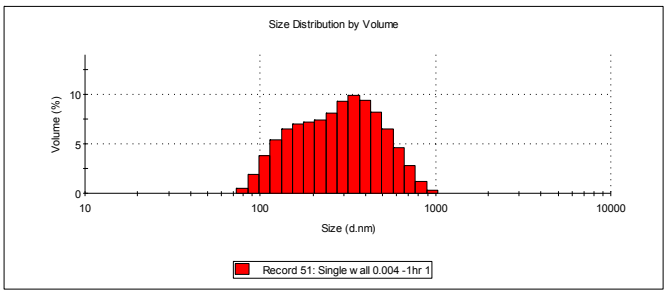

4 ng/cm^2

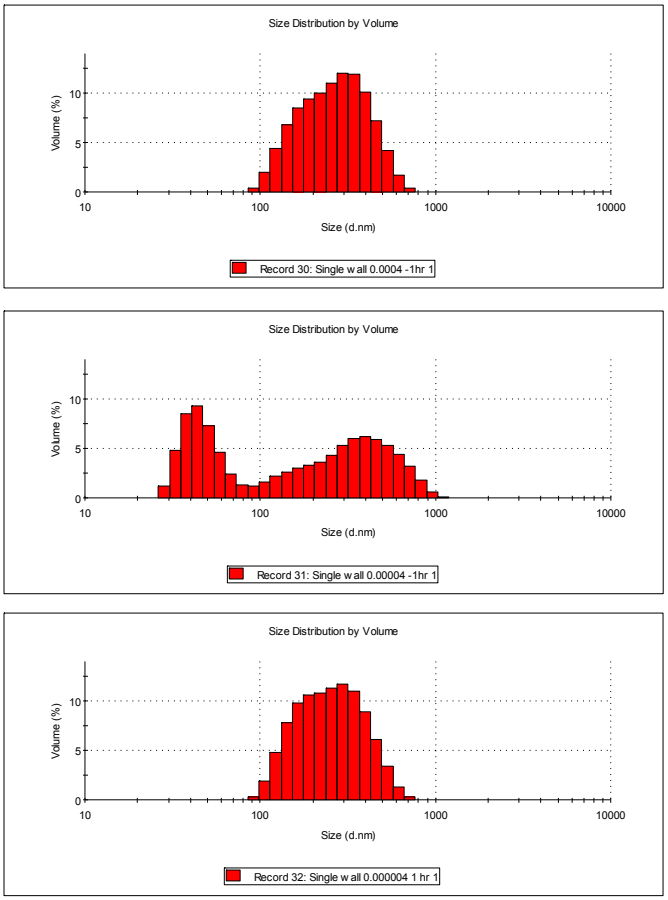

0.4 ng/cm^2

0.04 ng/cm^2

4 pg/cm^2

Figure 10 Particle Size Measurement of SWNTs at 1 h

The culture media containing different concentrations (4 µg/cm^2-4 pg/cm^2) of SWNTs was prepared in the same way as it was prepared for exposure to the cells and incubated at 37 °C for 1 h. The particle sizes were measured by using Zetasizer nano ZS90. A control that was prepared in the same way was also included.

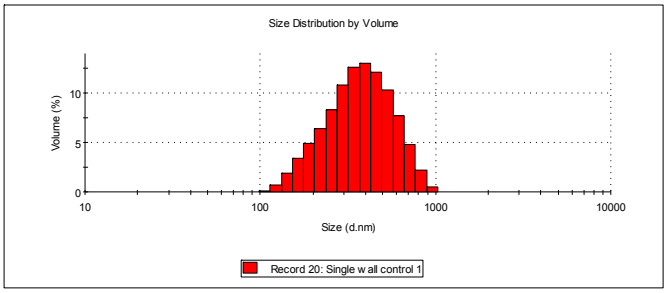

Control

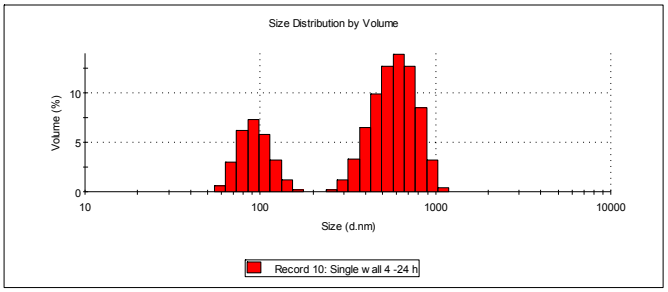

4 µg/cm^2

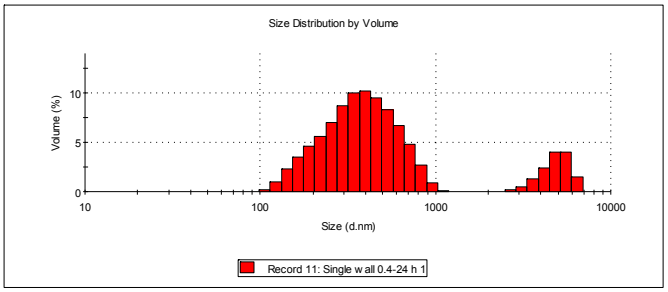

0.4 µg/cm^2

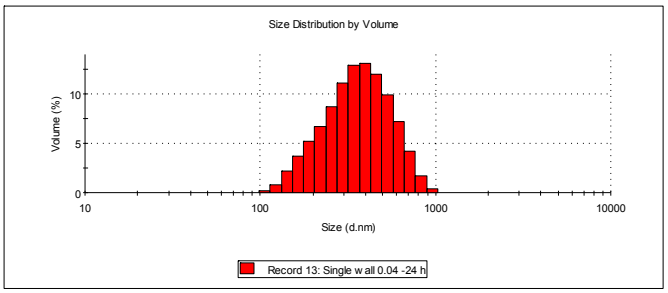

0.04 µg/cm^2

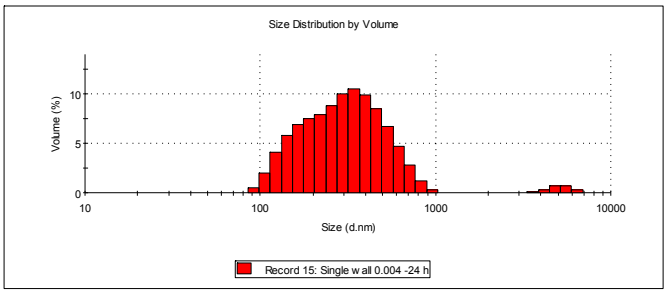

4 ng/cm^2

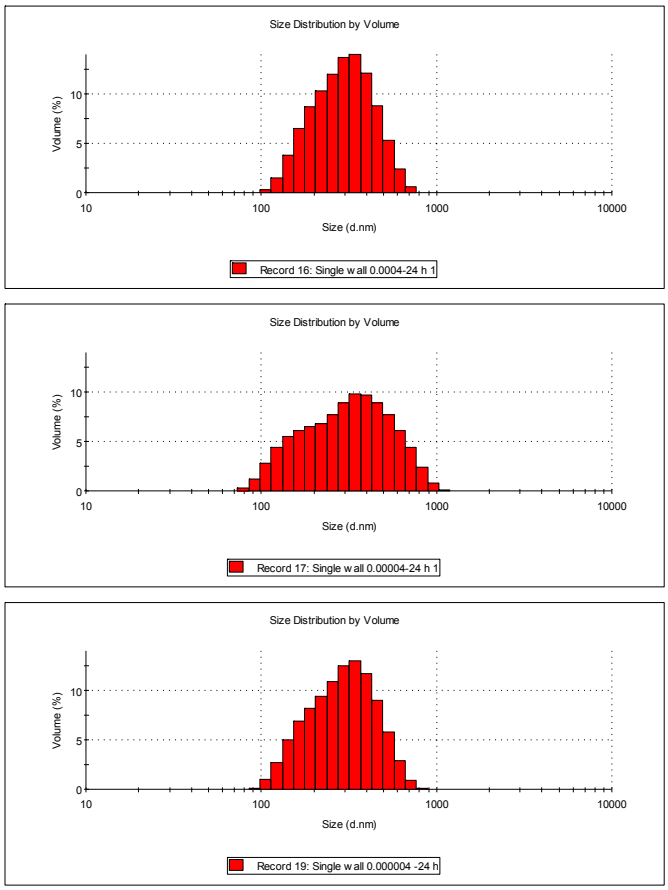

0.4 ng/cm^2

0.04 ng/cm^2

4 pg/cm^2

Figure 11 Particle Size Measurement of SWNTs at 24 h

The culture media containing different concentrations (4 µg/cm^2-4 pg/cm^2) of SWNTs was prepared in the same way as it was prepared for exposure to the cells and incubated at 37 °C for 24 h. The particle sizes were measured by using Zetasizer nano ZS90. A control that was prepared in the same way was also included.

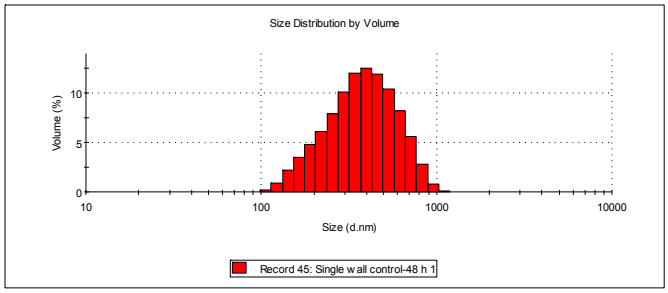

Control

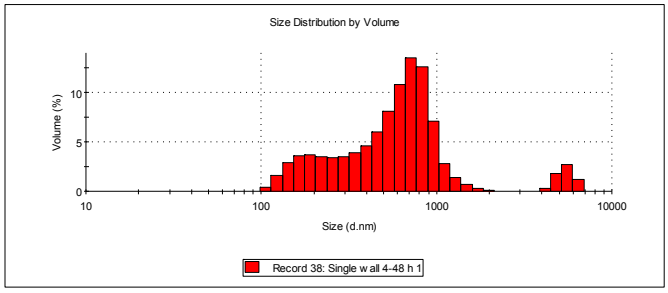

4 µg/cm^2

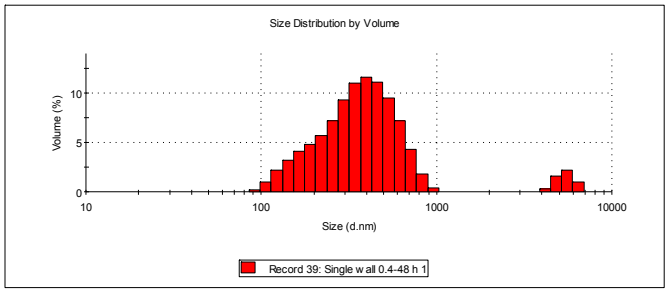

0.4 µg/cm^2

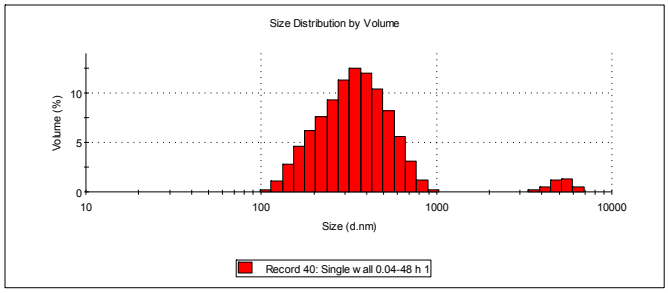

0.04 µg/cm^2

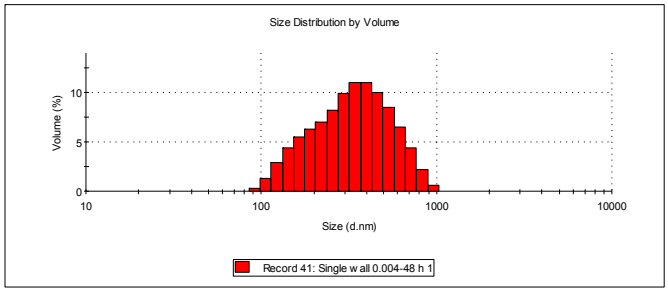

4 ng/cm^2

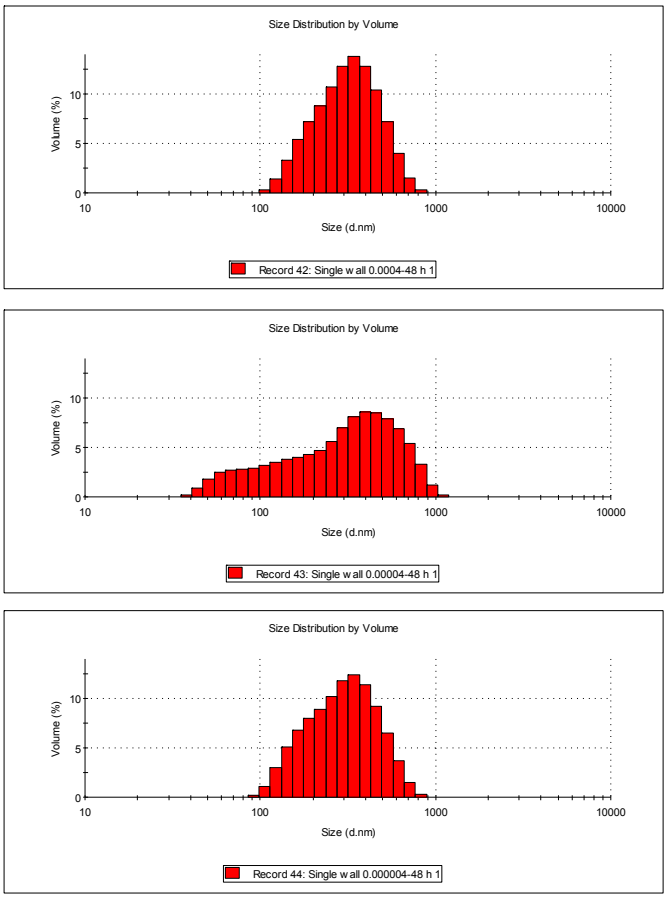

0.4 ng/cm^2

0.04 ng/cm^2

4 pg/cm^2

Figure 12 Particle Size Measurement of SWNTs at 48 h

The culture media containing different concentrations (4 µg/cm^2-4 pg/cm^2) of SWNTs was prepared in the same way as it was prepared for exposure to the cells and incubated at 37 °C for 24 h. The particle sizes were measured by using Zetasizer nano ZS90. A control that was prepared in the same way was also included.

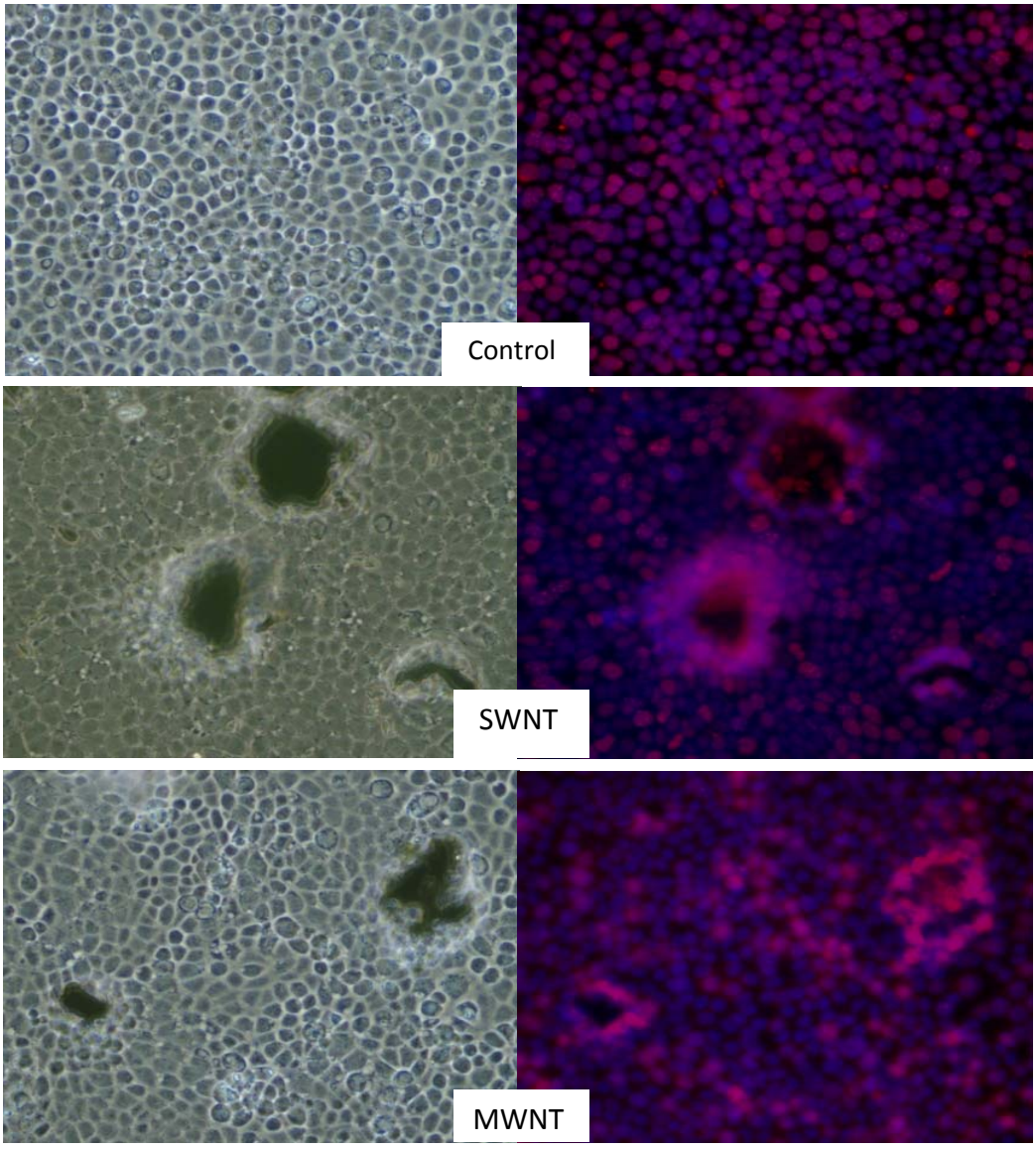

Figure 13 Effects of CNP Exposure on the Cellular Proliferation in the mpkCCD$_{cl4}$ Cell Line

Cells were seeded in 24-well plates and exposed to 40 µg/cm^2 of SWNT or MWNT for 48 h. The cells were fixed and stained with proliferating cell nuclear antigen (PCNA) to indicate the nuclei of proliferating cells and DAPI stain to all cell nuclei (red and blue respectively in the merged images on the right). The brightfield image (left-hand panels) clearly show the agglomerated nanoparticles as irregular black spots. The panels on the right indicate increased cellular proliferation (PCNA; red) in the areas surrounding the nanoparticles.

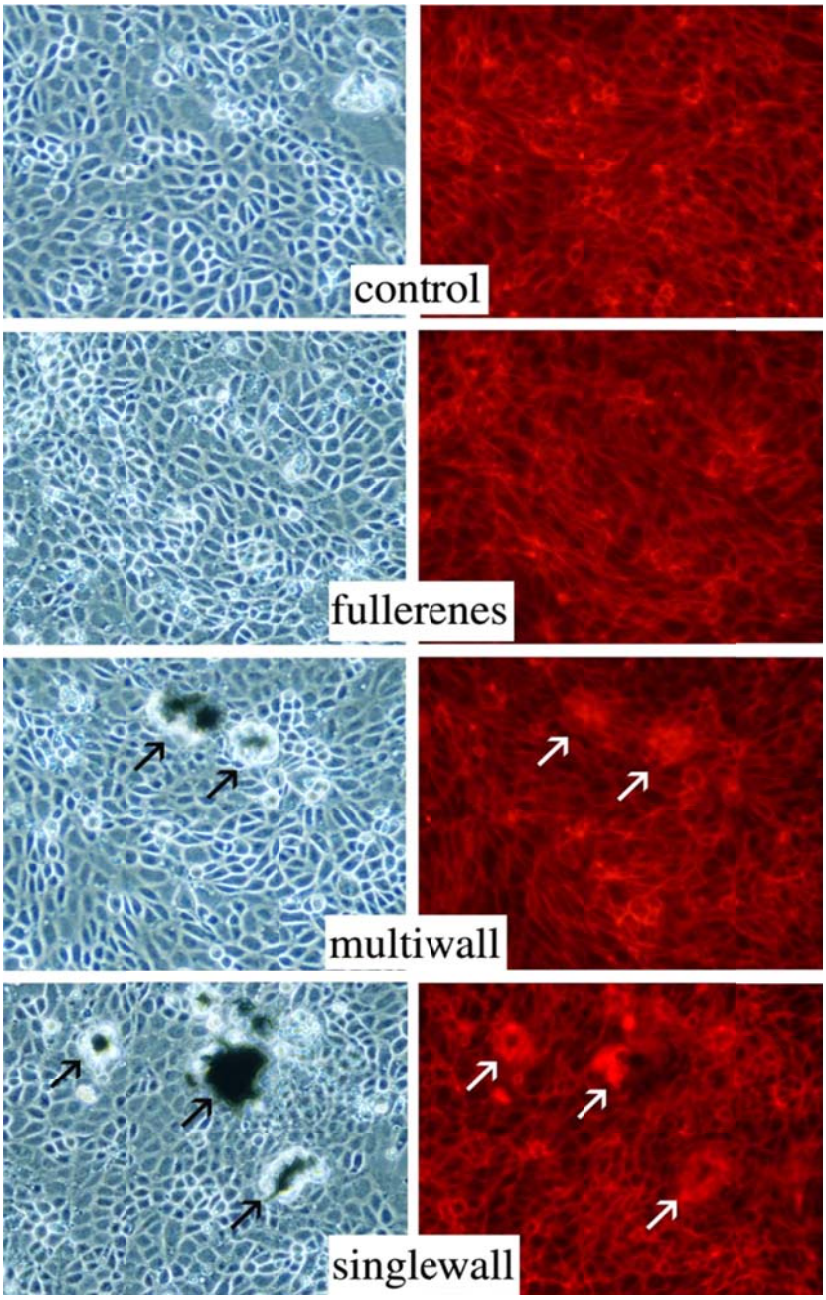

Figure 14 Effects of CNP Exposure on the Actin **C**ytoskeleton in the mpkCCD$_{cl4}$ Cell Line

Cells were seeded in 24-well plates and exposed to 40 µg/cm^2 of SWNT or MWNT for 48 h. Cells were fixed and actin was visualized using rhodamine-phalloidin. Cells treated with SWNT and MWNT show regions of filamentous actin accumulation (white arrows) at or near sites of CNT agglomeration (black arrows).

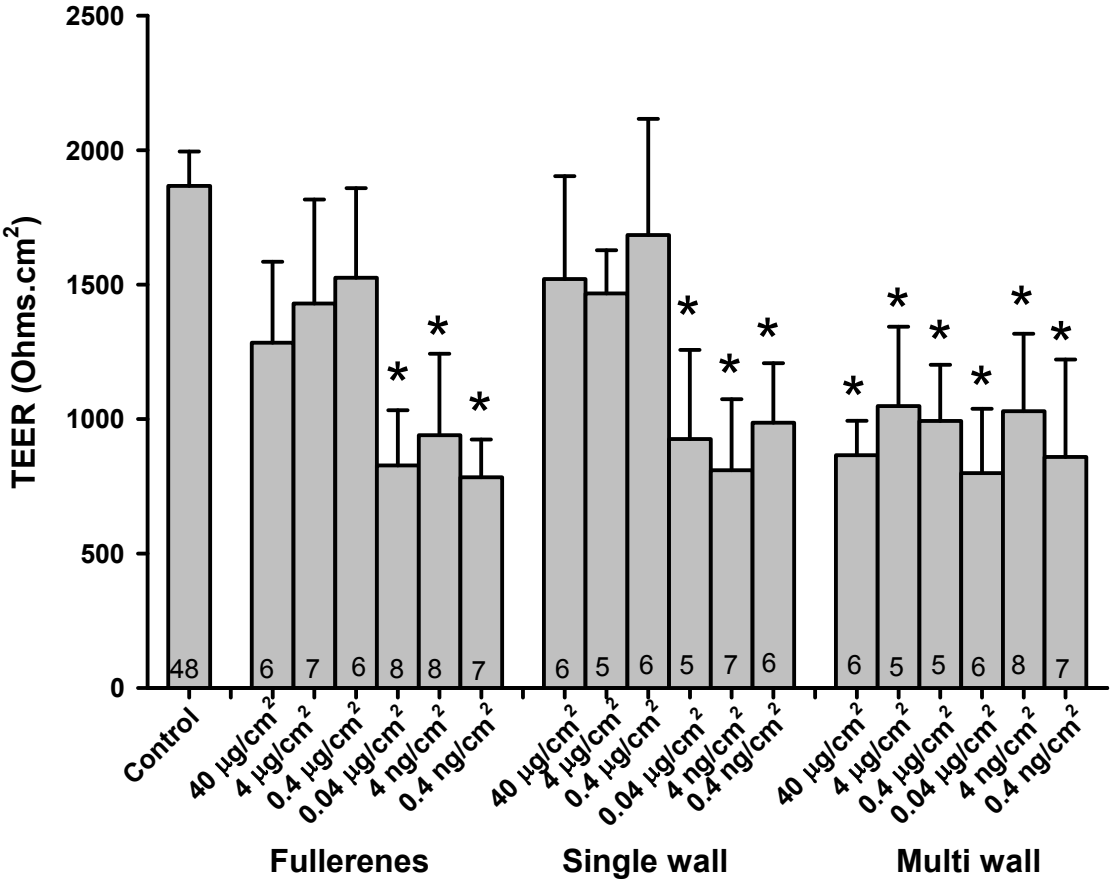

Figure 15 Effect of the Nanoparticle Incubation on the TEER in the mpkCCD$_{cl4}$ Cell Line

Cells were grown to confluency on transwell permeable supports and incubated for 48 h with media containing the indicated concentrations of nanoparticles. After the incubation the transwell filters were excised and mounted in Ussing chamber for the measurement of TEER. The bars represents the mean ±SEM. * indicates experiments where the mean value were significantly different than the mean control value. The values in the bars represent the number of replicate experiments.

Figure 16 Response of mpkCCD_{cl4} Renal Cells to ADH in Control and Nanotube Exposed Cultures

Cells were grown in transwell supports until confluent. The monolayer was then exposed to nanoparticle containing media for 48 h. The cells were mounted in Ussing chambers and the basal SCC was allowed to stabilize. ADH was added to the serosal bathing media at time zero. The hormone causes an immediate response that consists of a CFTR-mediated Cl^- secretory phase (~ 0–1 min) followed by an ENaC-mediated increase in Na^+ flux (~ 5–30 min). Amiloride, a specific inhibitor of ENaC, was used to terminate the experiment at time t = 30 min. This figure contains the data from control, 40 μg/cm^2 (highest dose) and 0.4 ng/cm^2 (lowest dose). Symbols=mean ± SEM for the number of experiments listed in legend.

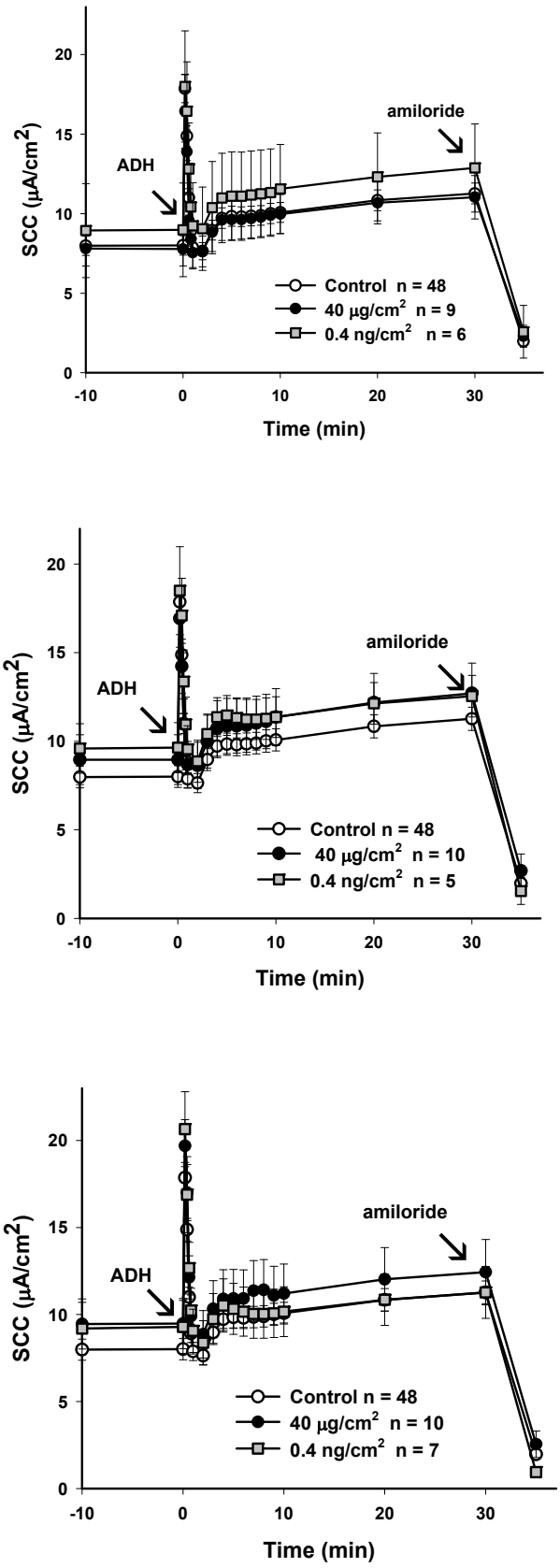
SCC (μA/cm²)
Time (min)
ADH
amiloride
Control n = 48
40 μg/cm² n = 9
0.4 ng/cm² n = 6
Control n = 48
40 μg/cm² n = 10
0.4 ng/cm² n = 5
Control n = 48
40 μg/cm² n = 10
0.4 ng/cm² n = 7

Figure 16

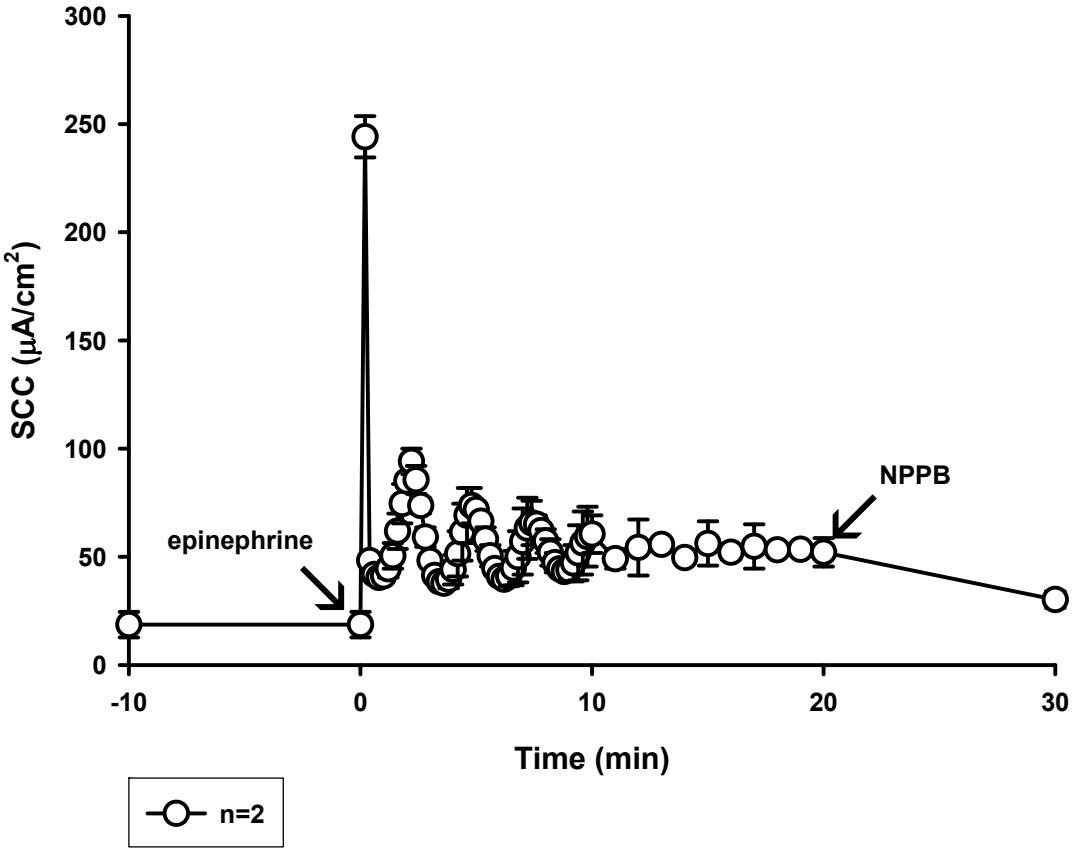

Figure 17 Response of Calu-3 Cells to Epinephrine

Confluent monolayers of Calu-3 cells were grown on permeable transwell membranes for 14 days, were excised, mounted in a Ussing chamber and the cells were allowed to develop a stable basal SCC. The graphs depict the continuous measurement of short circuit current (SCC), a measure of net ion transport of the nanoparticle exposed cells. At time=0, epinephrine (10^{-6}M) was added to the serosal bathing medium. At time=20 min, NPPB was added to inhibit the Cl^- secretion. The response consisted of several ion transport fluctuations characterized by progressively dampened peaks.

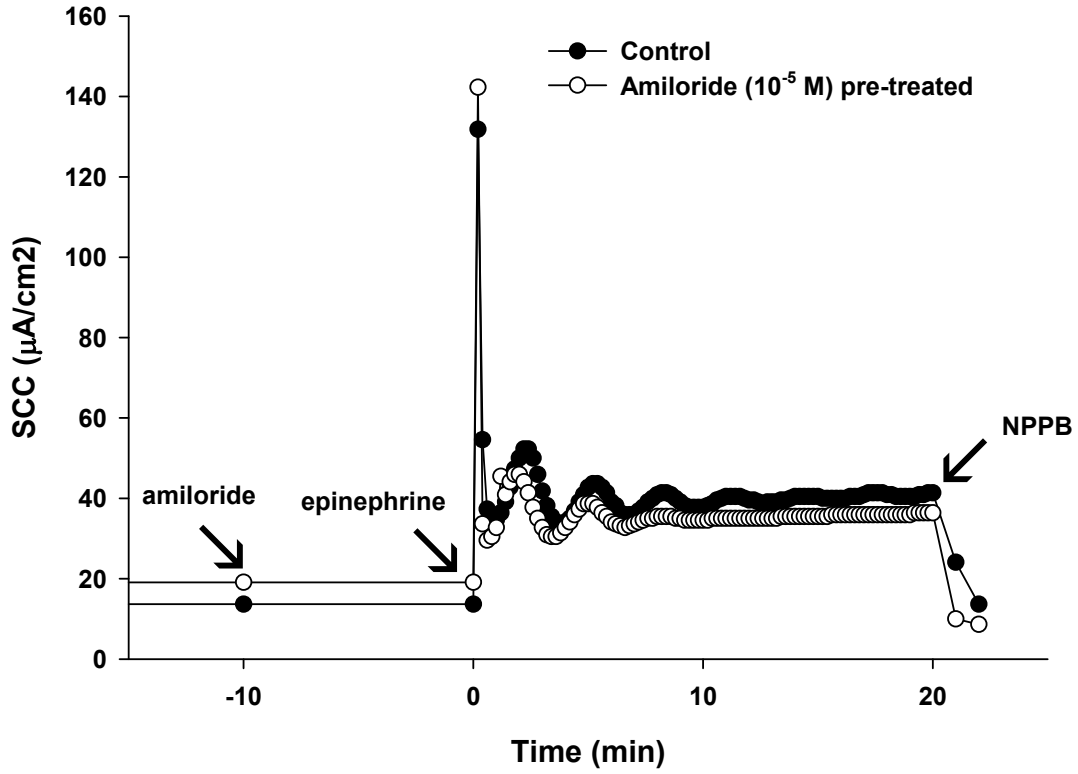

Figure 18 Effect of Amiloride Pretreatment on the Epinephrine Stimulated Ion Transport in the Calu-3 Cell Line

Confluent monolayers of Calu-3 cells grown on permeable transwell membranes for 14 days, were excised, mounted in a Ussing chamber and the cells were allowed to develop a stable basal short circuit current (SCC). The graphs depict the continuous measurement of SCC, a measure of net ion transport of the cells. ● Control cells ○ Cells that were pretreated with amiloride (10^{-5} M) for 10 min. At time = 0, epinephrine (10^{-6} M) was added to the serosal bathing medium. At time = 20 min, NPPB was added to inhibit the Cl^- secretion. This experiment is a representative of three experiments done in cultures grown in parallel.

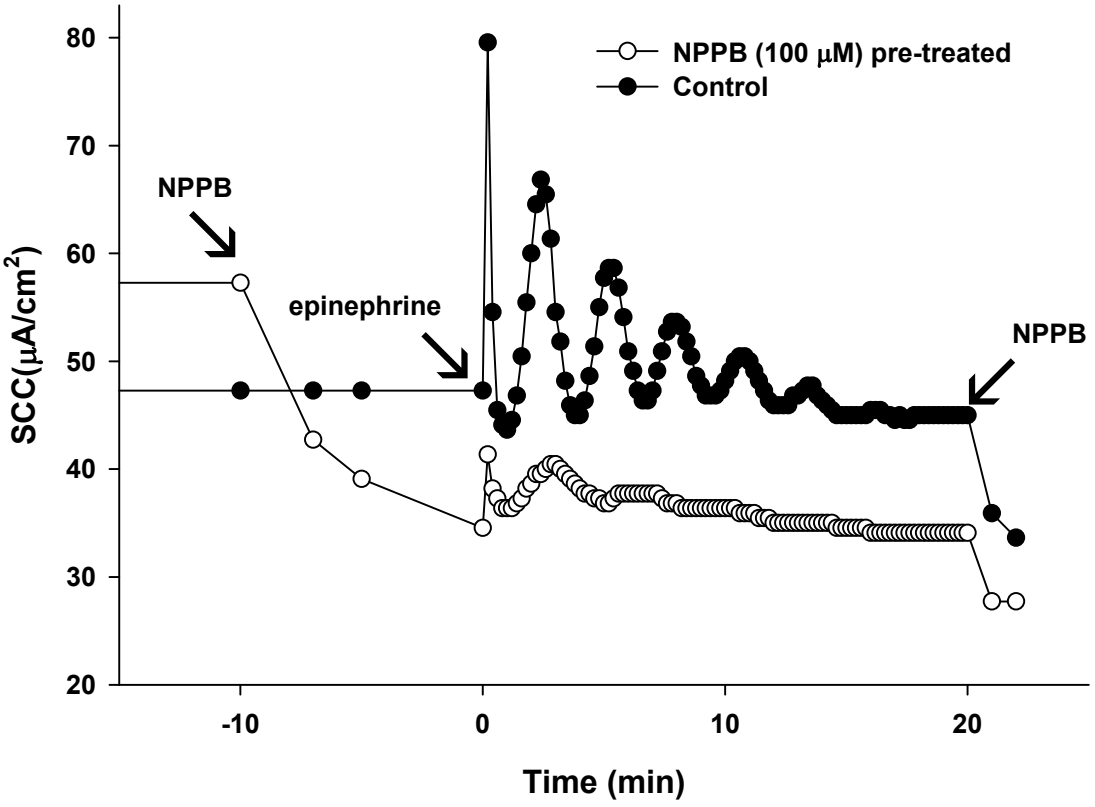

Figure 19 Effect of NPPB Pretreatment on the Epinephrine Stimulated Ion Transport in the Calu-3 Cell Line

Confluent monolayers of Calu-3 cells grown on permeable transwell membranes for 14 days, were excised, mounted in a Ussing chamber and the cells were allowed to develop a stable basal short circuit current (SCC). The graphs depict the continuous measurement of SCC, a measure of net ion transport of the cells. ● Control cells ○ The cells that were pretreated with NPPB (100 μM) for 10 min. At time = 0, epinephrine (10^{-6} M) was added to the serosal bathing medium. At time = 20 min, NPPB was added to inhibit the Cl^- secretion. This experiment is a representative of three experiment done in cultures grown in parallel.

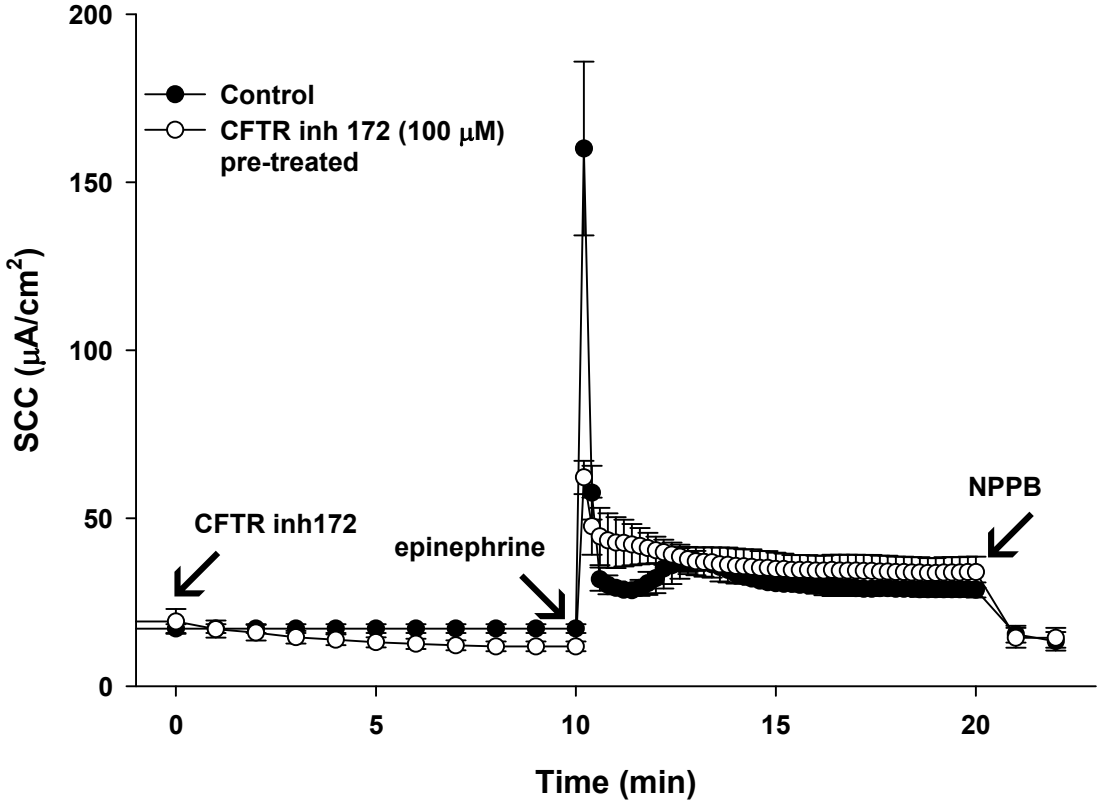

Figure 20 Effect of CFTR inh 172 Pretreatment on the Epinephrine Stimulated Ion Transport in the Calu-3 Cell Line

Confluent monolayers of Calu-3 cells grown on permeable transwell membranes for 14 days, were excised, mounted in a Ussing chamber and the cells were allowed to develop a stable basal short circuit current (SCC). The graphs depict the continuous measurement of SCC, a measure of net ion transport of the cells. ● Control cells ○ The cells that were pretreated with CFTR inh 172 (100 μM) for 10 min. At time = 10 min, epinephrine (10^{-6} M) was added to the serosal bathing medium. At time = 20 min, NPPB was added to inhibit the Cl^- secretion.(n=3).

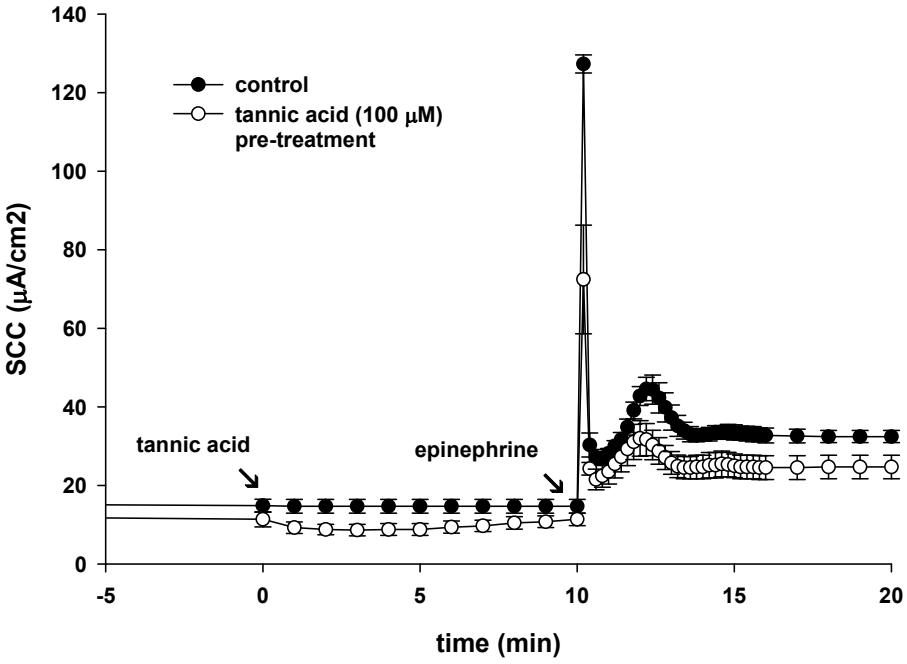

Figure 21 Effect of Tannic Acid Pretreatment on the Epinephrine Stimulated Ion Transport in the Calu-3 Cell Line

Confluent monolayers of Calu-3 cells grown on permeable transwell membranes for 14 days, were excised, mounted in a Ussing chamber and the cells were allowed to develop a stable basal short circuit current (SCC). The graphs depict the continuous measurement of SCC, a measure of net ion transport of the cells. ● Control cells ○ The cells that were pretreated with tannic acid (100 μM) for 10 min. At time = 10 min, epinephrine (10^{-6} M) was added to the serosal bathing medium. (n=3).

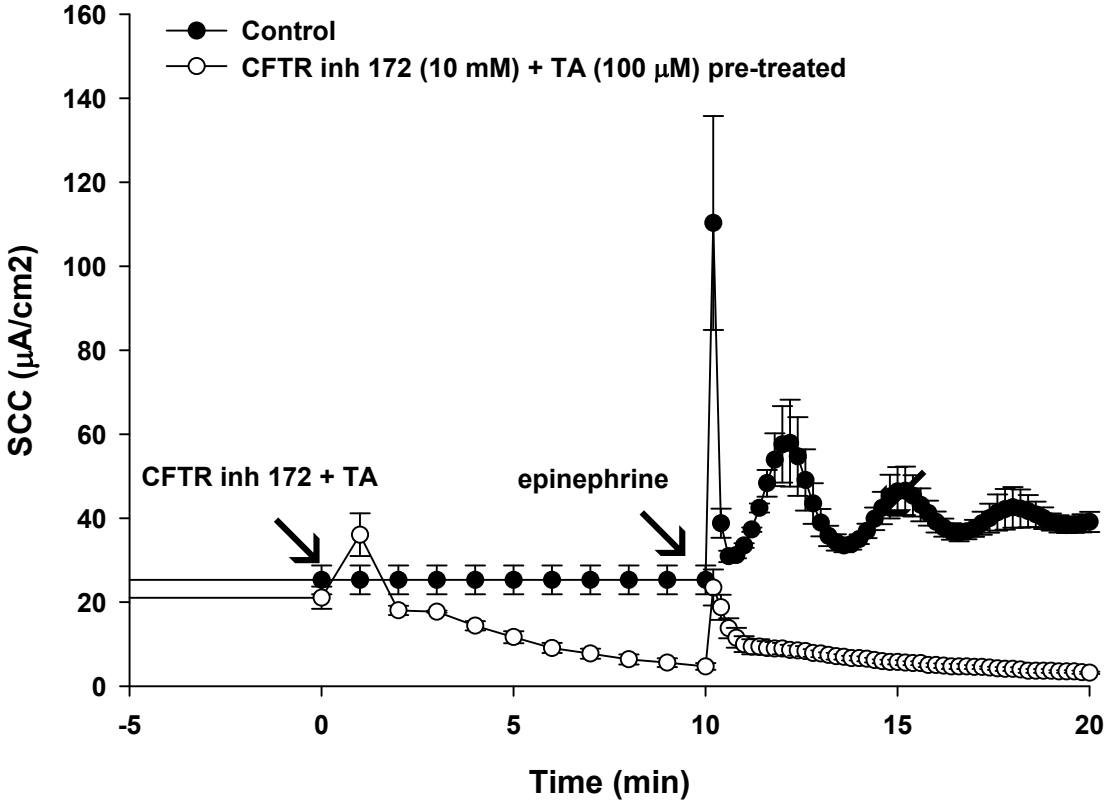

Figure 22 Effect of CFTR inh 172 and Tannic Acid Pretreatment on the Epinephrine Stimulated Ion Transport in the Calu-3 Cell Line

Confluent monolayers of Calu-3 cells grown on permeable transwell membranes for 14 days, were excised, mounted in a Ussing chamber and the cells were allowed to develop a stable basal short circuit current (SCC). The graphs depict the continuous measurement of SCC, a measure of net ion transport of the cells. ● Control cells ○ The cells that were pretreated with CFTR inh 172 (10 μM) and tannic acid (100 μM) for 10 min. At time =10 min, epinephrine (10^{-6} M) was added to the serosal bathing medium.

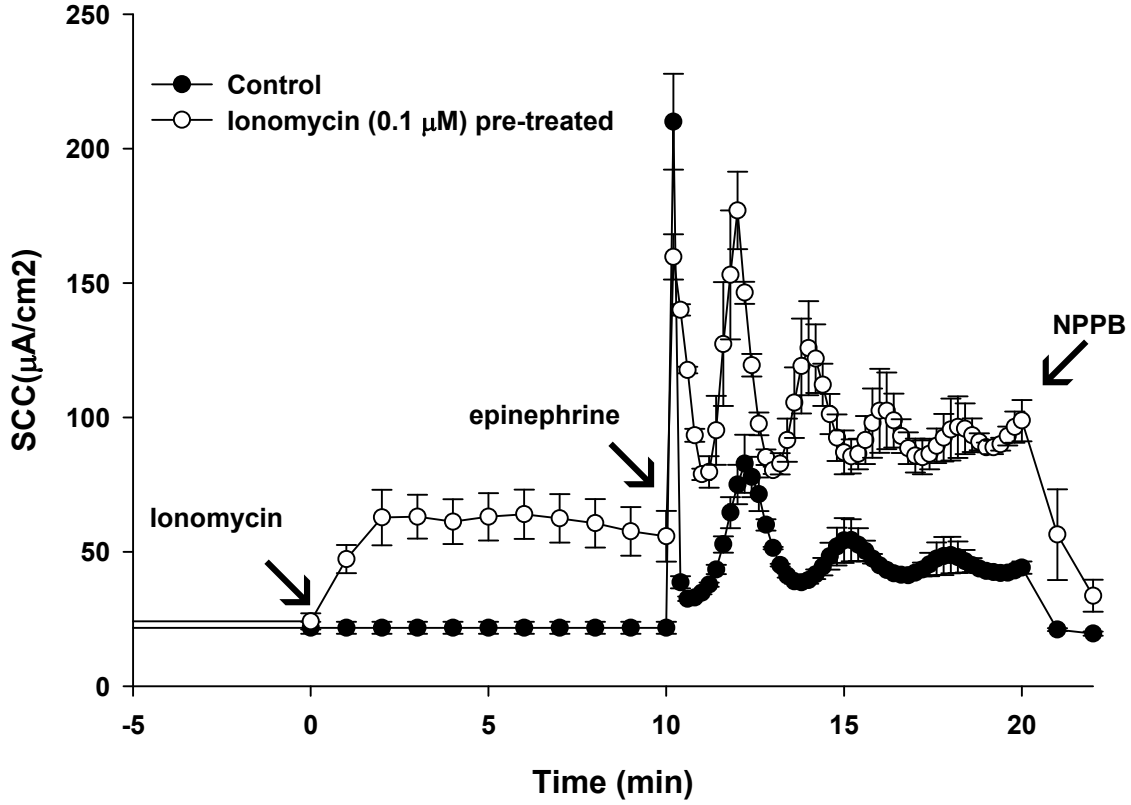

Figure 23 Effect of Ionomycin Pretreatment on the Epinephrine Stimulated Ion Transport in the Calu-3 Cell Line

Confluent monolayers of Calu-3 cells grown on permeable transwell membranes for 14 days, were excised, mounted in a Ussing chamber and the cells were allowed to develop a stable basal short circuit current (SCC). The graphs depict the continuous measurement of SCC, a measure of net ion transport of the cells. ● Control cells ○ The cells that were pretreated with ionomycin (0.1 μM) for 10 min. At time = 10 min, epinephrine (10^{-6} M) was added to the serosal bathing medium. At time = 20 min, NPPB was added to inhibit the Cl^- secretion.(n=3).

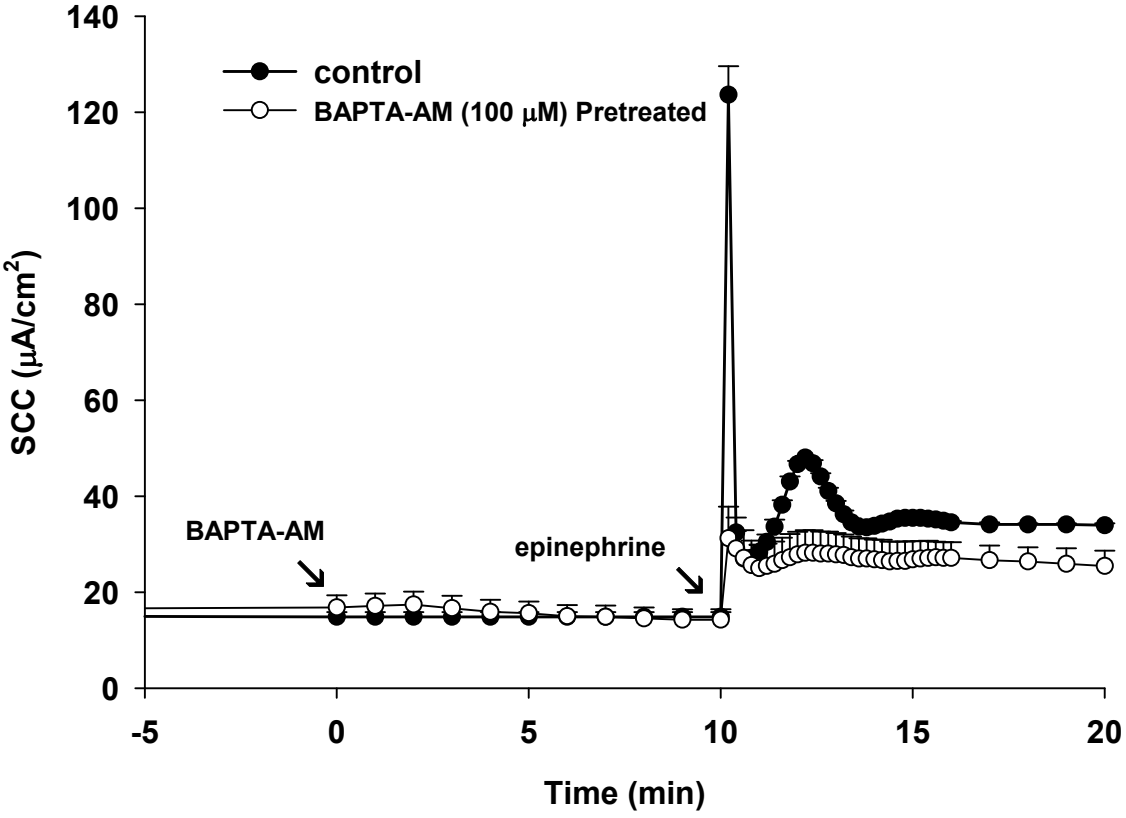

Figure 24 Effect of BAPTA-AM Pretreatment on the Epinephrine Stimulated Ion Transport in the Calu-3 Cell Line

Confluent monolayers of Calu-3 cells grown on permeable transwell membranes for 14 days, were excised, mounted in a Ussing chamber and the cells were allowed to develop a stable basal short circuit current (SCC). The graphs depict the continuous measurement of SCC, a measure of net ion transport of the cells. ● Control cells ○ The cells that were pretreated with BAPTA-AM (100 μM) for 10 min. At time = 10 min, epinephrine (10^{-6} M) was added to the serosal bathing medium. (n=3).

Figure 25 Effect of 48 h, 24 h and 1 h CNP Exposure on TEER of Calu-3 Cells

Calu-3 cells were grown for 14 days to form a high resistance monolayer on transwell membrane supports under air-liquid interface conditions and treated with CNPs for time periods as indicated in the figure. After the treatment time, the cells were excised from the transwells and mounted in Ussing chambers for measurement of transepithelial resistance, TEER. The number at the base of each bar indicates the number of separate cultures that were measured. Columns indicate means ±SEM * indicates that the value was statistically different from the control value ($P<0.05$) using a Students' t-test.

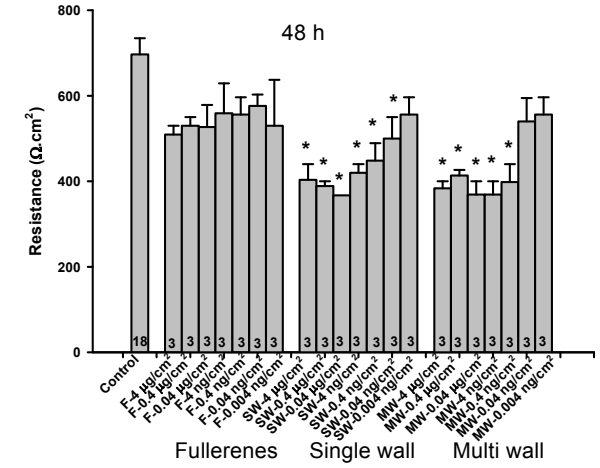
48 h
Resistance (Ω.cm²)
800
600
400
200
0
Control
F-4 µg/cm²
F-0.4 µg/cm²
F-0.04 µg/cm²
F-4 ng/cm²
F-0.4 ng/cm²
F-0.04 ng/cm²
F-0.004 ng/cm²
SW-4 µg/cm²
SW-0.4 µg/cm²
SW-0.04 µg/cm²
SW-4 ng/cm²
SW-0.4 ng/cm²
SW-0.04 ng/cm²
SW-0.004 ng/cm²
MW-4 µg/cm²
MW-0.4 µg/cm²
MW-0.04 µg/cm²
MW-4 ng/cm²
MW-0.4 ng/cm²
MW-0.04 ng/cm²
MW-0.004 ng/cm²
Fullerenes
Single wall
Multi wall

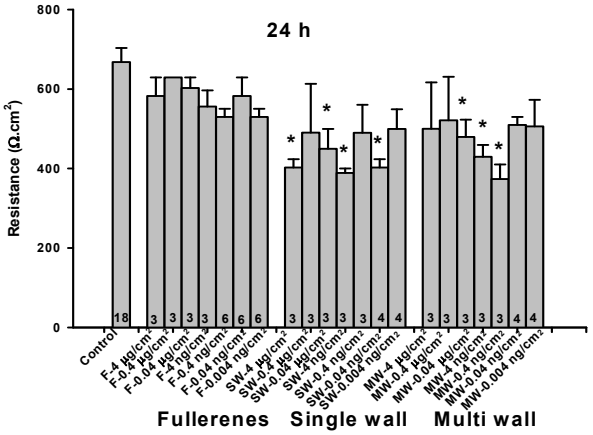
24 h
Resistance (Ω.cm²)
800
600
400
200
0
Control
Fullerenes
Single wall
Multi wall

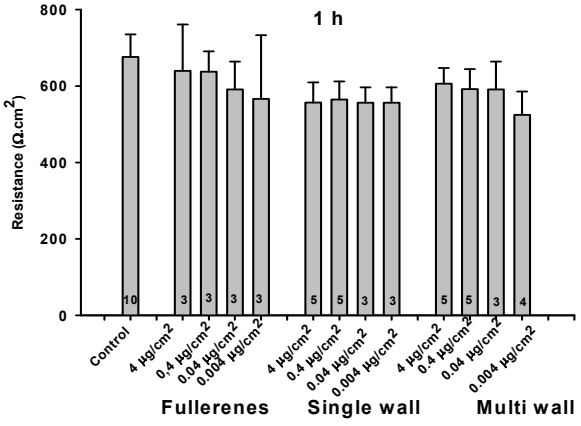
1 h
Resistance (Ω.cm²)
800
600
400
200
0
Control
4 µg/cm²
0,4 µg/cm²
0.04 µg/cm²
0.004 µg/cm²
Fullerenes
Single wall
Multi wall

Figure 25

Figure 26 Epinephrine-Stimulated Ion Transport in the Calu-3 Cell Line after 48 h Nanoparticle Incubation

The graphs depict the continuous measurement of SCC, in the control and nanoparticle exposed cells (fullerene, SWNT and MWNT respectively from top to bottom). The top figures illustrate the SCC plot of the highest and lowest exposure concentrations of fullerenes for 48 h. The middle and bottom graphs illustrate the responses of the highest and lowest nanotube concentrations that had a significant effect on epinephrine stimulated ion transport. When a stable baseline was achieved, epinephrine (10^{-6}M) was added to the cultures (Time T=0). NPPB (100 μM) was added 20 minutes after the epinephrine. The points on the graphs are means $\pm$ SEM of the number of experiments conducted. * indicates that the value was statistically different from the control value ($P<0.05$) using a Students' t-test.

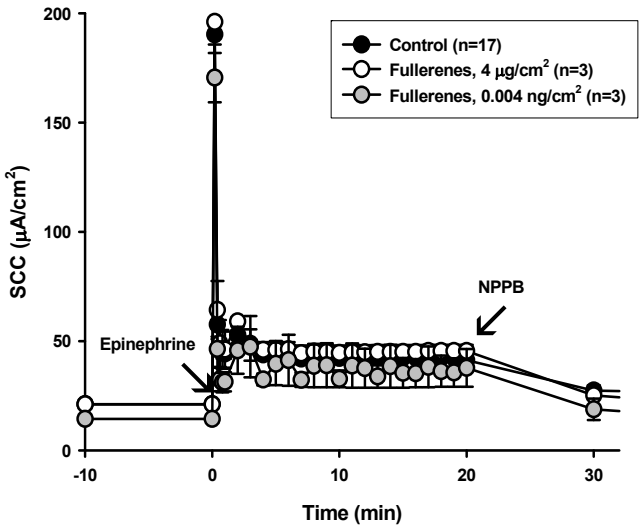
Control (n=17)
Fullerenes, 4 µg/cm² (n=3)
Fullerenes, 0.004 ng/cm² (n=3)
SCC (µA/cm²)
Epinephrine
NPPB
Time (min)

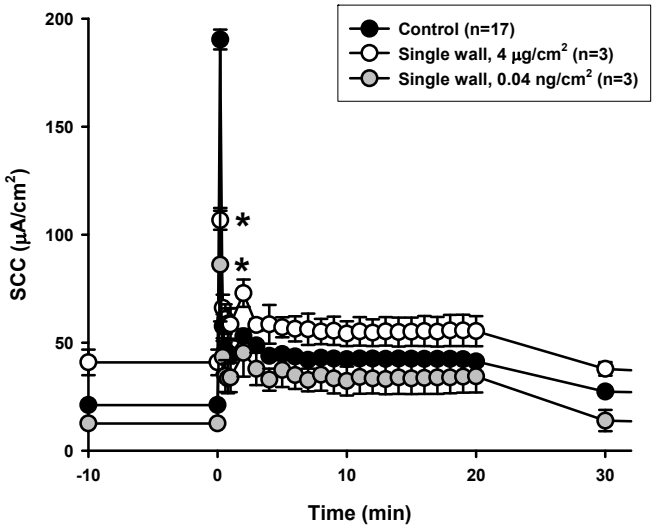
Control (n=17)
Single wall, 4 µg/cm² (n=3)
Single wall, 0.04 ng/cm² (n=3)
SCC (µA/cm²)
*
*
Time (min)

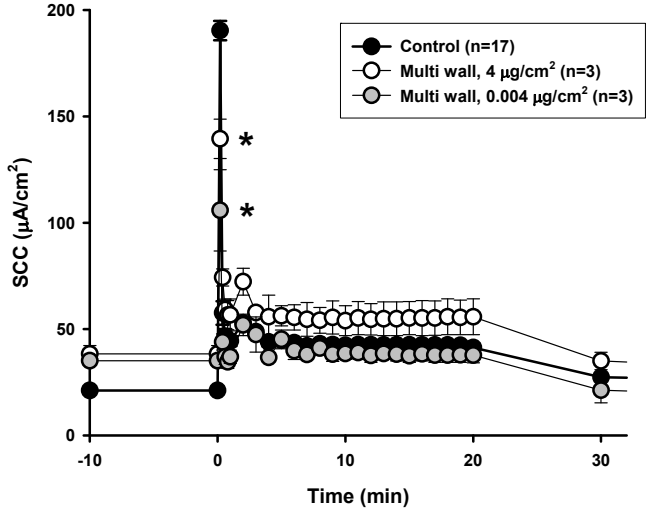
Control (n=17)
Multi wall, 4 µg/cm² (n=3)
Multi wall, 0.004 µg/cm² (n=3)
SCC (µA/cm²)
*
*
Time (min)

Figure 26

Figure 27 Epinephrine-Stimulated Ion Transport in the Calu-3 Cell Line After 24 hour Incubation with Nanoparticles

The graphs depict the continuous measurement of SCC, in the control and nanoparticle exposed cells (fullerene, SWNT and MWNT respectively from top to bottom). The top figures illustrate the SCC plot of the highest and lowest exposure concentrations of fullerenes for 24 h. The middle and bottom graphs illustrate the responses of the highest and lowest nanotube concentrations that had a significant effect on epinephrine stimulated ion transport. When a stable baseline was achieved, epinephrine (10^{-6}M) was added to the cultures (Time T=0). NPPB (100 μM) was added 20 minutes after the epinephrine. The points on the graphs are means $\pm$ SEM of the number of experiments conducted. * indicates that the value was statistically different from the control value ($P<0.05$) using a Students' t-test.

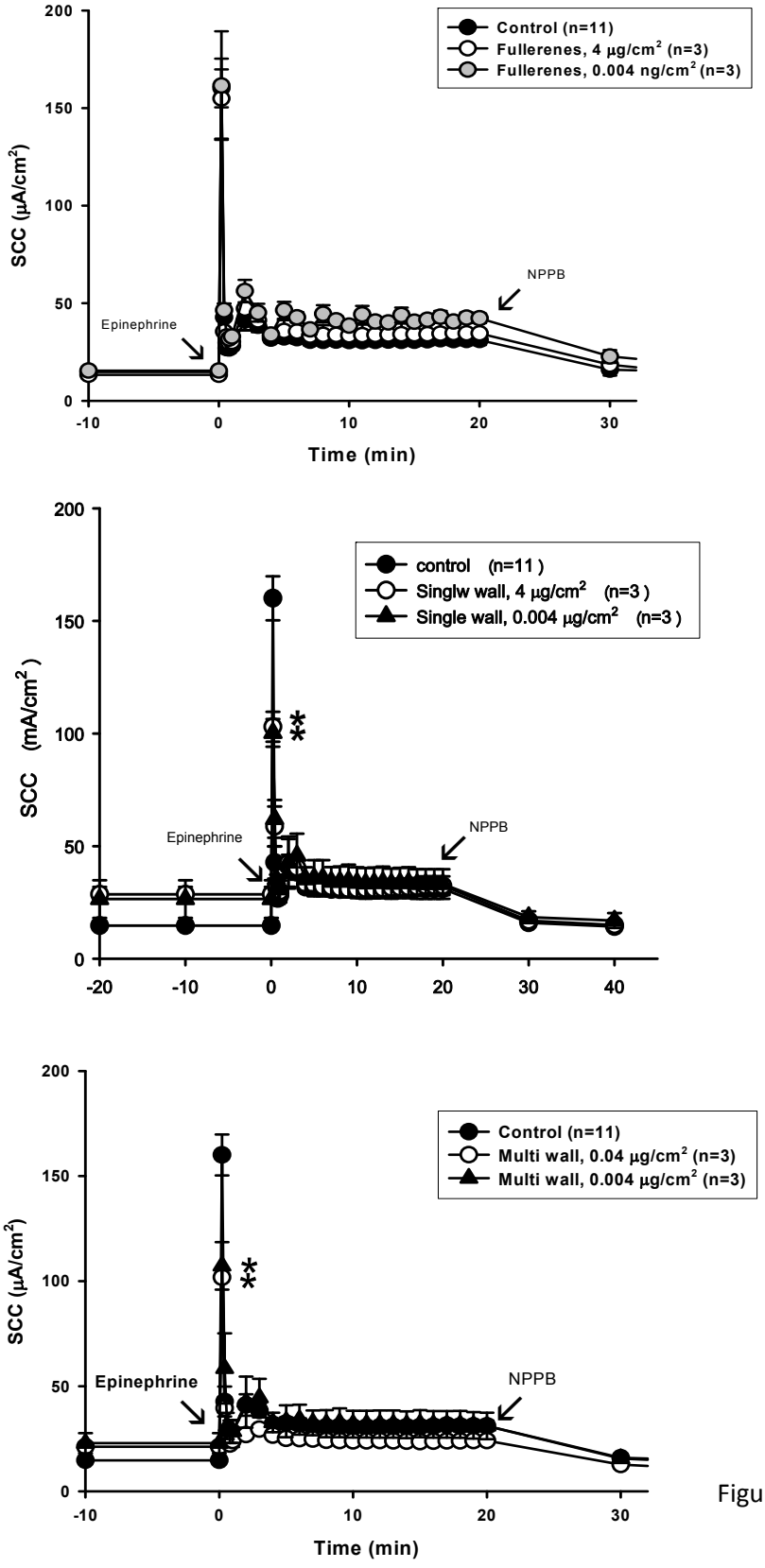
Control (n=11)
Fullerenes, 4 µg/cm² (n=3)
Fullerenes, 0.004 ng/cm² (n=3)
SCC (µA/cm²)
Epinephrine
NPPB
Time (min)
control (n=11)
Singlw wall, 4 µg/cm² (n=3)
Single wall, 0.004 µg/cm² (n=3)
SCC (mA/cm²)
**
Epinephrine
NPPB
Control (n=11)
Multi wall, 0.04 µg/cm² (n=3)
Multi wall, 0.004 µg/cm² (n=3)
SCC (µA/cm²)
**
Epinephrine
NPPB
Time (min)

Figure 27

Figure 28 Epinephrine-Stimulated Ion Transport in the Calu-3 Cell Line after 1 h Incubation with Nanoparticles

The graphs depict the continuous measurement of SCC, in the control and nanoparticle exposed cells (fullerene, SWNT and MWNT respectively from top to bottom). The top figures illustrate the SCC plot of the highest and lowest exposure concentrations of fullerenes for 1 h. The middle and bottom graphs illustrate the responses of the highest and lowest nanotube concentrations that had a significant effect on epinephrine stimulated ion transport. When a stable baseline was achieved, epinephrine (10^{-6}M) was added to the cultures (Time T=0). NPPB (100 µM) was added 20 minutes after the epinephrine. The points on the graphs are means $\pm$ SEM of the number of experiments conducted. None of the treated samples were significantly different than the control using a Students' t-test.

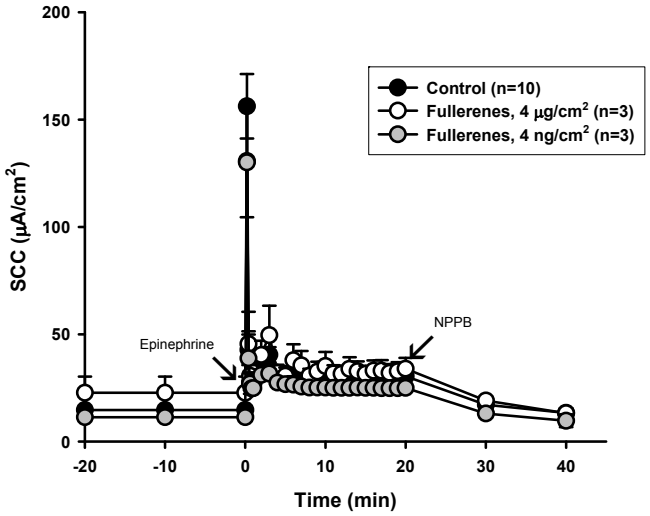
Control (n=10)
Fullerenes, 4 μg/cm² (n=3)
Fullerenes, 4 ng/cm² (n=3)
SCC (μA/cm²)
Epinephrine
NPPB
Time (min)

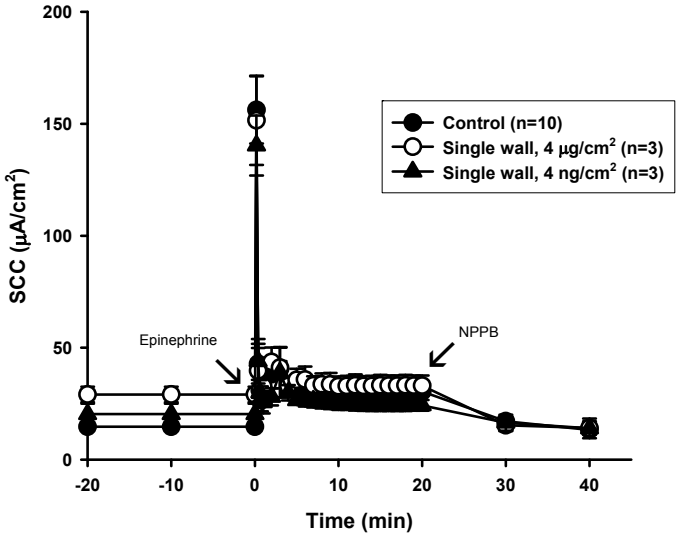
Control (n=10)
Single wall, 4 μg/cm² (n=3)
Single wall, 4 ng/cm² (n=3)
SCC (μA/cm²)
Epinephrine
NPPB
Time (min)

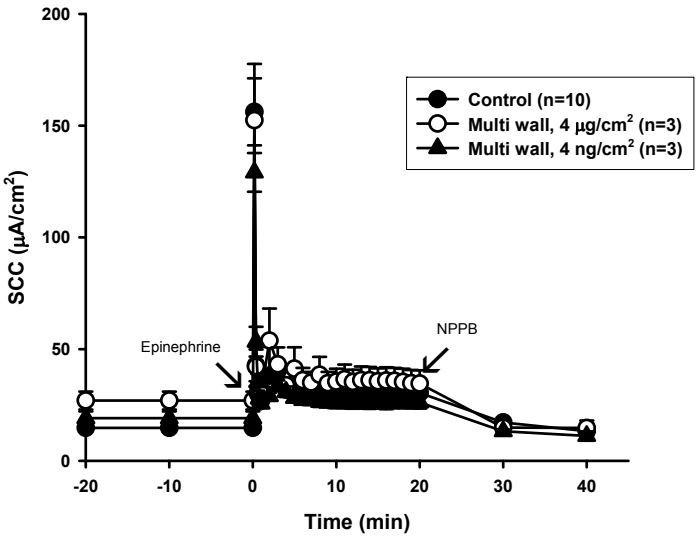
Control (n=10)
Multi wall, 4 μg/cm² (n=3)
Multi wall, 4 ng/cm² (n=3)
SCC (μA/cm²)
Epinephrine
NPPB
Time (min)

Figure 28

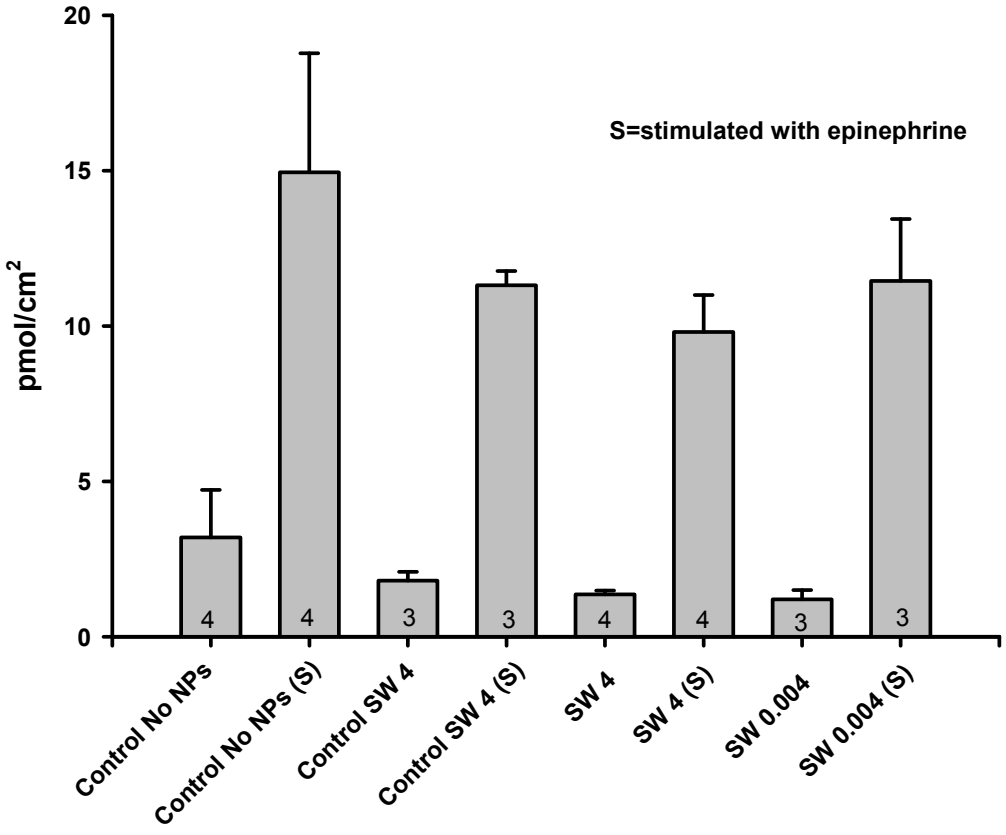

Figure 29 cAMP Concentration in Cells Treated with Single Walled Nanotubes at a Concentration of 4 and 0.004 μg/cm^2 vs Untreated Cells

The NPs are known to interfere in the colorimetric assays so a control with NPs added at the time of experiment was included. The values in the bars represent the number of replicates. The two controls (+/- nanoparticles at the time of experiment) did not differ significantly from each other. Neither of the treated samples had cAMP levels that were significantly different than controls under basal or stimulated conditions.

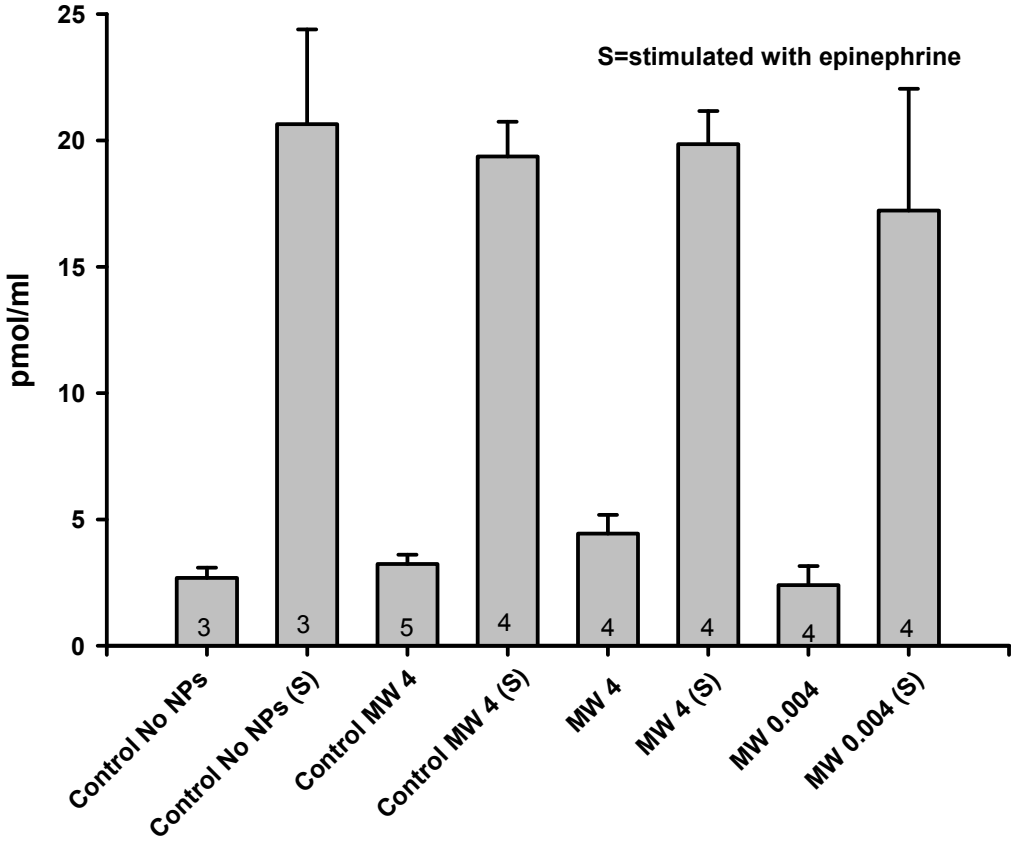

Figure 30 cAMP Concentration in Cells Treated with Multi Walled Nanotubes at a Concentration of 4 and 0.004 μg/cm^2 vs Untreated Cells

The NPs are known to interfere in the colorimetric assays so a control with NPs added at the time of experiment was included. The values in the bars represent the number of replicates. The two controls (+/- nanoparticles at the time of experiment) did not differ significantly from each other. Neither of the treated samples had cAMP levels that were significantly different than controls under basal or stimulated conditions.

Figure 31 Release of Cytokines by Calu-3 cells on Exposure to CNTs

Cell were grown on 6 well permeable supports for 14 days and exposed to two concentrations (4 and 0.004 μg/cm^2) of nanotubes (SWNT and MWNT) for the last 48 h of growth. Media was collected form apical (A) and basolateral (B) sides. Human Inflammation ELISA Strip for Profiling 8 Cytokines kit (Signosis, Sunnyvale CA) was used for determining eight cytokines; TNF-α (Tumor necrosis factor-alpha), IFNr (interferon regulator), G-CSF (granulocyte-colony stimulating factor), GM-CSF (granulocyte macrophage-colony stimulating factor), IL-1a (interleukin-1a), IL-8 (interleukin-8), IP-10 (Interferon inducible protein 10), and RANTES (regulated on activation, normal T expressed and secreted) in the apical and basolateral media according to the given protocol. The bars represent the average of three experiments.

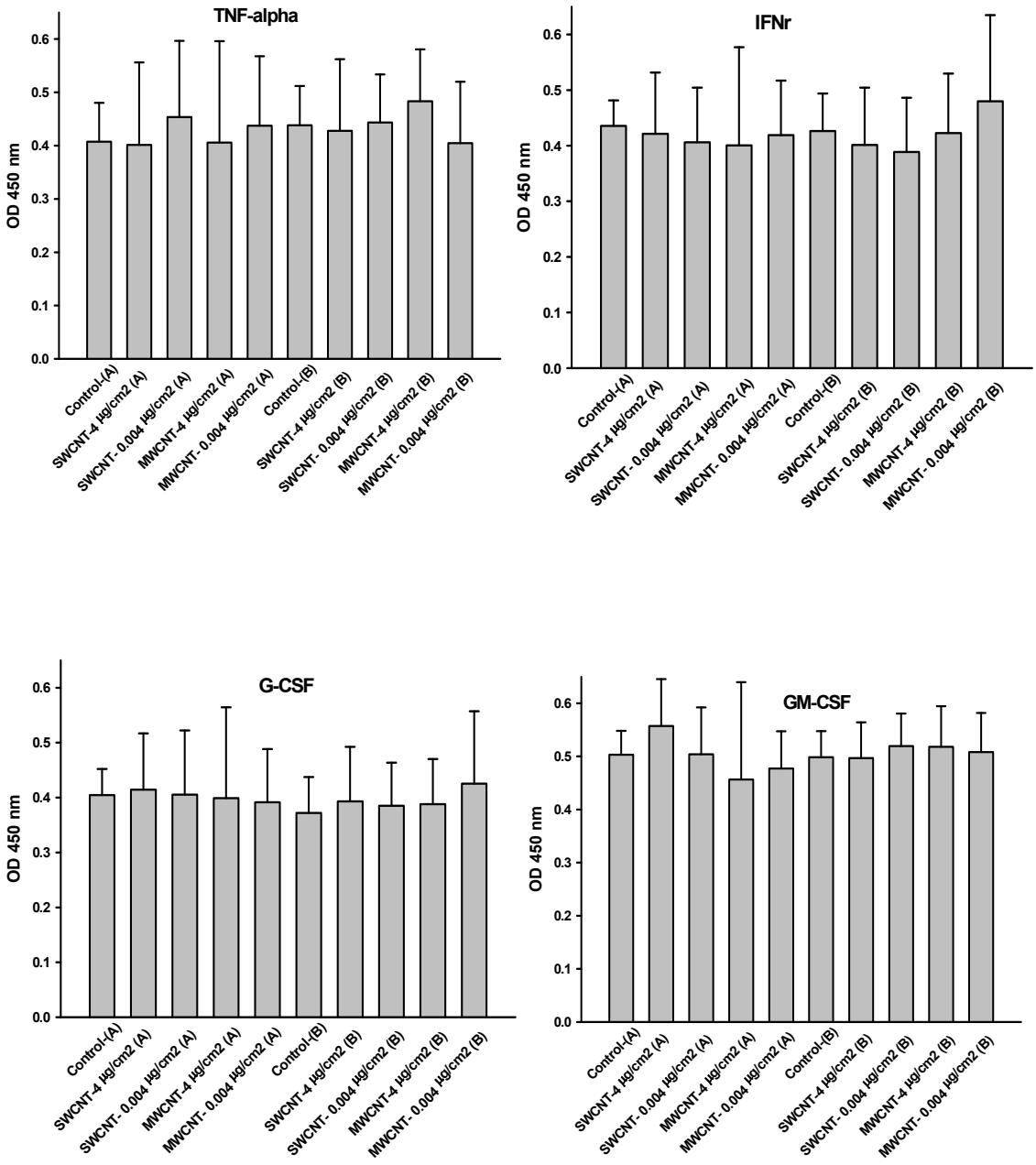
TNF-alpha
IFNr
G-CSF
GM-CSF
OD 450 nm
0.0
0.1
0.2
0.3
0.4
0.5
0.6
Control-(A)
SWCNT-4 µg/cm2 (A)
SWCNT- 0.004 µg/cm2 (A)
MWCNT-4 µg/cm2 (A)
MWCNT- 0.004 µg/cm2 (A)
Control-(B)
SWCNT-4 µg/cm2 (B)
SWCNT- 0.004 µg/cm2 (B)
MWCNT-4 µg/cm2 (B)
MWCNT- 0.004 µg/cm2 (B)

Figure 31

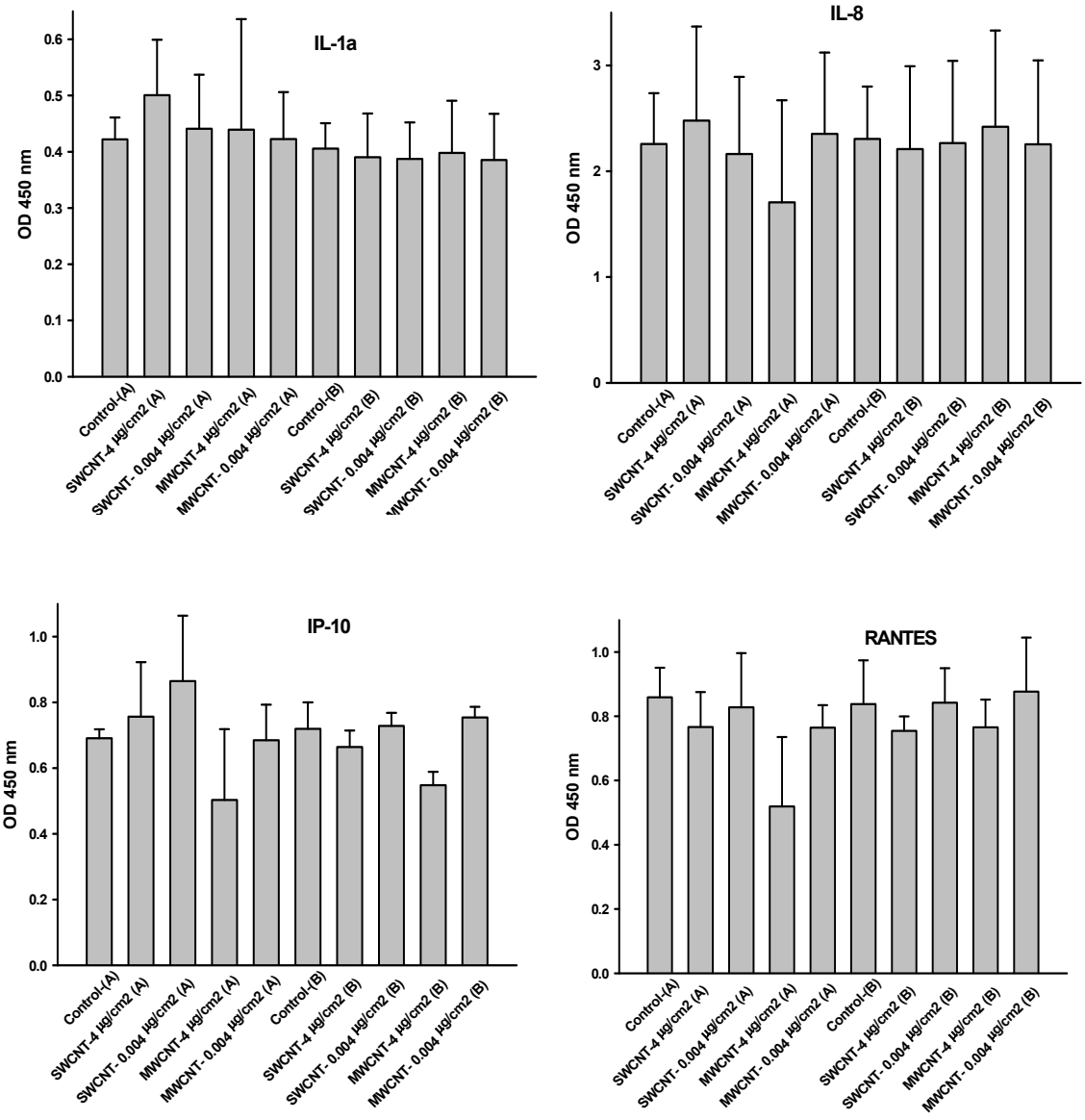
IL-1a
OD 450 nm
0.0
0.1
0.2
0.3
0.4
0.5
0.6
Control-(A)
SWCNT-4 µg/cm2 (A)
SWCNT- 0.004 µg/cm2 (A)
MWCNT-4 µg/cm2 (A)
MWCNT- 0.004 µg/cm2 (A)
Control-(B)
SWCNT-4 µg/cm2 (B)
SWCNT- 0.004 µg/cm2 (B)
MWCNT-4 µg/cm2 (B)
MWCNT- 0.004 µg/cm2 (B)
IL-8
OD 450 nm
0
1
2
3
Control-(A)
SWCNT-4 µg/cm2 (A)
SWCNT- 0.004 µg/cm2 (A)
MWCNT-4 µg/cm2 (A)
MWCNT- 0.004 µg/cm2 (A)
Control-(B)
SWCNT-4 µg/cm2 (B)
SWCNT- 0.004 µg/cm2 (B)
MWCNT-4 µg/cm2 (B)
MWCNT- 0.004 µg/cm2 (B)
IP-10
OD 450 nm
0.0
0.2
0.4
0.6
0.8
1.0
Control-(A)
SWCNT-4 µg/cm2 (A)
SWCNT- 0.004 µg/cm2 (A)
MWCNT-4 µg/cm2 (A)
MWCNT- 0.004 µg/cm2 (A)
Control-(B)
SWCNT-4 µg/cm2 (B)
SWCNT- 0.004 µg/cm2 (B)
MWCNT-4 µg/cm2 (B)
MWCNT- 0.004 µg/cm2 (B)
RANTES
OD 450 nm
0.0
0.2
0.4
0.6
0.8
1.0
Control-(A)
SWCNT-4 µg/cm2 (A)
SWCNT- 0.004 µg/cm2 (A)
MWCNT-4 µg/cm2 (A)
MWCNT- 0.004 µg/cm2 (A)
Control-(B)
SWCNT-4 µg/cm2 (B)
SWCNT- 0.004 µg/cm2 (B)
MWCNT-4 µg/cm2 (B)
MWCNT- 0.004 µg/cm2 (B)

Figure 31

LIST OF REFERENCES

LIST OF REFERENCES

1. Cherukuri P, Gannon CJ, Leeuw TK, Schmidt HK, Smalley RE, et al. (2006) Mammalian pharmacokinetics of carbon nanotubes using intrinsic near-infrared fluorescence. Proc Natl Acad Sci U S A 103: 18882-18886.
2. Panessa-Warren BJ, Warren JB, Wong SS, Misewich JA (2006) Biological cellular response to carbon nanoparticle toxicity. J of Phys-Cond Matter 18: S2185-S2201.
3. Cassee FR, Muijser H, Duistermaat E, Freijer JJ, Geerse KB, et al. (2002) Particle size-dependent total mass deposition in lungs determines inhalation toxicity of cadmium chloride aerosols in rats. Application of a multiple path dosimetry model. Arch Toxicol 76: 277-286.
4. Oberdorster G (1996) Significance of particle parameters in the evaluation of exposure-dose-response relationships of inhaled particles. Inhal Toxicol 8 Suppl: 73-89.
5. Dawson KA, Salvati A, Lynch I (2009) Nanotoxicology: nanoparticles reconstruct lipids. Nat Nanotechnol 4: 84-85.
6. Oberdorster G, Sharp Z, Atudorei V, Elder A, Gelein R, et al. (2004) Translocation of inhaled ultrafine particles to the brain. Inhal Toxicol 16: 437-445.
7. An H, Liu Q, Ji Q, Jin B (2010) DNA binding and aggregation by carbon nanoparticles. Biochem Biophys Res Commun 393: 571-576.
8. Tsuji JS, Maynard AD, Howard PC, James JT, Lam CW, et al. (2006) Research strategies for safety evaluation of nanomaterials, part IV: risk assessment of nanoparticles. Toxicol Sci 89: 42-50.
9. Oberdorster G, Oberdorster E, Oberdorster J (2005) Nanotoxicology: an emerging discipline evolving from studies of ultrafine particles. Environ Health Perspect 113: 823-839.
10. Borm PJ, Robbins D, Haubold S, Kuhlbusch T, Fissan H, et al. (2006) The potential risks of nanomaterials: a review carried out for ECETOC. Part Fibre Toxicol 3: 11.
11. Kreyling WG, Semmler M, Erbe F, Mayer P, Takenaka S, et al. (2002) Translocation of ultrafine insoluble iridium particles from lung epithelium to extrapulmonary organs is size dependent but very low. J Toxicol Environ Health A 65: 1513-1530.
12. Jani PU, Mccarthy DE, Florence AT (1994) Titanium-Dioxide (Rutile) Particle Uptake from the Rat Gi Tract and Translocation to Systemic Organs after Oral-Administration. Intern J of Pharm 105: 157-168.
13. Egbaria K, Weiner N (1990) Liposomes as a Topical Drug Delivery System. Abstracts of Papers of the Am Chem Soc 200: 14-Pmse.
14. Nigavekar SS, Sung LY, Llanes M, El-Jawahri A, Lawrence TS, et al. (2004) 3H dendrimer nanoparticle organ/tumor distribution. Pharm Res 21: 476-483.
15. Fiorito S, Serafino A, Andreola F, Togna A, Togna G (2006) Toxicity and biocompatibility of carbon nanoparticles. J Nanosci Nanotechnol 6: 591-599.
16. Lewinski N, Colvin V, Drezek R (2008) Cytotoxicity of nanoparticles. Small 4: 26-49.

17. Oberdorster E (2004) Manufactured nanomaterials (fullerenes, C60) induce oxidative stress in the brain of juvenile largemouth bass. Environ Health Perspect 112: 1058-1062.
18. Ema M, Kobayashi N, Naya M, Hanai S, Nakanishi J (2010) Reproductive and developmental toxicity studies of manufactured nanomaterials. Reprod Toxicol 30: 343-352.
19. Park EJ, Kim H, Kim Y, Yi J, Choi K, et al. (2010) Carbon fullerenes (C60s) can induce inflammatory responses in the lung of mice. Toxicol Appl Pharmacol 244: 226-233.
20. Kraszewski S, Tarek M, Treptow W, Ramseyer C (2010) Affinity of C60 neat fullerenes with membrane proteins: a computational study on potassium channels. ACS Nano 4: 4158-4164.
21. Kolosnjaj-Tabi J, Hartman KB, Boudjemaa S, Ananta JS, Morgant G, et al. (2010) In vivo behavior of large doses of ultrashort and full-length single-walled carbon nanotubes after oral and intraperitoneal administration to Swiss mice. ACS Nano 4: 1481-1492.
22. Warheit DB, Laurence BR, Reed KL, Roach DH, Reynolds GA, et al. (2004) Comparative pulmonary toxicity assessment of single-wall carbon nanotubes in rats. Toxicol Sci 77: 117-125.
23. Lam CW, James JT, McCluskey R, Hunter RL (2004) Pulmonary toxicity of single-wall carbon nanotubes in mice 7 and 90 days after intratracheal instillation. Toxicol Sci 77: 126-134.
24. Shvedova AA, Kisin E, Murray AR, Johnson VJ, Gorelik O, et al. (2008) Inhalation vs. aspiration of single-walled carbon nanotubes in C57BL/6 mice: inflammation, fibrosis, oxidative stress, and mutagenesis. Am J of Physiol-Lung Cell and Mol Physiol 295: L552-L565.
25. Kisin ER, Murray AR, Keane MJ, Shi XC, Schwegler-Berry D, et al. (2007) Single-walled carbon nanotubes: geno- and cytotoxic effects in lung fibroblast V79 cells. J Toxicol Environ Health A 70: 2071-2079.
26. Cui D, Tian F, Ozkan CS, Wang M, Gao H (2005) Effect of single wall carbon nanotubes on human HEK293 cells. Toxicol Lett 155: 73-85.
27. Bihari P, Holzer M, Praetner M, Fent J, Lerchenberger M, et al. (2010) Single-walled carbon nanotubes activate platelets and accelerate thrombus formation in the microcirculation. Toxicol 269: 148-154.
28. Poland CA, Duffin R, Kinloch I, Maynard A, Wallace WA, et al. (2008) Carbon nanotubes introduced into the abdominal cavity of mice show asbestos-like pathogenicity in a pilot study. Nat Nanotechnol 3: 423-428.
29. Muller J, Huaux F, Fonseca A, Nagy JB, Moreau N, et al. (2008) Structural defects play a major role in the acute lung toxicity of multiwall carbon nanotubes: toxicological aspects. Chem Res Toxicol 21: 1698-1705.
30. Han SG, Andrews R, Gairola CG (2010) Acute pulmonary response of mice to multi-wall carbon nanotubes. Inhal Toxicol 22: 340-347.
31. Monteiro-Riviere NA, Nemanich RJ, Inman AO, Wang YY, Riviere JE (2005) Multi-walled carbon nanotube interactions with human epidermal keratinocytes. Toxicol Lett 155: 377-384.
32. Ravichandran P, Periyakaruppan A, Sadanandan B, Ramesh V, Hall JC, et al. (2009) Induction of apoptosis in rat lung epithelial cells by multiwalled carbon nanotubes. J Biochem Mol Toxicol 23: 333-344.
33. Patlolla A, Knighten B, Tchounwou P (2010) Multi-walled carbon nanotubes induce cytotoxicity, genotoxicity and apoptosis in normal human dermal fibroblast cells. Ethn Dis 20: S1-65-72.

34. Witzmann FA, Monteiro-Riviere NA (2006) Multi-walled carbon nanotube exposure alters protein expression in human keratinocytes. Nanomed 2: 158-168.
35. Donaldson K, Brown D, Clouter A, Duffin R, MacNee W, et al. (2002) The pulmonary toxicology of ultrafine particles. J Aerosol Med 15: 213-220.
36. Donaldson K, Tran L, Jimenez LA, Duffin R, Newby DE, et al. (2005) Combustion-derived nanoparticles: a review of their toxicology following inhalation exposure. Part Fibre Toxicol 2: 10.
37. Oberdorster G (2001) Pulmonary effects of inhaled ultrafine particles. Int Arch Occup Environ Health 74: 1-8.
38. Nemmar A, Hoet PH, Vanquickenborne B, Dinsdale D, Thomeer M, et al. (2002) Passage of inhaled particles into the blood circulation in humans. Circulation 105: 411-414.
39. Semmler M, Seitz J, Erbe F, Mayer P, Heyder J, et al. (2004) Long-term clearance kinetics of inhaled ultrafine insoluble iridium particles from the rat lung, including transient translocation into secondary organs. Inhal Toxicol 16: 453-459.
40. Elder A, Oberdorster G (2006) Translocation and effects of ultrafine particles outside of the lung. Clin Occup Environ Med 5: 785-796.
41. Mills NL, Amin N, Robinson SD, Anand A, Davies J, et al. (2006) Do inhaled carbon nanoparticles translocate directly into the circulation in humans? Am J of Resp and Crit Care Med 173: 426-431.
42. Borm PJ, Kreyling W (2004) Toxicological hazards of inhaled nanoparticles--potential implications for drug delivery. J Nanosci Nanotechnol 4: 521-531.
43. Reddy AR, Reddy YN, Krishna DR, Himabindu V (2010) Multi wall carbon nanotubes induce oxidative stress and cytotoxicity in human embryonic kidney (HEK293) cells. Toxicol 272: 11-16.
44. Wang J, Zhou G, Chen C, Yu H, Wang T, et al. (2007) Acute toxicity and biodistribution of different sized titanium dioxide particles in mice after oral administration. Toxicol Lett 168: 176-185.
45. Yang RS, Chang LW, Wu JP, Tsai MH, Wang HJ, et al. (2007) Persistent tissue kinetics and redistribution of nanoparticles, quantum dot 705, in mice: ICP-MS quantitative assessment. Environ Health Perspect 115: 1339-1343.
46. Choi HS, Liu W, Misra P, Tanaka E, Zimmer JP, et al. (2007) Renal clearance of quantum dots. Nat Biotechnol 25: 1165-1170.
47. Reddy AR, Krishna DR, Reddy YN, Himabindu V (2010) Translocation and extra pulmonary toxicities of multi wall carbon nanotubes in rats. Toxicol Mech Methods 20: 267-272.
48. Bens M, Vallet V, Cluzeaud F, Pascual-Letallec L, Kahn A, et al. (1999) Corticosteroid-dependent sodium transport in a novel immortalized mouse collecting duct principal cell line. J Am Soc Nephrol 10: 923-934.
49. Shane MA, Nofziger C, Blazer-Yost BL (2006) Hormonal regulation of the epithelial Na+ channel: from amphibians to mammals. Gen Comp Endocrinol 147: 85-92.
50. Foster KA, Avery ML, Yazdanian M, Audus KL (2000) Characterization of the Calu-3 cell line as a tool to screen pulmonary drug delivery. Int J of Pharm 208: 1-11.
51. Shen BQ, Finkbeiner WE, Wine JJ, Mrsny RJ, Widdicombe JH (1994) Calu-3: a human airway epithelial cell line that shows cAMP-dependent Cl- secretion. Am J Physiol 266: L493-501.
52. Singh M, Krouse M, Moon S, Wine JJ (1997) Most basal I(SC) in Calu-3 human airway cells is bicarbonate-dependent Cl- secretion. Am J Physiol 272: L690-698.

53. Ryman-Rasmussen JP, Cesta MF, Brody AR, Shipley-Phillips JK, Everitt JI, et al. (2009) Inhaled carbon nanotubes reach the subpleural tissue in mice. Nat Nanotechnol 4: 747-751.
54. Buford MC, Hamilton RF, Jr., Holian A (2007) A comparison of dispersing media for various engineered carbon nanoparticles. Part Fibre Toxicol 4: 6.
55. Vippola M, Falck GC, Lindberg HK, Suhonen S, Vanhala E, et al. (2009) Preparation of nanoparticle dispersions for in-vitro toxicity testing. Hum Exp Toxicol 28: 377-385.
56. Worle-Knirsch JM, Pulskamp K, Krug HF (2006) Oops they did it again! Carbon nanotubes hoax scientists in viability assays. Nano Lett 6: 1261-1268.
57. Lee KJ, Nallathamby PD, Browning LM, Osgood CJ, Xu XH (2007) In vivo imaging of transport and biocompatibility of single silver nanoparticles in early development of zebrafish embryos. ACS Nano 1: 133-143.
58. Decker T, Lohmann-Matthes ML (1988) A quick and simple method for the quantitation of lactate dehydrogenase release in measurements of cellular cytotoxicity and tumor necrosis factor (TNF) activity. J Immunol Methods 115: 61-69.
59. Korzeniewski C, Callewaert DM (1983) An enzyme-release assay for natural cytotoxicity. J Immunol Methods 64: 313-320.
60. Stone V, Johnston H, Schins RP (2009) Development of in vitro systems for nanotoxicology: methodological considerations. Crit Rev Toxicol 39: 613-626.
61. Bolstad BM, Irizarry RA, Astrand M, Speed TP (2003) A comparison of normalization methods for high density oligonucleotide array data based on variance and bias. Bioinformatics 19: 185-193.
62. Heywood H (1970) "The origins and development of Particle Size Analysis", in "Particle size analysis"; Groves MJao, editor: The Society for analytical chemistry, London.
63. Allen T (1990) Particle size measurement: Chapman and Hall, NY.
64. Irani RRaC, C.F. (1971) "Particle Size: Measurement, Interpretation and Application": John Wiley & Sons, NY-London.
65. Measuring Zeta Potential: LaserDoppler Electrophoresis. WWW.MALVERN.CO.UK.
66. Lai X, Bacallao RL, Blazer-Yost BL, Hong D, Mason SB, et al. (2008) Characterization of the renal cyst fluid proteome in autosomal dominant polycystic kidney disease (ADPKD) patients. Proteomics Clin Appl 2: 1140-1152.
67. Keller A, Nesvizhskii AI, Kolker E, Aebersold R (2002) Empirical statistical model to estimate the accuracy of peptide identifications made by MS/MS and database search. Anal Chem 74: 5383-5392.
68. JD S (2002) "A direct approach to false discovery rates.". Journal of the Royal Statistical Society Series B-Statistical Methodology 64: 479-498.
69. Monroe ME, Shaw JL, Daly DS, Adkins JN, Smith RD (2008) MASIC: a software program for fast quantitation and flexible visualization of chromatographic profiles from detected LC-MS(/MS) features. Comput Biol Chem 32: 215-217.
70. Storey JD (2002) "A direct approach to false discovery rates.". Journal of the Royal Statistical Society Series B-Statistical Methodology 64: 479-498.
71. Grainger CI, Greenwell LL, Lockley DJ, Martin GP, Forbes B (2006) Culture of Calu-3 cells at the air interface provides a representative model of the airway epithelial barrier. Pharm Res 23: 1482-1490.
72. Moon S, Singh M, Krouse ME, Wine JJ (1997) Calcium-stimulated Cl- secretion in Calu-3 human airway cells requires CFTR. Am J Physiol 273: L1208-1219.

73. Jeffery PK (1983) Morphologic features of airway surface epithelial cells and glands. Am Rev Respir Dis 128: S14-20.
74. Liedtke CM, Cole TS (1998) Antisense oligonucleotide to PKC-epsilon alters cAMP-dependent stimulation of CFTR in Calu-3 cells. Am J Physiol 275: C1357-1364.
75. Ma T, Thiagarajah JR, Yang H, Sonawane ND, Folli C, et al. (2002) Thiazolidinone CFTR inhibitor identified by high-throughput screening blocks cholera toxin-induced intestinal fluid secretion. J Clin Invest 110: 1651-1658.
76. Caputo A, Caci E, Ferrera L, Pedemonte N, Barsanti C, et al. (2008) TMEM16A, a membrane protein associated with calcium-dependent chloride channel activity. Science 322: 590-594.
77. Schroeder BC, Cheng T, Jan YN, Jan LY (2008) Expression cloning of TMEM16A as a calcium-activated chloride channel subunit. Cell 134: 1019-1029.
78. Yang YD, Cho H, Koo JY, Tak MH, Cho Y, et al. (2008) TMEM16A confers receptor-activated calcium-dependent chloride conductance. Nature 455: 1210-1215.
79. Namkung W, Phuan PW, Verkman AS (2011) TMEM16A inhibitors reveal TMEM16A as a minor component of calcium-activated chloride channel conductance in airway and intestinal epithelial cells. J Biol Chem 286: 2365-2374.
80. Pauluhn J (2010) Subchronic 13-week inhalation exposure of rats to multiwalled carbon nanotubes: toxic effects are determined by density of agglomerate structures, not fibrillar structures. Toxicol Sci 113: 226-242.
81. Pauluhn J (2010) Multi-walled carbon nanotubes (Baytubes): approach for derivation of occupational exposure limit. Regul Toxicol Pharmacol 57: 78-89.
82. L'Azou B, Jorly J, On D, Sellier E, Moisan F, et al. (2008) In vitro effects of nanoparticles on renal cells. Part Fibre Toxicol 5: 22.
83. Amos AD WF, Chernoff EA, Hong D, Lai X, Ringham HN, Blazer-Yost BL (2008) Changes in cell function and protein expression of mouse renal principal cells, mpkCCD, after carbon nanoparticle (CNP) exposure. FASEB J 22: 942.
84. Murr LE, Garza KM, Soto KF, Carrasco A, Powell TG, et al. (2005) Cytotoxicity assessment of some carbon nanotubes and related carbon nanoparticle aggregates and the implications for anthropogenic carbon nanotube aggregates in the environment. Int J Environ Res Public Health 2: 31-42.
85. Kane AB, Hurt RH (2008) Nanotoxicology: the asbestos analogy revisited. Nat Nanotechnol 3: 378-379.
86. Wang L, Mercer RR, Rojanasakul Y, Qiu A, Lu Y, et al. (2010) Direct fibrogenic effects of dispersed single-walled carbon nanotubes on human lung fibroblasts. J Toxicol Environ Health A 73: 410-422.
87. Holt BD, Short PA, Rape AD, Wang YL, Islam MF, et al. (2010) Carbon nanotubes reorganize actin structures in cells and ex vivo. ACS Nano 4: 4872-4878.
88. Warner JR, McIntosh KB (2009) How common are extraribosomal functions of ribosomal proteins? Mol Cell 34: 3-11.
89. Leussink BT, Baelde HJ, Broekhuizen-van den Berg TM, de Heer E, van der Voet GB, et al. (2003) Renal epithelial gene expression profile and bismuth-induced resistance against cisplatin nephrotoxicity. Hum Exp Toxicol 22: 535-540.
90. Guo L, Von Dem Bussche A, Buechner M, Yan A, Kane AB, et al. (2008) Adsorption of essential micronutrients by carbon nanotubes and the implications for nanotoxicity testing. Small 4: 721-727.

91. Fuller CM, Benos DJ (1992) Cftr! Am J Physiol 263: C267-286.
92. Fischer H, Illek B, Sachs L, Finkbeiner WE, Widdicombe JH (2010) CFTR and calcium-activated chloride channels in primary cultures of human airway gland cells of serous or mucous phenotype. Am J Physiol Lung Cell Mol Physiol 299: L585-594.
93. Ito Y, Son M, Kume H, Yamaki K (2001) Novel effects of minocycline on Ca(2+)-dependent Cl(-) secretion in human airway epithelial Calu-3 cells. Toxicol Appl Pharmacol 176: 101-109.
94. Huang F, Rock JR, Harfe BD, Cheng T, Huang X, et al. (2009) Studies on expression and function of the TMEM16A calcium-activated chloride channel. Proc Natl Acad Sci U S A 106: 21413-21418.
95. Rock JR, O'Neal WK, Gabriel SE, Randell SH, Harfe BD, et al. (2009) Transmembrane protein 16A (TMEM16A) is a Ca2+-regulated Cl- secretory channel in mouse airways. J Biol Chem 284: 14875-14880.
96. Rock JR, Futtner CR, Harfe BD (2008) The transmembrane protein TMEM16A is required for normal development of the murine trachea. Dev Biol 321: 141-149.
97. Namkung W, Thiagarajah JR, Phuan PW, Verkman AS (2010) Inhibition of Ca2+-activated Cl- channels by gallotannins as a possible molecular basis for health benefits of red wine and green tea. FASEB J 24: 4178-4186.
98. Wei L, Vankeerberghen A, Cuppens H, Eggermont J, Cassiman JJ, et al. (1999) Interaction between calcium-activated chloride channels and the cystic fibrosis transmembrane conductance regulator. Pflugers Arch 438: 635-641.
99. Wei L, Vankeerberghen A, Cuppens H, Cassiman JJ, Droogmans G, et al. (2001) The C-terminal part of the R-domain, but not the PDZ binding motif, of CFTR is involved in interaction with Ca(2+)-activated Cl- channels. Pflugers Arch 442: 280-285.
100. Reddy MM, Quinton PM (2003) Functional interaction of CFTR and ENaC in sweat glands. Pflugers Arch 445: 499-503.
101. Bachhuber T, Konig J, Voelcker T, Murle B, Schreiber R, et al. (2005) Cl- interference with the epithelial Na+ channel ENaC. J Biol Chem 280: 31587-31594.
102. Ji HL, Chalfant ML, Jovov B, Lockhart JP, Parker SB, et al. (2000) The cytosolic termini of the beta- and gamma-ENaC subunits are involved in the functional interactions between cystic fibrosis transmembrane conductance regulator and epithelial sodium channel. J Biol Chem 275: 27947-27956.
103. Stutts MJ, Rossier BC, Boucher RC (1997) Cystic fibrosis transmembrane conductance regulator inverts protein kinase A-mediated regulation of epithelial sodium channel single channel kinetics. J Biol Chem 272: 14037-14040.
104. Rotoli BM, Bussolati O, Bianchi MG, Barilli A, Balasubramanian C, et al. (2008) Non-functionalized multi-walled carbon nanotubes alter the paracellular permeability of human airway epithelial cells. Toxicol Lett 178: 95-102.
105. Haws C, Finkbeiner WE, Widdicombe JH, Wine JJ (1994) CFTR in Calu-3 human airway cells: channel properties and role in cAMP-activated Cl- conductance. Am J Physiol 266: L502-512.
106. Brouwer D (2010) Exposure to manufactured nanoparticles in different workplaces. Toxicology 269: 120-127.
107. Schneider T, Brouwer DH, Koponen IK, Jensen KA, Fransman W, et al. (2011) Conceptual model for assessment of inhalation exposure to manufactured nanoparticles. J Expo Sci Environ Epidemiol.

108. Lam CW, James JT, McCluskey R, Arepalli S, Hunter RL (2006) A review of carbon nanotube toxicity and assessment of potential occupational and environmental health risks. Crit Rev Toxicol 36: 189-217.
109. Maynard AD, Baron PA, Foley M, Shvedova AA, Kisin ER, et al. (2004) Exposure to carbon nanotube material: aerosol release during the handling of unrefined single-walled carbon nanotube material. J Toxicol Environ Health A 67: 87-107.
110. Hirase T, Staddon JM, Saitou M, Ando-Akatsuka Y, Itoh M, et al. (1997) Occludin as a possible determinant of tight junction permeability in endothelial cells. J Cell Sci 110 (Pt 14): 1603-1613.
111. Balda MS, Matter K (1998) Tight junctions. J Cell Sci 111 (Pt 5): 541-547.
112. Denker BM, Nigam SK (1998) Molecular structure and assembly of the tight junction. Am J Physiol 274: F1-9.
113. Matter K, Aijaz S, Tsapara A, Balda MS (2005) Mammalian tight junctions in the regulation of epithelial differentiation and proliferation. Curr Opin Cell Biol 17: 453-458.
114. Kallakury BV, Sheehan CE, Ross JS (2001) Co-downregulation of cell adhesion proteins alpha- and beta-catenins, p120CTN, E-cadherin, and CD44 in prostatic adenocarcinomas. Hum Pathol 32: 849-855.
115. Morton RA, Ewing CM, Nagafuchi A, Tsukita S, Isaacs WB (1993) Reduction of E-cadherin levels and deletion of the alpha-catenin gene in human prostate cancer cells. Cancer Res 53: 3585-3590.
116. Voeller HJ, Truica CI, Gelmann EP (1998) Beta-catenin mutations in human prostate cancer. Cancer Res 58: 2520-2523.
117. Winder SJ, Ayscough KR (2005) Actin-binding proteins. J Cell Sci 118: 651-654.
118. Birkenfeld J, Betz H, Roth D (2003) Identification of cofilin and LIM-domain-containing protein kinase 1 as novel interaction partners of 14-3-3 zeta. Biochem J 369: 45-54.
119. Xing H, Zhang S, Weinheimer C, Kovacs A, Muslin AJ (2000) 14-3-3 proteins block apoptosis and differentially regulate MAPK cascades. EMBO J 19: 349-358.
120. Gourlay CW, Ayscough KR (2005) The actin cytoskeleton: a key regulator of apoptosis and ageing? Nat Rev Mol Cell Biol 6: 583-589.
121. Haniu H, Matsuda Y, Takeuchi K, Kim YA, Hayashi T, et al. (2010) Proteomics-based safety evaluation of multi-walled carbon nanotubes. Toxicol Appl Pharmacol 242: 256-262.
122. Dong PX, Wan B, Guo LH (2011) In vitro toxicity of acid-functionalized single-walled carbon nanotubes: Effects on murine macrophages and gene expression profiling. Nanotoxicology.
123. Goldberg AL (2003) Protein degradation and protection against misfolded or damaged proteins. Nature 426: 895-899.
124. Ross CA, Poirier MA, Wanker EE, Amzel M (2003) Polyglutamine fibrillogenesis: the pathway unfolds. Proc Natl Acad Sci U S A 100: 1-3.
125. Sjakste N STaVU (2002) Role of the ubiquitin-proteasome degradation pathway in carcinogenesis, tumor progression and susceptibility to tumor treatment. Exp Onc 24: 243-248.
126. Miyamoto Y, Saiwaki T, Yamashita J, Yasuda Y, Kotera I, et al. (2004) Cellular stresses induce the nuclear accumulation of importin alpha and cause a conventional nuclear import block. J Cell Biol 165: 617-623.

127. Hirano S, Fujitani Y, Furuyama A, Kanno S (2010) Uptake and cytotoxic effects of multi-walled carbon nanotubes in human bronchial epithelial cells. Toxicol Appl Pharmacol 249: 8-15.
128. Cha MH, Rhim T, Kim KH, Jang AS, Paik YK, et al. (2007) Proteomic identification of macrophage migration-inhibitory factor upon exposure to TiO2 particles. Mol Cell Proteomics 6: 56-63.
129. Ramesh GT, Sarkar S, Sharma C, Yog R, Periakaruppan A, et al. (2007) Analysis of stress responsive genes induced by single-walled carbon nanotubes in BJ foreskin cells. Journal of Nanoscience and Nanotechnology 7: 584-592.
130. Thiele M, Bernhagen J (2005) Link between macrophage migration inhibitory factor and cellular redox regulation. Antioxid Redox Signal 7: 1234-1248.
131. Teeguarden JG, Webb-Robertson BJ, Waters KM, Murray AR, Kisin ER, et al. (2011) Comparative proteomics and pulmonary toxicity of instilled single-walled carbon nanotubes, crocidolite asbestos, and ultrafine carbon black in mice. Toxicol Sci 120: 123-135.

VITA

VITA

Amiraj Banga

EDUCATIONAL QUALIFICATIONS

Punjab Agricultural University, Ludhiana, Punjab, India

M.S. in Microbiology ..... **December 2002**

Punjab University, Chandigarh, India

B.S. in Biology..... **June 2000**

AWARDS

Indiana University-Purdue University Indianapolis, IN

Student Travel Grant by Center of Membrane Biosciences .....**Spring 2011**

Educational Enhancement Grant by Graduate Student Organization.....**Spring 2009**

Educational Enhancement Grant by Graduate Student Organization.....**Spring 2008**

School of Science Graduate Student Council Travel Award .....**Spring 2008**

Purdue University, West Lafayette, IN

Purdue Travel Grant by Purdue Graduate Student Government .....**Spring 2008**

TEACHING EXPERIENCE

Indiana University-Purdue University Indianapolis, IN

Teaching Assistant, Concepts of Biology.....**Spring 2009, Spring 2010, Fall 2010**

Guest lectures, (4), Physiology.....**Fall 2009, Fall 2010**

Shaheed Udham Singh College of Engineering and Technology, Mohali, Punjab, India

Lecturer Biotechnology.....**February 2004-March 2006**

RESEARCH EXPERIENCE

Punjab Agricultural University, Ludhiana, Punjab, India

Senior Research Fellow ..... **January-December 2003**

PUBLICATIONS

Abstract entitled "Functional effects of carbon nanotubes on airway epithelial cells" has been published by Indiana Physiological Society, Indianapolis, Indiana

February 5, 2011

Research paper entitled "Effect of carbon nanoparticles on barrier function of renal epithelial cells" has been published by the journal Nanotoxicology
Blazer-Yost, B.L., A. J. Banga, A. Amos, E. Chernoff, X. Lai, C. Li, S. Mitra and F.A. Witzmann. Effect of carbon nanoparticles on barrier function of renal epithelial cells. Nanotoxicology, November 10, 2010 [Epub ahead of print]

November 2010

Abstract entitled "Functional effects of nanoparticle exposure on airway epithelial cells" has been published by U.S. EPA Nanotechnology Grantees Meeting, Portland, Oregon

November 8-9, 2010

Abstract entitled "Effect of carbon nanoparticle exposure on protein expression in barrier epithelial cells" has been published by Nanotoxicology 2010, Edinburgh, Scotland

June 2-4, 2010

Abstract entitled "Effect of carbon nanoparticle exposure on cellular function of barrier epithelial cells" has been published by Nanotoxicology 2010, Edinburgh, Scotland

June 2-4, 2010

Research paper entitled "Evaluation of paddy straw composts for *Agaricus bisporus* production' has been published by the 'Indian Journal of Ecology" (2004) 31 (2) : 120-123

June 2004

Abstract entitled "Evaluation of paddy straw composts for *Agaricus bisporus* production" has been published by the 43rd Annual Conference of 'Association of Microbiologists of India', India

December 11-13, 2002

PRESENTATIONS

Presented the poster entitled "Functional effects of carbon nanotubes on airway epithelial cells" at Experimental Biology Pre-Epithelial Meeting 2011, Washington DC

A**pril 11, 2011**

Delivered a talk at Experimental Biology Pre-Epithelial Meeting 2011, Washington DC, on "Effects of nanoparticle exposure on airway epitehlial cells"

April 9, 2011

Presented the poster entitled "Functional effects of carbon nanotubes on airway epithelial cells" at Indiana Physiological Society meeting, Indianapolis, Indiana

February 5, 2011

Delivered a talk on "Sensory organs" at a graduate Physiology class (Physiology 557), IUPUI, Indianapolis, Indiana

December 23, 2010

Delivered a talk at a U.S. Environmental Protection Act Nanotechnology Grantees meeting in conjunction with Society of Environmental Toxicology and Chemistry, North America 31st Annual meeting on "Effects of nanoparticle exposure on airway epithelial cells" at Portland, Oregon

November 9, 2010

Delivered a lecture on "Functional effects of nanoparticle toxicity on airway epithelial cell function" at 45th Annual Biological Transport Meeting (affiliated with American Physiological Society) in Jamestown, Kentucky

June 22, 2010

Delivered a talk on "Skeletal system" at an undergraduate physiology class (Biology K103), IUPUI, Indianapolis, Indiana

January 16, 2010

Delivered a talk on "Female reproductive system and polycystic ovarian syndrome" at a graduate Physiology classes (Physiology 557), IUPUI, Indianapolis, Indiana

November 17, 2009

Presented a poster entitled "Structural and functional effects of nanoparticle exposure on renal epithelial cell function" at Annual Indiana University School of Medicine-Clinical and Translational Science Institute scientific poster session, Indiana University School of Medicine, Indianapolis, Indiana

September 16, 2009

Delivered a lecture on "Structural and functional effects of nanoparticle toxicity on barrier epithelial cell function" at 44th Annual Biological Transport Meeting (affiliated with American Physiological Society) in Jamestown, Kentucky

June 22, 2009

Presented a poster entitled "Structural and functional effects of nanoparticle toxicity on renal epithelial cell function" at IUPUI Research Day at IUPUI, Indianapolis, Indiana

April 24, 2009

Presented a poster entitled "Structural and functional effects of nanoparticle toxicity on renal epithelial cell function" at Indiana Clinical and Translational Science Institute meeting at Indianapolis, Indiana

January 8, 2009

Delivered a lecture on "Role of serum and glucocorticoid induced kinase (Sgk) in renal function" at the 43rd Annual Biological Transport Meeting (affiliated with American Physiological Society) in Jamestown, Kentucky

June 17, 2008

Presented a poster entitled "Evaluation of paddy straw composts for *Agaricus bisporus* production" at the 43rd Annual Conference of Association of Microbiologists of India, Hisar, India

December 12, 2002